Sparse representations and quadratic approximations in path integral techniques for stochastic response analysis of diverse systems/structures

Apostolos Psaros Andriopoulos

Submitted in partial fulfillment of the
requirements for the degree of
Doctor of Philosophy
in the Graduate School of Arts and Sciences

Columbia University
2019

© 2019
Apostolos Psaros Andriopoulos
All rights reserved

Abstract

Sparse representations and quadratic approximations in path integral techniques for stochastic response analysis of diverse systems/structures

Apostolos Psaros Andriopoulos

Uncertainty propagation in engineering mechanics and dynamics is a highly challenging problem that requires development of analytical/numerical techniques for determining the stochastic response of complex engineering systems. In this regard, although Monte Carlo simulation (MCS) has been the most versatile technique for addressing the above problem, it can become computationally daunting when faced with high-dimensional systems or with computing very low probability events. Thus, there is a demand for pursuing more computationally efficient methodologies.

Recently, a Wiener path integral (WPI) technique, whose origins can be found in theoretical physics, has been developed in the field of engineering dynamics for determining the response transition probability density function (PDF) of nonlinear oscillators subject to non-white, non-Gaussian and non-stationary excitation processes. In the present work, the Wiener path integral technique is enhanced, extended and generalized with respect to three main aspects; namely, versatility, computational efficiency and accuracy.

Specifically, the need for increasingly sophisticated modeling of excitations has led recently to the utilization of fractional calculus, which can be construed as a generalization of classical calculus. Motivated by the above developments, the WPI technique is extended herein to account for stochastic excitations modeled via fractional-order filters. To this aim, relying on a variational formulation and on the most probable path approximation yields a deterministic fractional boundary value problem to be solved numerically for obtaining the oscillator joint response PDF.

Further, appropriate multi-dimensional bases are constructed for approximating, in a computationally efficient manner, the non-stationary joint response PDF. In this regard, two distinct approaches are pursued. The first employs expansions based on Kronecker

products of bases (e.g., wavelets), while the second utilizes representations based on positive definite functions. Next, the localization capabilities of the WPI technique are exploited for determining PDF points in the joint space-time domain to be used for evaluating the expansion coefficients at a relatively low computational cost.

Subsequently, compressive sampling procedures are employed in conjunction with group sparsity concepts and appropriate optimization algorithms for decreasing even further the associated computational cost. It is shown that the herein developed enhancement renders the technique capable of treating readily relatively high-dimensional stochastic systems. More importantly, it is shown that this enhancement in computational efficiency becomes more prevalent as the number of stochastic dimensions increases; thus, rendering the herein proposed sparse representation approach indispensable, especially for high-dimensional systems.

Next, a quadratic approximation of the WPI is developed for enhancing the accuracy degree of the technique. Concisely, following a functional series expansion, higher-order terms are accounted for, which is equivalent to considering not only the most probable path but also fluctuations around it. These fluctuations are incorporated into a state-dependent factor by which the exponential part of each PDF value is multiplied. This localization of the state-dependent factor yields superior accuracy as compared to the standard most probable path WPI approximation where the factor is constant and state-invariant. An additional advantage relates to efficient structural reliability assessment, and in particular, to direct estimation of low probability events (e.g., failure probabilities), without possessing the complete transition PDF.

Overall, the developments in this thesis render the WPI technique a potent tool for determining, in a reliable manner and with a minimal computational cost, the stochastic response of nonlinear oscillators subject to an extended range of excitation processes. Several numerical examples, pertaining to both nonlinear dynamical systems subject to external excitations and to a special class of engineering mechanics problems with stochastic media properties, are considered for demonstrating the reliability of the developed techniques. In

all cases, the degree of accuracy and the computational efficiency exhibited are assessed by comparisons with pertinent MCS data.

Contents

List of Figures

Acknowledgements

I am very privileged to have worked with Professor Ioannis Kougioumtzoglou, whom I greatly thank for his constant support, guidance, and patience. Throughout the course of my doctoral studies he has been and continues to be my advisor, an invaluable collaborator, and a spectacular source of inspiration, encouragement and ideas. By always being available for his students, listening to us and adapting our research according to our interests and skills, and by providing us with intelligent personal and career advices, he succeeds to foster scientific independence and integrity in us; qualities that are indispensable to young researchers. Certainly, all the above are exemplified by the fact that every single discussion we had during these past four years resulted in amplified excitement and curiosity about both our common research endeavors and scientific inquiry in general.

I am also very grateful to Professor George Deodatis for his insight and support during my studies at Columbia University. Moreover, I would like to thank the rest of the thesis committee, Professors Andrew Smyth, Shiho Kawashima and Karl Sigman, who spent the time to provide me with helpful feedback. Their comments were extremely valuable.

Last but not least, I wish to express my deepest gratitude to my family and friends for their love and motivation all these years. They were the ones who truly helped me endure and overcome the sporadic, but intense, hardships of my Ph.D. life.

Chapter 1

Introduction

1.1 Stochastic engineering dynamics

1.1.1 Persistent and current challenges due to increasingly complex modeling

Addressing the challenge of uncertainty propagation in engineering dynamics relates to the development of analytical and numerical methodologies for determining response and reliability statistics of complex systems, i.e., for solving stochastic (partial) differential equations of the form

$$\mathcal{F}[\boldsymbol{x}] = \boldsymbol{f} \tag{1.1}$$

where $\mathcal{F}[\cdot]$ is an operator (nonlinear, differential, etc.); $\boldsymbol{f}$ is the external excitation; and $\boldsymbol{x}$ is the system response to be determined. Note that ever-increasing computational capabilities, novel signal processing techniques, advanced experimental setups, as well as progress in emerging and transformative technologies (e.g., nano-mechanics, energy harvesting, etc.) have contributed to a highly sophisticated mathematical modeling of Eq. (1.1). Irrespective of the scale of the problem (nano- to macro-), common challenges include:

A) Stochastic environment and media properties: Uncertainty modeling precedes the chal-

lenge of uncertainty propagation and relates to the development of methodologies (e.g., spectral analysis techniques) for analyzing available measured data (e.g., time-histories), and subsequently, for estimating pertinent stochastic models. In real-life situations, measured data most often exhibit a *time-* and *space-varying behavior*. For instance, most environmental excitations (e.g., earthquakes, winds, etc.) exhibit statistics that vary with time. Similarly, considering the example of functionally graded materials, properties such as the elasticity modulus may exhibit statistics that vary with space. Further, most often there are *limited* and *incomplete data* due to several reasons, such as cost (e.g., expensive sensor maintenance in harsh conditions and remote areas), data loss or corruption (e.g., sensor failures, power outages, etc), as well as limited bandwidth and storage capacities. Thus, development of potent joint time/space-frequency analysis techniques, which can account for incomplete data as well, is necessary for more accurate excitation/system modeling. Indicatively, statistical estimators based on wavelets in conjunction with compressive sampling concepts and tools have been developed recently for uncertainty modeling based on available realizations with missing data (e.g., [27, 201]). Furthermore, with the recent advent of multi-scale computational analyses, researchers and engineers are faced with the challenge of interpreting and translating *measured data at multiple scales* into pertinent stochastic models (e.g., [76]). In this regard, there is a need for developing robust multi-scale statistical descriptors and stochastic models capable of capturing complex uncertainty relationships. Also, the recent exploitation of diverse sensor technologies, and the availability of *massive amounts of measured data*, facilitates a higher-order modeling and representation of stochastic processes, which would be unfeasible a few years ago due to lack of sufficient data (e.g., [162]). As a result, modern statistical estimators necessitate, in general, the realistic modeling of the system parameters in the operator $\mathcal{F}[\cdot]$ (e.g., media / material properties), and of the excitation $\boldsymbol{f}$ in Eq. (1.1), as *non-Gaussian*, *non-white*, and *non-stationary stochastic processes*. This reflects a significantly more complex uncertainty modeling, especially in comparison to early developments in the field of stochastic engineering dynamics where the "Gaussian

white noise process" assumption used to be routinely employed. Of course, although this assumption facilitated significantly the solution of the governing equations, it also yielded an oversimplification of the model.

B) System complexity & high dimensionality: Classical continuum (or discretized) mechanics theories have been traditionally used for modeling the operator $\mathcal{F}[\cdot]$ in Eq. (1.1). Nevertheless, the need for more accurate media behavior modeling has led recently to advanced mathematical tools such as *fractional calculus* (e.g., [139, 155, 156]). Besides the fact that fractional calculus can be construed as a generalization of classical calculus (and as such provides with enhanced modeling flexibility), it has been successfully employed in theoretical and applied mechanics for developing *non-local* continuum mechanics theories (e.g., [40, 184]), as well as for *viscoelastic* material modeling (e.g., [39]). Note that the fractional derivative operator $\boldsymbol{D}^{\beta}[\boldsymbol{x}]$ has also a clear and intuitive physical interpretation in the field of viscoelasticity. For $\beta = 0$, $\boldsymbol{D}^{\beta}[\boldsymbol{x}]$ degenerates to $\boldsymbol{D}^{\beta}[\boldsymbol{x}] = \boldsymbol{x}$, modeling a purely elastic restoring force in engineering dynamics. For $\beta = 1$, $\boldsymbol{D}^{\beta}[\boldsymbol{x}]$ degenerates to $\boldsymbol{D}^{\beta}[\boldsymbol{x}] = \dot{\boldsymbol{x}}$, modeling a purely viscous restoring force. What if the material has a visco-elastic behavior? Is it possible that this is captured by a fractional order ($0 \leq \beta < 1$) derivative? Indeed, experimental viscoelastic response data obtained via creep and relaxation tests agree extremely well with such kind of modeling [39, 72, 137]. Finally, the above unconventional modeling is also typically coupled with complex *nonlinearities* and *hysteresis* (e.g., [122]), and with *high-dimensional multi-degree-of-freedom* system modeling.

Overall, from a mathematics perspective, Eq. (1.1) takes the form of a *high-dimensional system of coupled nonlinear stochastic (fractional/partial) differential equations*. In many cases, even the deterministic solution of such equations is an open issue and an active research topic. Clearly, solving the stochastic counterparts of these equations becomes significantly more challenging. In this regard, "partially" solving Eq. (1.1) and obtaining the first few response moments only (e.g., mean and standard deviation) is often inadequate for properly

analyzing, designing and optimizing engineering systems and structures. Instead, a *complete stochastic characterization* of the system response requires (the significantly more difficult task of) determining the joint response transition probability density function (PDF). This would allow for an optimal and robust design methodology based, for instance, on low probability events (e.g., failures), and/or on other alternative constraints and requirements related to extreme/peak response statistics.

1.1.2 State-of-the-art solution techniques and limitations

Available techniques for solving the governing equations and determining the stochastic response of dynamical systems modeled via Eq. (1.1) can be broadly divided into two categories: a) those that can determine accurately low probability events, but can handle a very small number of stochastic dimensions/degrees-of-freedom due to *prohibitive computational cost*; and b) those that can readily treat high-dimensional systems, but provide *reliable estimates for low-order response statistics only* (e.g., mean and standard deviation). This is often inadequate for proper system analysis, design and optimization. To elaborate further, in stochastic engineering dynamics Eq. (1.1) takes typically the following form of stochastic differential equations (SDEs); that is,

$$\boldsymbol{M}\ddot{\boldsymbol{x}} + \boldsymbol{C}\dot{\boldsymbol{x}} + \boldsymbol{K}\boldsymbol{x} + \boldsymbol{g}\left(\boldsymbol{x}, \dot{\boldsymbol{x}}, \boldsymbol{D}^{\beta}\left[\boldsymbol{x}\right]\right) = \boldsymbol{f}(t) \tag{1.2}$$

where $\boldsymbol{M}$, $\boldsymbol{C}$, $\boldsymbol{K}$ denote the mass, damping and stiffness matrices, respectively, and $\boldsymbol{g}\left(\cdot\right)$ is a general nonlinear function which can account for hysteretic as well as for fractional derivative modeling.

Although Monte Carlo simulation (MCS) (e.g., [9, 47, 77, 163, 173, 188]) has been the most versatile tool for solving the stochastic Eq. (1.2), there are many cases where *MCS can be computationally prohibitive*. This is especially true when either high-dimensional complex systems are considered (thus, even only one deterministic analysis is time-consuming), or the

system response quantity of interest has a very low probability of occurrence (thus, millions of deterministic analyses are required to acquire a reasonably accurate estimate). During the past years significant progress has been made in enhancing the computational efficiency of MCS by developing various "smart" MCS schemes such as importance sampling, subset simulation, and sequential methods (e.g., [9, 47]). These schemes have been coupled with surrogate models (e.g., Kriging), and order reduction methodologies (e.g., [80]) to further decrease the computational cost. However, in many cases the cost still remains prohibitive. In addition, the above "hybrid" schemes may impose significant approximations, which can reduce effectively the accuracy and reliability of the simulations, especially when the goal is to determine low probability events (e.g., failures).

Thus, there is a *need for developing alternative analytical and/or numerical techniques* for determining the response of stochastic dynamical systems. Indicative techniques include moments equations, statistical linearization, stochastic averaging, perturbation approaches, discrete Chapman-Kolmogorov equation schemes, Fokker-Planck equation solution techniques, probability density evolution methods, (generalized) polynomial chaos expansions, and dynamically orthogonal field equations (e.g., [53, 63, 73, 79, 88, 105, 112, 114, 118, 135, 154, 158, 167, 171, 182]).

Historically, perturbation approaches were among the first ones to be employed for solving random vibration problems (e.g., [29]). However, they exhibit *satisfactory accuracy only for low nonlinearity magnitudes*; thus, rendering them inadequate for a wide range of strongly nonlinear engineering systems. Further, statistical linearization (and related moments equations approaches) has been one of the most versatile and popular approximate methodologies for determining the stochastic response of nonlinear systems in a computationally efficient manner (e.g., [154]). The main objective of the methodology relates to the replacement of the original nonlinear system with an "equivalent linear" one by appropriately minimizing the error vector corresponding to the difference between the two systems. According to the standard implementation of the methodology, the minimization criterion typically relates to

the mean square error, while the Gaussian assumption for the system response PDFs is commonly adopted (e.g., [154]). Although there exist more sophisticated implementations of the statistical linearization, which relax the aforementioned assumptions and/or employ various other minimization criteria (e.g., [167]), these versions typically lack versatility. In fact, one of the reasons for the wide utilization of the standard statistical linearization methodology has been, undoubtedly, its versatility in addressing a wide range of nonlinear behaviors under the same mathematical framework. In particular, the Gaussian response assumption in conjunction with the mean square error minimization criterion facilitates the derivation of closed form expressions for the equivalent linear elements (e.g., mass, stiffness, and damping coefficients, etc.) as functions of the response statistics. Nevertheless, primarily due to the Gaussian response assumption, the standard methodology is generally *restricted to the determination of first- and second-order response statistics only*. The interested reader may find a detailed presentation of the methodology in the two dedicated books on the topic by [154] and by [167], and in various review papers (e.g., [31, 54, 166, 172]).

Furthermore, relying on preliminary work in the field of theoretical physics (e.g., [189]), Naess and co-workers pioneered in stochastic engineering dynamics a numerical solution scheme by utilizing a discrete version of the Chapman-Kolmogorov equation, and by propagating the response PDF in short time steps (e.g., [23, 128]). Nevertheless, although the scheme exhibits excellent accuracy in predicting even the tails of the system response PDF, its performance is hindered eventually by *excessive computational cost with increasing dimensionality* (e.g., [5]). This is due to the fact that a multi-convolution integral needs to be computed for each and every time step, while the time increment is required to be short. Due to other different reasons, alternative probability density evolution schemes (e.g., [112]) and Fokker-Planck equation solution strategies (e.g., [152, 169]), as well as approaches based on polynomial chaos and other expansions [63, 73, 182], also become eventually *inefficient computationally* with an increasing number of dimensions. In this regard, various order reduction approaches have been employed routinely over the last few decades for decreasing

the dimensionality of the original system of equations. Indicatively, stochastic averaging has been a potent dimension reduction tool, used for obtaining approximate solutions to problems involving the vibration response of lightly damped systems to broad-band random excitation (e.g., [153, 202]). The main aspects of the technique relate to a Markovian approximation of an appropriately chosen amplitude of the system response, as well as to a dimension reduction of the original $2m$-dimensional problem to an m-dimensional problem. Nevertheless, the price to pay for reducing the complexity of the original problem is the introduction of various approximations, which unavoidably limit the range of applicability of the approach.

Overall, it becomes clear that the development of versatile solution techniques, which exhibit both high accuracy and low computational cost (and thus, can treat high-dimensional problems), is paramount for advancing the field of stochastic engineering dynamics. In the following section, the mathematical tool of path integral with its major impact on theoretical physics is briefly introduced.

1.2 The path integral technique

From a mathematics point of view, the path integral concept refers to the generalization of integral calculus to functionals. It was first introduced by Wiener [192] (see also preliminary work by Daniell [32]), and was reinvented in a different form by Feynman [61] leading to a reformulation of quantum mechanics. Notwithstanding the obvious similarities between the Wiener and the Feynman integrals, the Wiener path integral relates to stochastic processes and is real-valued, whereas the Feynman path integral is complex-valued as a consequence of a fundamental quantity in quantum mechanics, i.e., the probability amplitude. Interestingly, although the development by Wiener preceded that by Feynman, the applications of the Feynman integral in most branches of modern physics have proven extremely fruitful as a guide for the formulation and development of new ideas and approaches in the description

of physical phenomena. Indicative application areas include the theories of superfluidity, of unified electromagnetic and weak interactions, and of quantum chromodynamics. Clearly, the importance of path integral in theoretical physics as a conceptual and computational tool can hardly be disputed, while a number of books provide the fundamentals and details on the machinery of Feynman path integrals (e.g., [21, 62, 98, 161]).

Note, however, that very few of the aforementioned developments relate to the field of engineering mechanics and dynamics. To address this issue, Kougioumtzoglou and co-workers have recently adapted, extended, and applied the Wiener path integral (WPI) methodology for the stochastic response analysis and reliability assessment of complex dynamical systems of engineering interest. Indicatively, the developed WPI techniques are capable of determining the joint response transition PDF of multi-degree-of-freedom (MDOF) nonlinear/hysteretic systems, even when endowed with fractional derivative terms (e.g., [37, 100, 103]). Furthermore, they can address certain one-dimensional mechanics problems with random material/media properties [101], systems subject to non-white and non-Gaussian stochastic processes [146], as well as a class of nonlinear electromechanical energy harvesters [143].

1.3 Objectives and organization of thesis

Despite the aforementioned developments, the WPI technique is limited to systems subject to excitation processes modeled via filters involving integer-order derivatives only. In this regard, the need for increasingly sophisticated modeling of excitations has led recently to the use of fractional-order filters for describing stochastic loads acting on structural systems. For instance, the widely used in earthquake engineering Kanai-Tajimi power spectrum has been recently enhanced by utilizing a fractional-order filter for circumventing certain limitations of the original standard model [6, 93, 183]. Further, from a computational efficiency perspective, since a WPI-based analytical determination of the PDF is a highly challenging task, a

numerical implementation of the technique is typically required. To this aim, although recent work in [104] reduced the computational complexity by, potentially, several orders of magnitude as compared to the original formulation and numerical implementation of the technique, the related computational cost, which follows a power-law function of the number of stochastic dimensions, restricts the applicability of the methodology to relatively low-dimensional systems. Finally, according to the standard WPI solution approach (e.g., [100]) the path integral is approximated by utilizing only the "most probable path". Even though such an approach has proven to be reliable for the stochastic response determination of a wide class of problems (e.g., [100, 103, 146]) an enhancement in terms of accuracy is potentially feasible by utilizing functional series expansions and higher-order approximations. In this regard, the objective of the present work is to address the above limitations and thus, improve and extend the WPI technique in terms of versatility, computational efficiency, and accuracy.

First, the current state-of-the-art of the technique is presented in Chapter 2. Specifically, by employing the WPI methodology an exact closed-form expression for the joint response PDF of MDOF systems subject to white noise excitation processes and governed by first-order SDEs is derived. As the analytical evaluation of such an expression is a highly challenging task, an approximate WPI technique based on the most probable path is developed and the determination of the PDF reduces to the solution of a deterministic boundary value problem (BVP). Next, the corresponding exact and approximate expressions, as well as the related BVPs for addressing MDOF systems subject to white and non-white/non-Gaussian excitation processes and governed by second-order SDEs are derived. For both first- and second-order systems, since for a linear version of the governing SDE the solution of the related BVP is amenable to a closed-form analytical solution, the PDF is also given in closed-form. However, for general nonlinear systems this is not the case and, in this regard, it is shown that the solution of one BVP is required for the determination of a single point of the PDF; i.e., for obtaining a single PDF measurement. Further, adopt-

ing a brute-force numerical solution approach, for each time instant an effective domain of values is considered for the joint response PDF and one BVP is solved for each and every point of the PDF. Clearly, the computational cost of such a numerical implementation of the technique is prohibitive especially for high-dimensional systems and the necessity for a more computationally efficient implementation is highlighted. Note that a first attempt towards this direction has been proposed in [104].

In Chapter 3 the WPI technique is extended to account for stochastic excitations modeled via fractional-order filters. To this aim, considering two general classes for the form of the excitation process, the governing second-order SDE that is coupled with a fractional-order filter is either written as a fourth-order SDE (as is the case for non-white/non-Gaussian excitation processes modeled via integer-order filters) or as a second-order SDE that is coupled with a set of constraints to be satisfied at all times. In both cases, the original stochastic problem reduces to a set of deterministic problems to be solved for the determination of the joint response PDF. Specifically, considering that the system is written as a fourth-order SDE the PDF is obtained by solving a set of fractional-order BVPs (see e.g., [1, 8, 11, 95, 116]). For the case where a set of constraints is introduced in order to account for the filter equation, the original stochastic problem reduces to a set of fractional-order optimal control problems (e.g., [2, 3, 117]).

In Chapter 4 the problem of obtaining in a computationally efficient manner the joint response PDF of stochastically excited nonlinear oscillators is addressed. Specifically, by employing appropriate time-dependent expansion bases (e.g., wavelets), the task of determining the PDF is formulated as a multivariate approximation problem. As a result, the solution of the problem amounts to acquiring a number of PDF measurements equal to the number of the expansion coefficients and solving a linear system of equations for the determination of the expansion coefficients. Therefore, the WPI technique is generalized to account explicitly for the time dimension in its formulation and implementation. It is shown that the gain in terms of computational cost is notable, measured even at several orders of magnitude

for some cases. In addition, for enhancing the WPI technique in terms of computational efficiency even further, the case of collecting a number of measurements smaller than the number of the expansion coefficients is considered next. By following such a compressive sampling approach, the approximation problem takes the form of an underdetermined linear system, which has either no solution, or an infinite number of solutions. However, it is shown that if the coefficients vector is known to be sparse in the selected basis, i.e., only a few of its components are non-zero, a unique solution can be obtained. Overall, it is shown that a compressive sampling treatment in conjunction with an appropriate optimization algorithm can reduce drastically the required number of PDF measurements.

In Chapter 5 a novel WPI-based stochastic response determination technique is developed for diverse dynamical systems/structures. The developed technique, which can construed as an enhancement of the standard most probable path approach described in Chapter 2, relies on functional series expansions and quadratic approximations for accounting for fluctuations around the most probable path. As a result, by introducing a "localized" and state dependent fluctuation factor yields an increased accuracy degree. An additional significant advantage of this enhancement as compared to earlier developments relates to the fact that low probability events (e.g., failure probabilities) can be estimated directly in a computationally efficient manner by determining only a few points of the joint response PDF. In other words, the normalization step in the standard approach, which required the evaluation of the joint response PDF over its entire effective domain, is circumvented.

Finally, Chapter 6 provides a summary of the main research findings and conclusions of this work. Indicative future research directions are also provided.

Chapter 2

Wiener path integral formalism

2.1 Markov processes and stochastic differential equations

This section serves as a brief background on Markov processes, the associated Chapman-Kolmogorov and Fokker-Planck equations, as well as their relation to a corresponding stochastic differential equation governing the dynamics of the system. Consider a Markov stochastic vector process, $\boldsymbol{\alpha}(t)$, where $\boldsymbol{\alpha} = [\alpha_j]_{n\times 1}$, for which the Chapman-Kolmogorov equation is satisfied (e.g., [171]) for any three distinct time instants $t_{l-1} \leq t_l \leq t_{l+1}$, i.e.,

$$p(\boldsymbol{\alpha}_{l+1}, t_{l+1}|\boldsymbol{\alpha}_{l-1}, t_{l-1}) = \int_{-\infty}^{\infty} p(\boldsymbol{\alpha}_{l+1}, t_{l+1}|\boldsymbol{\alpha}_l, t_l) p(\boldsymbol{\alpha}_l, t_l|\boldsymbol{\alpha}_{l-1}, t_{l-1}) \mathrm{d}\boldsymbol{\alpha}_l \tag{2.1}$$

The sample paths are continuous functions of t with probability one, if for any $\delta > 0$ the Lindeberg condition (e.g., [74])

$$\lim_{\epsilon\to 0} \frac{1}{\epsilon} \int_{|\boldsymbol{\alpha}_{l+1}-\boldsymbol{\alpha}_l|>\delta} p(\boldsymbol{\alpha}_{l+1}, t_{l+1}|\boldsymbol{\alpha}_l, t_l) \mathrm{d}\boldsymbol{\alpha}_{l+1} = 0 \tag{2.2}$$

holds true, where $\epsilon = t_{l+1} - t_l$. Next, the process $\boldsymbol{\alpha}$ is termed diffusion process (e.g., [67, 171]), if the drift vector $\boldsymbol{A}(\boldsymbol{\alpha}, t) = [A_j(\boldsymbol{\alpha}, t)]_{n\times 1}$ and the diffusion matrix $\boldsymbol{B}(\boldsymbol{\alpha}, t) = [B_{jk}(\boldsymbol{\alpha}, t)]_{n\times n}$

can be defined, respectively, as

$$A_j(\boldsymbol{\alpha}_l, t_l) = \lim_{\epsilon \to 0} \frac{\mathbb{E}\left[\alpha_{jl+1} - \alpha_{jl}\right]}{\epsilon} \tag{2.3}$$

and

$$B^2_{jk}(\boldsymbol{\alpha}_l, t_l) = \lim_{\epsilon \to 0} \frac{\mathbb{E}\left[(\alpha_{jl+1} - \alpha_{jl})(\alpha_{kl+1} - \alpha_{kl})\right]}{\epsilon} \tag{2.4}$$

Further, employing the Chapman-Kolmogorov Eq. (2.1) leads to the well-known Fokker-Planck equation (e.g., [7, 78])

$$\frac{\partial p}{\partial t} = -\sum_j \frac{\partial}{\partial \alpha_j}\left(A_j(\boldsymbol{\alpha}, t)p\right) + \frac{1}{2}\sum_{j,k} \frac{\partial}{\partial \alpha_j}\frac{\partial}{\partial \alpha_k}\left(\widetilde{B}_{jk}(\boldsymbol{\alpha}, t)p\right) \tag{2.5}$$

where $p = p(\boldsymbol{\alpha}_{l+1}, t_{l+1}|\boldsymbol{\alpha}_l, t_l)$ and $\widetilde{\boldsymbol{B}}(\boldsymbol{\alpha}, t) = \boldsymbol{B}(\boldsymbol{\alpha}, t)\boldsymbol{B}^T(\boldsymbol{\alpha}, t)$. The Fokker-Planck Eq. (2.5) is related to a first-order stochastic differential equation of the form

$$\mathrm{d}\boldsymbol{\alpha} = \boldsymbol{A}(\boldsymbol{\alpha}, t)\mathrm{d}t + \boldsymbol{B}(\boldsymbol{\alpha}, t)\mathrm{d}\boldsymbol{W} \tag{2.6}$$

where $\boldsymbol{W}$ represents the Wiener process (also known as Brownian motion), which is a Markov process with independent increments; i.e., $\boldsymbol{W}(t_{l+1}) = \boldsymbol{W}(t_l) + \Delta\boldsymbol{W}(t_l, t_{l+1})$, $\forall\ l \geq 0$, with $\Delta\boldsymbol{W}(t_l, t_{l+1})$ being statistically independent from any other increment $\Delta\boldsymbol{W}$. Also, $\boldsymbol{W}$ has continuous, nowhere differentiable, sample paths and is a Gaussian stochastic process; see also [171]. Notwithstanding some loss of mathematical rigor (e.g., [67, 138]), Eq. (2.6) is often written, alternatively, as

$$\dot{\boldsymbol{\alpha}} = \boldsymbol{A}(\boldsymbol{\alpha}, t) + \boldsymbol{B}(\boldsymbol{\alpha}, t)\boldsymbol{\eta}(t) \tag{2.7}$$

where the dot above a variable denotes differentiation with respect to time t and $\boldsymbol{\eta}$ denotes a zero-mean and delta-correlated Gaussian white noise stochastic process of intensity one; i.e., $\mathbb{E}\left[\eta_j(t)\right] = 0$ and $\mathbb{E}\left[\eta_j(t_l)\eta_k(t_{l+1})\right] = \delta_{jk}\delta(t_l - t_{l+1})$, for any $j, k \in \{1, \ldots, n\}$, where δ_{jk} is the

Kronecker delta, and $\delta(t)$ is the Dirac delta function. Regarding the relation between the Wiener and white noise processes, $\boldsymbol{\eta}(t)$ can be defined as an infinitesimal jump of the Wiener process, i.e., $\boldsymbol{\eta}\mathrm{d}t = \mathrm{d}\boldsymbol{W}$; and, thus, it is often (informally) written as the time derivative of the Wiener process in the form $\boldsymbol{\eta} = \frac{\mathrm{d}\boldsymbol{W}}{\mathrm{d}t}$; see also [67] and [138] for a more detailed discussion on the topic.

In the short-time limit the transition PDF has been shown to admit a Gaussian distribution (e.g., [67, 152]) of the form

$$p(\boldsymbol{\alpha}_{l+1}, t_{l+1}|\boldsymbol{\alpha}_l, t_l) = \left[\sqrt{(2\pi\epsilon)^n \det\left[\widetilde{\boldsymbol{B}}(\boldsymbol{\alpha}_l, t_l)\right]}\right]^{-1} \times \exp\left(-\frac{1}{2}\frac{[\boldsymbol{\alpha}_{l+1} - \boldsymbol{\alpha}_l - \epsilon\boldsymbol{A}(\boldsymbol{\alpha}_l, t_l)]^T \left[\widetilde{\boldsymbol{B}}(\boldsymbol{\alpha}_l, t_l)\right]^{-1} [\boldsymbol{\alpha}_{l+1} - \boldsymbol{\alpha}_l - \epsilon\boldsymbol{A}(\boldsymbol{\alpha}_l, t_l)]}{\epsilon}\right) \tag{2.8}$$

Note that the expression in Eq. (2.8) as a candidate for the short-time transition PDF is not restrictive, and other alternative non-Gaussian forms can be used (e.g., [109, 152]).

2.2 Functional integral over the space of paths

In this section, the solution of the general stochastic differential Eq. (2.7) is obtained in closed-form by expressing the joint transition PDF of the process $\boldsymbol{\alpha}$ as a Wiener path integral over the space of all possible paths that the process can follow. To this aim, the short-time transition PDF representation of Eq. (2.8) is employed to evaluate the probability that $\boldsymbol{\alpha}$ follows a specific sample path. In passing, note that, for notation simplicity, both the stochastic process and a sample path of the process are denoted by $\boldsymbol{\alpha}$. Nevertheless, when $\boldsymbol{\alpha}$ is used appropriate comments are provided for clarifying whether it refers to the stochastic process or a sample path. Next, consider the probability of the process $\boldsymbol{\alpha}$ propagating through some infinitesimally thin tube surrounding a path $\boldsymbol{\alpha}(t)$, $\forall\ t \in [t_i, t_f]$, with fixed initial and final states $\{t_i, \boldsymbol{\alpha}_i\}$ and $\{t_f, \boldsymbol{\alpha}_f\}$, respectively. This can be construed as the

probability of a compound event and is expressed (e.g., [21, 152]) as a product of probabilities of the form of Eq. (2.8), i.e.,

$$\mathcal{P}\left[\boldsymbol{\alpha}(t)\right] = \lim_{\substack{\epsilon\to 0\\ L\to\infty}} \left\{ \left[\prod_{l=0}^{L} \left(\left[\sqrt{(2\pi\epsilon)^n \det\left[\widetilde{\boldsymbol{B}}(\boldsymbol{\alpha}_l, t_l)\right]} \right]^{-1} \right) \right] \left[\prod_{l=1}^{L}\prod_{j=1}^{n} \mathrm{d}\alpha_{jl}\right] \right.$$
$$\left. \times \exp\left(-\sum_{l=0}^{L} \frac{1}{2} \frac{\left[\boldsymbol{\alpha}_{l+1} - \boldsymbol{\alpha}_l - \epsilon \boldsymbol{A}(\boldsymbol{\alpha}_l, t_l)\right]^T \left[\widetilde{\boldsymbol{B}}(\boldsymbol{\alpha}_l, t_l)\right]^{-1} \left[\boldsymbol{\alpha}_{l+1} - \boldsymbol{\alpha}_l - \epsilon \boldsymbol{A}(\boldsymbol{\alpha}_l, t_l)\right]}{\epsilon} \right) \right\} \tag{2.9}$$

where the time domain is discretized into $L+2$ points, ϵ apart, as

$$t_i = t_0 < t_1 < \cdots < t_{L+1} = t_f \tag{2.10}$$

and the path $\boldsymbol{\alpha}(t)$ is represented by its values $\boldsymbol{\alpha}_l$ at the discrete time points t_l, for $l \in \{0, \ldots, L+1\}$. Also, $\mathrm{d}\alpha_{jl}$ denote the (infinite in number) infinitesimal "gates" through which the path propagates. Note that the number of probabilities multiplied in Eq. (2.9) is equal to $L+1$, while the number of "gates" is L, since the final point $\boldsymbol{\alpha}_f$ is fixed. In the continuous limit, Eq. (2.9) can be written as

$$\mathcal{P}\left[\boldsymbol{\alpha}(t)\right] = \exp\left(-\int_{t_i}^{t_f} \mathcal{L}\left[\boldsymbol{\alpha}, \dot{\boldsymbol{\alpha}}\right] \mathrm{d}t \right) \prod_{j=1}^{n} \mathcal{D}[\alpha_j(t)] \tag{2.11}$$

where $\mathcal{L}\left[\boldsymbol{\alpha}, \dot{\boldsymbol{\alpha}}\right]$ denotes the Lagrangian functional of the system expressed as

$$\mathcal{L}\left[\boldsymbol{\alpha}, \dot{\boldsymbol{\alpha}}\right] = \frac{1}{2} \left[\dot{\boldsymbol{\alpha}} - \boldsymbol{A}(\boldsymbol{\alpha}, t)\right]^T \left[\widetilde{\boldsymbol{B}}(\boldsymbol{\alpha}, t)\right]^{-1} \left[\dot{\boldsymbol{\alpha}} - \boldsymbol{A}(\boldsymbol{\alpha}, t)\right] \tag{2.12}$$

and $\mathcal{D}[\alpha_j(t)]$, for $j \in \{1, \ldots, n\}$, is a functional measure (a rigorous generalization of the notion of volume; see [71] for more details) given by

$$\mathcal{D}[\alpha_j(t)] = \prod_{t=t_i}^{t_f} \frac{\mathrm{d}\alpha_j(t)}{\sqrt{2\pi \left(\det\left[\widetilde{\boldsymbol{B}}(\boldsymbol{\alpha}, t)\right]\right)^{1/n} \mathrm{d}t}} \equiv \prod_{l=0}^{L} \frac{1}{\sqrt{2\pi \left(\det\left[\widetilde{\boldsymbol{B}}(\boldsymbol{\alpha}_l, t_l)\right]\right)^{1/n} \epsilon}} \prod_{l=1}^{L} \mathrm{d}\alpha_{jl} \tag{2.13}$$

For the special case where the diffusion matrix $\boldsymbol{B}(\boldsymbol{\alpha}, t)$ is diagonal, Eqs. (2.12) and (2.13) degenerate to

$$\mathcal{L}\left[\boldsymbol{\alpha}, \dot{\boldsymbol{\alpha}}\right] = \frac{1}{2} \sum_{j=1}^{n} \frac{\left[\dot{\alpha}_j - A_j(\boldsymbol{\alpha}, t)\right]^2}{\widetilde{B}_{jj}(\boldsymbol{\alpha}, t)} \tag{2.14}$$

and

$$\mathcal{D}[\alpha_j(t)] = \prod_{t=t_i}^{t_f} \frac{\mathrm{d}\alpha_j(t)}{\sqrt{2\pi \widetilde{B}_{jj}(\boldsymbol{\alpha}, t)\mathrm{d}t}} \tag{2.15}$$

respectively.

It is noted that although the mathematically rigorous term for $\mathcal{P}\left[\boldsymbol{\alpha}(t)\right]$ is probability density functional, in this thesis the terms "probability density functional" and "probability of each path" are used interchangeably for convenience. Further, it is rather intuitive to argue that the respective probabilities of each and every path need to be accounted for, and loosely speaking, "summed up" in order to evaluate the total probability of $\boldsymbol{\alpha}$ starting from $\boldsymbol{\alpha}_i$ at time t_i and ending up at $\boldsymbol{\alpha}_f$ at time t_f (e.g., [62]). In this regard, by utilizing Eq. (2.9) in conjunction with Eqs. (2.11)-(2.13), the joint transition PDF is expressed as the limit of an L-dimensional integral with $L \to \infty$ in the form

$$\begin{aligned} p(\boldsymbol{\alpha}_f, t_f | \boldsymbol{\alpha}_i, t_i) = \lim_{\substack{\epsilon \to 0 \\ L \to \infty}} \int_{-\infty}^{\infty} \cdots \int_{-\infty}^{\infty} \exp\left(-\sum_{l=0}^{L} \mathcal{L}\left[\boldsymbol{\alpha}_j, \dot{\boldsymbol{\alpha}}_j\right] \epsilon\right) \\ \times \prod_{j=1}^{n} \prod_{l=0}^{L} \frac{1}{\sqrt{2\pi \left(\det\left[\widetilde{\boldsymbol{B}}(\boldsymbol{\alpha}_l, t_l)\right]\right)^{1/n} \epsilon}} \prod_{l=1}^{L} \mathrm{d}\alpha_{jl} \end{aligned} \tag{2.16}$$

Next, it can be shown, based on a Trotter product formula treatment (e.g., [161]), that

the discrete approximation of the transition PDF in Eq. (2.16) converges in the continuous limit to a functional integral over the space of paths that satisfy certain properties (e.g., [21]). Specifically, denoting the set of all paths with initial state $\boldsymbol{\alpha}_i$ at time t_i and final state $\boldsymbol{\alpha}_f$ at time t_f by $\mathcal{C}\{\boldsymbol{\alpha}_i, t_i; \boldsymbol{\alpha}_f, t_f\}$, the joint transition PDF takes the form

$$p(\boldsymbol{\alpha}_f, t_f|\boldsymbol{\alpha}_i, t_i) = \int_{\mathcal{C}\{\boldsymbol{\alpha}_i, t_i; \boldsymbol{\alpha}_f, t_f\}} \exp\left(-\int_{t_i}^{t_f} \mathcal{L}\left[\boldsymbol{\alpha}, \dot{\boldsymbol{\alpha}}\right] \mathrm{d}t\right) \mathcal{D}[\boldsymbol{\alpha}(t)] \tag{2.17}$$

where

$$\mathcal{D}[\boldsymbol{\alpha}(t)] = \prod_{j=1}^{n} \mathcal{D}[\alpha_j(t)] \tag{2.18}$$

or, alternatively,

$$p(\boldsymbol{\alpha}_f, t_f|\boldsymbol{\alpha}_i, t_i) = \int_{\mathcal{C}\{\boldsymbol{\alpha}_i, t_i; \boldsymbol{\alpha}_f, t_f\}} \exp\left(-\mathcal{S}\left[\boldsymbol{\alpha}, \dot{\boldsymbol{\alpha}}\right]\right) \mathcal{D}[\boldsymbol{\alpha}(t)] \tag{2.19}$$

where $\mathcal{S}\left[\boldsymbol{\alpha}, \dot{\boldsymbol{\alpha}}\right]$ is typically referred to in the theoretical physics literature as stochastic action and is given by

$$\mathcal{S}\left[\boldsymbol{\alpha}, \dot{\boldsymbol{\alpha}}\right] = \int_{t_i}^{t_f} \mathcal{L}\left[\boldsymbol{\alpha}, \dot{\boldsymbol{\alpha}}\right] \mathrm{d}t \tag{2.20}$$

To elaborate further, the functional integral of Eqs. (2.17)-(2.19) is also known as Wiener path integral, which for a process $\boldsymbol{\alpha}$ can be generally written as [21]

$$\int_{\mathcal{C}\{\boldsymbol{\alpha}_i, t_i; \boldsymbol{\alpha}_f, t_f\}} \mathcal{F}[\boldsymbol{\alpha}(t)] \mathcal{G}[\boldsymbol{\alpha}(t)] \mathcal{D}[\boldsymbol{\alpha}(t)] \tag{2.21}$$

In Eq. (2.21) $\mathcal{G}[\boldsymbol{\alpha}(t)]$ is a functional distribution providing the probability of occurrence of some function within the infinitesimal vicinity of $\boldsymbol{\alpha}(t)$; $\mathcal{F}[\boldsymbol{\alpha}(t)]$ is an arbitrary functional of $\boldsymbol{\alpha}(t)$; and $\mathcal{D}[\boldsymbol{\alpha}(t)]$ is a functional measure generalizing the measure of Eq. (2.13). For the special case of a Wiener process, i.e, $\boldsymbol{\alpha} = \boldsymbol{W}$, the product $\mathcal{G}[\boldsymbol{\alpha}(t)]\mathcal{D}[\boldsymbol{\alpha}(t)]$, also referred to as Wiener measure (e.g., [21, 161, 192]) represents the probability density functional of $\boldsymbol{W}(t)$

given by

$$\mathcal{P}[\boldsymbol{W}(t)] = \mathcal{G}[\boldsymbol{W}(t)]\mathcal{D}[\boldsymbol{W}(t)] = \exp\left(-\int_{t_i}^{t_f} \frac{1}{2}\sum_{j=1}^{n} \dot{W}_j^2 \, \mathrm{d}t\right) \prod_{j=1}^{n}\prod_{t=t_i}^{t_f} \frac{\mathrm{d}W_j(t)}{\sqrt{2\pi \mathrm{d}t}} \tag{2.22}$$

The notation in Eq. (2.22) is somewhat misleading since, as mentioned earlier, the sample paths of the Wiener process are nowhere differentiable. Nevertheless, the general Wiener path integral of Eq. (2.21) can be construed as a shorthand notation for the continuous limit (i.e., $L \to \infty$) of an L-dimensional integral similar to the one of Eq. (2.16). In this regard, a Volterra approach for handling functionals can be employed, according to which $\mathcal{P}[\boldsymbol{W}(t)]$ can be represented as the limit, for $L \to \infty$, of a function of L variables. Note that although there are more mathematically elegant definitions of the Wiener path integral, based for instance on probabilistic measure theory (see also [21]), the Volterra approach appears to be a convenient tool for numerical implementation and approximation purposes. Further, for the general case where a process $\boldsymbol{\alpha}$ is expressed as an arbitrary function of the Wiener process $\boldsymbol{W}$, it is clear that an appropriate "change of variables" treatment is required for evaluating the probability density functional $\mathcal{P}[\boldsymbol{\alpha}(t)]$ (e.g., [21, 71]). For instance, if the relationship between $\boldsymbol{\alpha}$ and $\boldsymbol{W}$ takes the form of a stochastic differential equation such as in Eq. (2.6), the functional change of variables involves a stochastic integral, and thus, a discretization rule (also known as prescription) needs to be selected. Typical choices include the Itô (prepoint) and the Stratonovich (midpoint) discretization rules [67, 78]. Note that different discretization schemes lead to different Jacobian transformation matrices in the functional change of variables, yielding eventually different probabilities $\mathcal{P}[\boldsymbol{\alpha}(t)]$ in Eqs. (2.9) and (2.11) [21, 193]. However, within the context of path integration and under certain conditions such discretization rules are called equivalent classes of discretization and for $L \to \infty$ converge to identical final results for determining the joint transition PDF [21, 109, 110]. In the present thesis, without loss of generality, the Itô discretization rule is utilized.

2.3 Functional series expansion and most probable path approximation

The analytical evaluation of the Wiener path integral of Eq. (2.19) for determining the joint transition PDF of the process $\boldsymbol{\alpha}$ is, clearly, a rather challenging task. Although an analytical solution treatment may be feasible for relatively simple forms of the stochastic differential Eq. (2.7), approximate solution techniques are required for the general case. In this regard, an indicative approximate approach pertains to employing a perturbation expansion for the expression of Eq. (2.19) and approximating $p(\boldsymbol{\alpha}_f, t_f|\boldsymbol{\alpha}_i, t_i)$ by truncating the resulting series [75, 96]. An alternative rather popular in theoretical physics solution approach is adopted in this thesis. This relates to utilizing a functional Taylor-kind series expansion of the stochastic action $\mathcal{S}$ in Eq. (2.19). In particular, $\boldsymbol{\alpha}(t)$ is expressed as

$$\boldsymbol{\alpha}(t) = \boldsymbol{\alpha}_c(t) + \hat{\mathbf{A}}(t) \tag{2.23}$$

and the stochastic action $\mathcal{S}$ as

$$\mathcal{S}\left[\boldsymbol{\alpha}\right] = \mathcal{S}\left[\boldsymbol{\alpha}_c + \hat{\mathbf{A}}\right] = \mathcal{S}[\boldsymbol{\alpha}_c] + \delta\mathcal{S}\left[\boldsymbol{\alpha}_c, \hat{\mathbf{A}}\right] + \frac{1}{2!}\delta^2\mathcal{S}\left[\boldsymbol{\alpha}_c, \hat{\mathbf{A}}\right] + \dots \tag{2.24}$$

where $\boldsymbol{\alpha}_c(t)$ is the path associated with the maximum probability of occurrence $\mathcal{P}\left[\boldsymbol{\alpha}_c(t)\right]$ and $\hat{\mathbf{A}}(t)$ denotes the fluctuations around $\boldsymbol{\alpha}_c(t)$. It is worth noting that the above definition generalizes, loosely speaking, the PDF mode concept to the case of paths and probability density functionals. Thus, it is not surprising that $\boldsymbol{\alpha}_c(t)$ is referred to in the literature extensively as the most probable path. In Eq. (2.24) $\mathcal{S}\left[\boldsymbol{\alpha}, \dot{\boldsymbol{\alpha}}\right]$ is denoted as $\mathcal{S}\left[\boldsymbol{\alpha}\right]$ for simplicity, and $\delta\mathcal{S}\left[\boldsymbol{\alpha}_c, \hat{\mathbf{A}}\right]$ represents the functional differential (or variation) of $\mathcal{S}$ evaluated on $\boldsymbol{\alpha}_c$.

This takes the form

$$\delta\mathcal{S}\left[\boldsymbol{\alpha}_c, \hat{\mathbf{A}}\right] = \int_{t_i}^{t_f} \sum_{j=1}^{n} \left(\frac{\partial \mathcal{L}}{\partial \alpha_j}\bigg|_{\boldsymbol{\alpha}=\boldsymbol{\alpha}_c} \hat{A}_j(t) + \frac{\partial \mathcal{L}}{\partial \dot{\alpha}_j}\bigg|_{\boldsymbol{\alpha}=\boldsymbol{\alpha}_c} \frac{\mathrm{d}}{\mathrm{d}t}\hat{A}_j(t) \right) \mathrm{d}t \tag{2.25}$$

Further, since maximum probability $\mathcal{P}\left[\boldsymbol{\alpha}(t)\right]$ in Eq. (2.11) (see also Eq. (2.20)) corresponds to minimum $\mathcal{S}\left[\boldsymbol{\alpha}, \dot{\boldsymbol{\alpha}}\right]$, $\boldsymbol{\alpha}_c(t)$ is associated with an extremum of the functional $\mathcal{S}\left[\boldsymbol{\alpha}, \dot{\boldsymbol{\alpha}}\right]$ in Eq. (2.19); i.e., it is the solution of the variational problem

$$\textit{minimize } \mathcal{S}[\boldsymbol{\alpha}_c], \textit{ subject to } \boldsymbol{\alpha}_c \in \mathcal{C}\{\boldsymbol{\alpha}_i, t_i; \boldsymbol{\alpha}_f, t_f\} \tag{2.26}$$

In this context, calculus of variations dictates that the first variation of $\mathcal{S}\left[\boldsymbol{\alpha}, \dot{\boldsymbol{\alpha}}\right]$ vanishes for $\boldsymbol{\alpha}(t) = \boldsymbol{\alpha}_c(t)$ [56, 70], i.e.,

$$\delta\mathcal{S}\left[\boldsymbol{\alpha}_c, \hat{\mathbf{A}}\right] = 0 \tag{2.27}$$

Therefore, Eq. (2.24) becomes

$$\mathcal{S}\left[\boldsymbol{\alpha}\right] = \mathcal{S}[\boldsymbol{\alpha}_c] + \frac{1}{2!}\delta^2\mathcal{S}\left[\boldsymbol{\alpha}_c, \hat{\mathbf{A}}\right] + \dots \tag{2.28}$$

Next, combining Eq. (2.25) and the extremality condition of Eq. (2.27) yields [70] the system of Euler-Lagrange (EL) equations (e.g., [56])

$$\frac{\partial \mathcal{L}}{\partial \alpha_{c,j}} - \frac{\mathrm{d}}{\mathrm{d}t}\frac{\partial \mathcal{L}}{\partial \dot{\alpha}_{c,j}} = 0, \quad \text{for } j = 1, \dots, n \tag{2.29}$$

in conjunction with $2 \times n$ boundary conditions

$$\left.\begin{aligned} \alpha_{c,j}(t_i) &= \alpha_{i,j} \\ \alpha_{c,j}(t_f) &= \alpha_{f,j} \end{aligned}\right\} \quad \text{for } j = 1, \dots, n \tag{2.30}$$

where the most probable path is written as $\boldsymbol{\alpha}_c(t) = \left[\alpha_{c,j}(t)\right]_{n\times 1}$, and the boundary conditions (at initial and final time instants) are written as $\boldsymbol{\alpha}_i = \left[\alpha_{i,j}\right]_{n\times 1}$ and $\boldsymbol{\alpha}_f = \left[\alpha_{f,j}\right]_{n\times 1}$. The

system of Eqs. (2.29)-(2.30) represents a rather standard deterministic BVP, which can be solved analytically for relatively simple forms of the Lagrangian functional $\mathcal{L}\left[\boldsymbol{\alpha}, \dot{\boldsymbol{\alpha}}\right]$. For instance, a linear version of the governing stochastic differential Eq. (2.7) yields a Lagrangian functional of quadratic form, for which Eqs. (2.29)-(2.30) are amenable to an analytical solution treatment. Nevertheless, for the general case, the deterministic BVP of Eqs. (2.29)-(2.30) can be solved via standard numerical approaches (e.g., via a classical variational finite element solution methodology). Next, it is readily seen that obtaining the most probable path enables the approximation of the stochastic action $\mathcal{S}\left[\boldsymbol{\alpha}, \dot{\boldsymbol{\alpha}}\right]$ by retaining only the first term in Eq. (2.28) and collectively treating the rest of the terms in the expansion as a constant. In this regard, the series expansion of Eq. (2.28) takes the form

$$\mathcal{S}\left[\boldsymbol{\alpha}, \dot{\boldsymbol{\alpha}}\right] = \mathcal{S}\left[\boldsymbol{\alpha}_c, \dot{\boldsymbol{\alpha}}_c\right] + \log\left(C^{-1}\right) \tag{2.31}$$

where C is a constant, and thus, the transition PDF of Eq. (2.19) becomes

$$p(\boldsymbol{\alpha}_f, t_f | \boldsymbol{\alpha}_i, t_i) = C \ \exp\left(-\mathcal{S}\left[\boldsymbol{\alpha}_c, \dot{\boldsymbol{\alpha}}_c\right]\right) \tag{2.32}$$

Finally, the constant C can be evaluated by the normalization condition

$$\int_{-\infty}^{\infty} p(\boldsymbol{\alpha}_f, t_f | \boldsymbol{\alpha}_i, t_i) \mathrm{d}\boldsymbol{\alpha}_f = 1 \tag{2.33}$$

It is worth mentioning that functional series expansions of the form of Eq. (2.24) have been widely used in quantum mechanics for calculating quantum-mechanical probability amplitudes (e.g., [19, 161]). In this regard, depending on the number of terms retained in the series expansion various approximation schemes have been proposed, typically referred to as semiclassical or Wentzel-Kramers-Brillouin approximations (e.g., [21, 161]).

2.4 Nonlinear multi-degree-of-freedom systems subject to stochastic excitation

2.4.1 Gaussian white noise stochastic excitation

Consider an m-degree-of-freedom (m-DOF) nonlinear dynamical system with stochastic external excitation

$$\boldsymbol{M}\ddot{\boldsymbol{x}} + \boldsymbol{C}\dot{\boldsymbol{x}} + \boldsymbol{K}\boldsymbol{x} + \boldsymbol{g}(\boldsymbol{x}, \dot{\boldsymbol{x}}) = \boldsymbol{w}(t) \tag{2.34}$$

where $\boldsymbol{x}$ is the displacement vector process ($\boldsymbol{x} = [x_1 \dots x_m]^T$); $\boldsymbol{M}$, $\boldsymbol{C}$, $\boldsymbol{K}$ correspond to the $m \times m$ mass, damping and stiffness matrices, respectively; $\boldsymbol{g}(\boldsymbol{x}, \dot{\boldsymbol{x}})$ denotes an arbitrary nonlinear vector function; and $\boldsymbol{w}(t)$ is a white noise stochastic vector process with $\mathbb{E}[\boldsymbol{w}(t_l)] = \boldsymbol{0}$ and $\mathbb{E}[\boldsymbol{w}(t_l)\boldsymbol{w}^T(t_l - t_{l+1})] = \boldsymbol{S}_{\boldsymbol{w}}\delta(t_l - t_{l+1})$, where $\boldsymbol{S}_{\boldsymbol{w}} \in \mathbb{R}^{m\times m}$ is a real, symmetric, non-negative and non-singular deterministic parameter matrix, and t_l, t_{l+1} are two arbitrary time instants (see also [154]). Eq. (2.34) can be cast in a state variable formulation (e.g., [152]), and take the form of Eq. (2.7), where

$$\boldsymbol{\alpha} = \begin{bmatrix} \boldsymbol{x} \\ \dot{\boldsymbol{x}} \end{bmatrix} = \begin{bmatrix} \boldsymbol{\alpha}_1 \\ \boldsymbol{\alpha}_2 \end{bmatrix} \tag{2.35}$$

$$\boldsymbol{A}(\boldsymbol{\alpha}, t) = \begin{bmatrix} \boldsymbol{\alpha}_2 \\ \boldsymbol{M}^{-1}\left(-\boldsymbol{C}\boldsymbol{\alpha}_2 - \boldsymbol{K}\boldsymbol{\alpha}_1 - \boldsymbol{g}(\boldsymbol{\alpha}_1, \boldsymbol{\alpha}_2)\right) \end{bmatrix} = \begin{bmatrix} \boldsymbol{A}_1 \\ \boldsymbol{A}_2 \end{bmatrix} \tag{2.36}$$

and

$$\boldsymbol{B}(\boldsymbol{\alpha}, t) = \begin{bmatrix} \boldsymbol{0}_{m\times m} & \boldsymbol{0}_{m\times m} \\ \boldsymbol{0}_{m\times m} & \boldsymbol{M}^{-1}\sqrt{\boldsymbol{S}_{\boldsymbol{w}}} \end{bmatrix} \tag{2.37}$$

where the square root of matrix $\boldsymbol{S}_{\boldsymbol{w}}$ is given by $\sqrt{\boldsymbol{S}_{\boldsymbol{w}}}\sqrt{\boldsymbol{S}_{\boldsymbol{w}}}^T = \boldsymbol{S}_{\boldsymbol{w}}$. In this regard, the m-dimensional second-order SDE of Eq. (2.34) becomes a $2m$-dimensional first-order SDE for

the process $\boldsymbol{\alpha} = [\boldsymbol{x}, \dot{\boldsymbol{x}}]^T = [\boldsymbol{\alpha}_1, \boldsymbol{\alpha}_2]^T$.

Note, however, that the diffusion matrix $\boldsymbol{B}(\boldsymbol{\alpha}, t)$ (as well as $\widetilde{\boldsymbol{B}} = \boldsymbol{B}\boldsymbol{B}^T$) in Eq. (2.37) is singular, and thus, Eq. (2.17) cannot be used directly. In fact, the challenge of accounting for singular diffusion matrices in conjunction with path integral formulations has received considerable attention in the literature (see [26, 45, 48, 51, 83, 119, 123, 134, 144, 194]). The singularity of matrix $\boldsymbol{B}$ can be bypassed by expressing it as

$$\boldsymbol{B} = \lim_{\delta \to 0} \begin{bmatrix} \sqrt{\delta}\boldsymbol{I}_{m\times m} & \boldsymbol{0}_{m\times m} \\ \boldsymbol{0}_{m\times m} & \boldsymbol{M}^{-1}\sqrt{\boldsymbol{S}_{\boldsymbol{w}}} \end{bmatrix} \tag{2.38}$$

and thus,

$$\widetilde{\boldsymbol{B}} = \lim_{\delta \to 0} \begin{bmatrix} \delta\boldsymbol{I}_{m\times m} & \boldsymbol{0}_{m\times m} \\ \boldsymbol{0}_{m\times m} & \widetilde{\boldsymbol{B}}_{ns} \end{bmatrix} \tag{2.39}$$

where δ is an arbitrary number that goes to 0, $\boldsymbol{I}_{m\times m}$ denotes the $m \times m$ identity matrix and $\widetilde{\boldsymbol{B}}_{ns}$ is the non-singular part of $\widetilde{\boldsymbol{B}}$ given by

$$\widetilde{\boldsymbol{B}}_{ns} = \boldsymbol{M}^{-1}\sqrt{\boldsymbol{S}_{\boldsymbol{w}}}\left[\boldsymbol{M}^{-1}\sqrt{\boldsymbol{S}_{\boldsymbol{w}}}\right]^T = \boldsymbol{M}^{-1}\boldsymbol{S}_{\boldsymbol{w}}\left[\boldsymbol{M}^T\right]^{-1} \tag{2.40}$$

Therefore, Eqs. (2.12)-(2.13) can be readily utilized and the transition PDF of $\boldsymbol{\alpha}$ is written in the form of Eq. (2.17) as

$$p(\boldsymbol{\alpha}_f, t_f|\boldsymbol{\alpha}_i, t_i) = \int_{\mathcal{C}\{\boldsymbol{\alpha}_i, t_i; \boldsymbol{\alpha}_f, t_f\}} \exp\left(-\int_{t_i}^{t_f} \mathcal{L}\left[\boldsymbol{\alpha}, \dot{\boldsymbol{\alpha}}\right]\ \mathrm{d}t\right) \mathcal{D}[\boldsymbol{\alpha}_1(t)]\mathcal{D}[\boldsymbol{\alpha}_2(t)] \tag{2.41}$$

with

$$\mathcal{L}\left[\boldsymbol{\alpha}, \dot{\boldsymbol{\alpha}}\right] = \lim_{\delta \to 0} \frac{1}{2}\left[\frac{1}{\delta}\left[\dot{\boldsymbol{\alpha}}_1 - \boldsymbol{\alpha}_2\right]^T\left[\dot{\boldsymbol{\alpha}}_1 - \boldsymbol{\alpha}_2\right] + \left[\dot{\boldsymbol{\alpha}}_2 - \boldsymbol{A}_2\right]^T\left[\widetilde{\boldsymbol{B}}_{ns}\right]^{-1}\left[\dot{\boldsymbol{\alpha}}_2 - \boldsymbol{A}_2\right]\right] \tag{2.42}$$

and

$$\mathcal{D}[\boldsymbol{\alpha}_1(t)] = \lim_{\delta\to 0}\prod_{j=1}^{m}\prod_{t=t_i}^{t_f}\frac{\mathrm{d}\alpha_{1,j}(t)}{\sqrt{2\pi\delta\mathrm{d}t}} \tag{2.43}$$

and

$$\mathcal{D}[\boldsymbol{\alpha}_2(t)] = \prod_{j=1}^{m}\prod_{t=t_i}^{t_f}\frac{\mathrm{d}\alpha_{2,j}(t)}{\sqrt{2\pi\left(\det\left[\widetilde{\boldsymbol{B}}_{ns}\right]\right)^{1/m}\mathrm{d}t}} \tag{2.44}$$

where the expressions

$$\widetilde{\boldsymbol{B}}^{-1} = \lim_{\delta\to 0}\begin{bmatrix}\frac{1}{\delta}\boldsymbol{I}_{m\times m} & \boldsymbol{0}_{m\times m}\\ \boldsymbol{0}_{m\times m} & \widetilde{\boldsymbol{B}}_{ns}^{-1}\end{bmatrix} \tag{2.45}$$

with

$$\widetilde{\boldsymbol{B}}_{ns}^{-1} = \boldsymbol{M}^T{\boldsymbol{S}_{\boldsymbol{w}}}^{-1}\boldsymbol{M} \tag{2.46}$$

and $\det\widetilde{\boldsymbol{B}} = \lim_{\delta\to 0}\det\left[\delta\boldsymbol{I}\right]\det\left[\widetilde{\boldsymbol{B}}_{ns}\right] = \lim_{\delta\to 0}\delta^m\det\left[\widetilde{\boldsymbol{B}}_{ns}\right]$ have been used for expressing the inverse and the determinant of $\widetilde{\boldsymbol{B}}$, respectively. Further, by combining Eqs. (2.16) and (2.42), and by employing the delta function identity

$$\lim_{\delta\to 0}\frac{1}{\sqrt{2\pi\delta\epsilon}}\exp\left(-\frac{1}{2\delta}(\dot{\alpha}_{1,jl}-\alpha_{2,jl})^2\epsilon\right) = \frac{1}{\epsilon}\delta(\dot{\alpha}_{1,jl}-\alpha_{2,jl}) \tag{2.47}$$

for every $j\in\{1,\ldots,m\}$ and for every $l\in\{0,\ldots,L\}$, and by denoting the delta functionals as

$$\delta\left[\dot{\alpha}_{1,j}-\alpha_{2,j}\right] = \prod_{l=0}^{L}\delta(\dot{\alpha}_{1,jl}-\alpha_{2,jl}) \tag{2.48}$$

and

$$\delta\left[\dot{\boldsymbol{\alpha}}_1-\boldsymbol{\alpha}_2\right] = \prod_{j=1}^{m}\delta\left[\dot{\alpha}_{1,j}-\alpha_{2,j}\right] \tag{2.49}$$

the transition PDF of $\boldsymbol{\alpha}$ takes the form

$$p(\boldsymbol{\alpha}_f,t_f|\boldsymbol{\alpha}_i,t_i) = \int_{\mathcal{C}\{\boldsymbol{\alpha}_i,t_i;\boldsymbol{\alpha}_f,t_f\}}\exp\left(-\int_{t_i}^{t_f}\mathcal{L}\left[\boldsymbol{\alpha},\dot{\boldsymbol{\alpha}}\right]\,\mathrm{d}t\right)\delta[\dot{\boldsymbol{\alpha}}_1-\boldsymbol{\alpha}_2]\widetilde{\mathcal{D}}[\boldsymbol{\alpha}_1(t)]\widetilde{\mathcal{D}}[\boldsymbol{\alpha}_2(t)] \tag{2.50}$$

where

$$\widetilde{\mathcal{D}}[\boldsymbol{\alpha}_1(t)] = \prod_{j=1}^{m} \prod_{t=t_i}^{t_f} \frac{\mathrm{d}\alpha_{1,j}(t)}{\sqrt{2\pi \left(\det \left[\widetilde{\boldsymbol{B}}_{ns}\right]\right)^{1/m} (\mathrm{d}t)^3}} \tag{2.51}$$

and

$$\widetilde{\mathcal{D}}[\boldsymbol{\alpha}_2(t)] = \prod_{j=1}^{m} \prod_{t=t_i}^{t_f} \mathrm{d}\alpha_{2,j}(t) \tag{2.52}$$

For simplicity, in Eq. (2.50) the modified Lagrangian is again denoted by $\boldsymbol{\mathcal{L}}[\boldsymbol{\alpha}, \dot{\boldsymbol{\alpha}}]$ and is given as

$$\boldsymbol{\mathcal{L}}[\boldsymbol{\alpha}, \dot{\boldsymbol{\alpha}}] = \frac{1}{2} [\dot{\boldsymbol{\alpha}}_2 - \boldsymbol{A}_2]^T \left[\widetilde{\boldsymbol{B}}_{ns}\right]^{-1} [\dot{\boldsymbol{\alpha}}_2 - \boldsymbol{A}_2] \tag{2.53}$$

or by using Eq. (2.46) as

$$\begin{aligned} \boldsymbol{\mathcal{L}}[\boldsymbol{\alpha}, \dot{\boldsymbol{\alpha}}] = \frac{1}{2} [\boldsymbol{M}\dot{\boldsymbol{\alpha}}_2 + \boldsymbol{C}\boldsymbol{\alpha}_2 + \boldsymbol{K}\boldsymbol{\alpha}_1 + \boldsymbol{g}(\boldsymbol{\alpha}_1, \boldsymbol{\alpha}_2)]^T \boldsymbol{S_w}^{-1} \\ \times [\boldsymbol{M}\dot{\boldsymbol{\alpha}}_2 + \boldsymbol{C}\boldsymbol{\alpha}_2 + \boldsymbol{K}\boldsymbol{\alpha}_1 + \boldsymbol{g}(\boldsymbol{\alpha}_1, \boldsymbol{\alpha}_2)] \end{aligned} \tag{2.54}$$

Following integration over paths $\boldsymbol{\alpha}_2(t)$ by using the delta functional $\delta[\dot{\boldsymbol{\alpha}}_1 - \boldsymbol{\alpha}_2]$ and the functional measure $\widetilde{\mathcal{D}}[\boldsymbol{\alpha}_2(t)]$ [193], Eq. (2.50) becomes

$$\begin{aligned} &p(\boldsymbol{x}_f, \dot{\boldsymbol{x}}_f, t_f | \boldsymbol{x}_i, \dot{\boldsymbol{x}}_i, t_i) \\ &\quad = \int_{\mathcal{C}\{\boldsymbol{x}_i, \dot{\boldsymbol{x}}_i, t_i; \boldsymbol{x}_f, \dot{\boldsymbol{x}}_f, t_f\}} \exp\left(-\int_{t_i}^{t_f} \boldsymbol{\mathcal{L}}[\boldsymbol{x}, \dot{\boldsymbol{x}}, \ddot{\boldsymbol{x}}] \ \mathrm{d}t\right) \prod_{j=1}^{m} \delta(\dot{x}_j(t_i) - \dot{x}_{i,j}) \widetilde{\mathcal{D}}[\boldsymbol{x}(t)] \end{aligned} \tag{2.55}$$

or

$$\begin{aligned} &p(\boldsymbol{x}_f, \dot{\boldsymbol{x}}_f, t_f | \boldsymbol{x}_i, \dot{\boldsymbol{x}}_i, t_i) \\ &\quad = \int_{\mathcal{C}\{\boldsymbol{x}_i, \dot{\boldsymbol{x}}_i, t_i; \boldsymbol{x}_f, \dot{\boldsymbol{x}}_f, t_f\}} \exp\left(-\boldsymbol{\mathcal{S}}[\boldsymbol{x}, \dot{\boldsymbol{x}}, \ddot{\boldsymbol{x}}]\right) \prod_{j=1}^{m} \delta(\dot{x}_j(t_i) - \dot{x}_{i,j}) \widetilde{\mathcal{D}}[\boldsymbol{x}(t)] \end{aligned} \tag{2.56}$$

where the Lagrangian with respect to the process $\boldsymbol{x}$ is given by

$$\mathcal{L}\left[\boldsymbol{x}, \dot{\boldsymbol{x}}, \ddot{\boldsymbol{x}}\right] = \frac{1}{2}\left[\boldsymbol{M}\ddot{\boldsymbol{x}} + \boldsymbol{C}\dot{\boldsymbol{x}} + \boldsymbol{K}\boldsymbol{x} + \boldsymbol{g}(\boldsymbol{x}, \dot{\boldsymbol{x}})\right]^T \boldsymbol{S_w}^{-1} \times \left[\boldsymbol{M}\ddot{\boldsymbol{x}} + \boldsymbol{C}\dot{\boldsymbol{x}} + \boldsymbol{K}\boldsymbol{x} + \boldsymbol{g}(\boldsymbol{x}, \dot{\boldsymbol{x}})\right] \quad (2.57)$$

and the functional measure $\widetilde{\mathcal{D}}[\boldsymbol{x}(t)]$ is given by

$$\widetilde{\mathcal{D}}[\boldsymbol{x}(t)] = \prod_{j=1}^{m}\prod_{t=t_i}^{t_f} \frac{\mathrm{d}x_j(t)}{\sqrt{2\pi\left(\det\left[\widetilde{\boldsymbol{B}}_{ns}\right]\right)^{1/m}(\mathrm{d}t)^3}} \quad (2.58)$$

In passing, it is noted that $\prod_{j=1}^{m}\delta(\dot{x}_j(t_i) - \dot{x}_{i,j})$ in Eqs. (2.55)-(2.56) ensures that in a discrete approximation of the path integral (as in Eq. (2.16)) the first-order derivative of $\boldsymbol{x}$ for every degree of freedom j is equal to the initial conditions $\dot{\boldsymbol{x}}_i$.

Further, the extremality condition of Eq. (2.27) is written as

$$\delta\mathcal{S}\left[\boldsymbol{x}_c, \boldsymbol{X}\right] = 0 \quad (2.59)$$

where the first variation of the functional $\mathcal{S}\left[\boldsymbol{x}, \dot{\boldsymbol{x}}, \ddot{\boldsymbol{x}}\right]$ given by [70]

$$\delta\mathcal{S}\left[\boldsymbol{x}_c, \boldsymbol{X}\right] = \int_{t_i}^{t_f}\sum_{j=1}^{m}\left(\frac{\partial\mathcal{L}}{\partial x_j}\bigg|_{\boldsymbol{x}=\boldsymbol{x}_c} X_j + \frac{\partial\mathcal{L}}{\partial\dot{x}_j}\bigg|_{\boldsymbol{x}=\boldsymbol{x}_c}\frac{\mathrm{d}}{\mathrm{d}t}X_j + \frac{\partial\mathcal{L}}{\partial\ddot{x}_j}\bigg|_{\boldsymbol{x}=\boldsymbol{x}_c}\frac{\mathrm{d}^2}{\mathrm{d}t^2}X_j\right)\mathrm{d}t \quad (2.60)$$

yields the EL equations

$$\frac{\partial\mathcal{L}}{\partial x_{c,j}} - \frac{\mathrm{d}}{\mathrm{d}t}\frac{\partial\mathcal{L}}{\partial\dot{x}_{c,j}} + \frac{\mathrm{d}^2}{\mathrm{d}t^2}\frac{\partial\mathcal{L}}{\partial\ddot{x}_{c,j}} = 0, \quad \text{for } j = 1, \ldots, m \quad (2.61)$$

in conjunction with $4 \times m$ boundary conditions

$$\left.\begin{aligned} x_{c,j}(t_i) &= x_{i,j} \\ x_{c,j}(t_f) &= x_{f,j} \\ \dot{x}_{c,j}(t_i) &= \dot{x}_{i,j} \\ \dot{x}_{c,j}(t_f) &= \dot{x}_{f,j} \end{aligned}\right\} \quad \text{for } j = 1, \ldots, m \tag{2.62}$$

where the most probable path is written as $\boldsymbol{x}_c(t) = [x_{c,j}(t)]_{m\times 1}$, $\boldsymbol{X}(t)$ denotes the fluctuations around $\boldsymbol{x}_c(t)$, and the boundary conditions (at initial and final time instants) are written as $\boldsymbol{x}_i = [x_{i,j}]_{m\times 1}$, $\boldsymbol{x}_f = [x_{f,j}]_{m\times 1}$, $\dot{\boldsymbol{x}}_i = [\dot{x}_{i,j}]_{m\times 1}$, and $\dot{\boldsymbol{x}}_f = [\dot{x}_{f,j}]_{m\times 1}$. Finally, the most probable path approximation of the PDF given by Eq. (2.32) becomes

$$p(\boldsymbol{x}_f, \dot{\boldsymbol{x}}_f, t_f | \boldsymbol{x}_i, \dot{\boldsymbol{x}}_i, t_i) = C \ \exp\left(-\mathcal{S}\left[\boldsymbol{x}_c, \dot{\boldsymbol{x}}_c, \ddot{\boldsymbol{x}}_c\right]\right) \tag{2.63}$$

where

$$\mathcal{S}\left[\boldsymbol{x}, \dot{\boldsymbol{x}}, \ddot{\boldsymbol{x}}\right] = \int_{t_i}^{t_f} \mathcal{L}\left[\boldsymbol{x}, \dot{\boldsymbol{x}}, \ddot{\boldsymbol{x}}\right] \mathrm{d}t \tag{2.64}$$

and C is given by the normalization condition of Eq. (2.33) which for the system of Eq. (2.34) is written as

$$\int_{-\infty}^{\infty} p(\boldsymbol{x}_f, \dot{\boldsymbol{x}}_f, t_f | \boldsymbol{x}_i, \dot{\boldsymbol{x}}_i, t_i) \mathrm{d}\boldsymbol{x}_f \mathrm{d}\dot{\boldsymbol{x}}_f = 1 \tag{2.65}$$

2.4.2 Non-white, non-Gaussian, and non-stationary stochastic excitation

Consider the m-DOF nonlinear dynamical system of Eq. (2.34) subject to a non-white and non-Gaussian, in general, excitation stochastic process. In this regard, the equation governing the dynamics of the system is given as

$$\boldsymbol{M}\ddot{\boldsymbol{x}} + \boldsymbol{C}\dot{\boldsymbol{x}} + \boldsymbol{K}\boldsymbol{x} + \boldsymbol{g}(\boldsymbol{x}, \dot{\boldsymbol{x}}) = \boldsymbol{f}(t) \tag{2.66}$$

$\boldsymbol{f}(t)$ is a non-stationary, non-white, and non-Gaussian vector process expressed as [112, 154]

$$\boldsymbol{f}(t) = \boldsymbol{\Gamma}(t)\boldsymbol{\xi}(t) \tag{2.67}$$

where $\boldsymbol{\Gamma}(t)$ is a diagonal matrix of deterministic time-modulating functions $\gamma_j(t)$, $j \in \{1, \dots, m\}$, and $\boldsymbol{\xi}(t)$ is given as the response of the nonlinear "filter" equation (e.g., [154])

$$\boldsymbol{P}\ddot{\boldsymbol{\xi}} + \boldsymbol{Q}\dot{\boldsymbol{\xi}} + \boldsymbol{R}\boldsymbol{\xi} + \boldsymbol{s}(\boldsymbol{\xi}, \dot{\boldsymbol{\xi}}) = \boldsymbol{w}(t) \tag{2.68}$$

where $\boldsymbol{P}$, $\boldsymbol{Q}$, $\boldsymbol{R}$ denote coefficient matrices; $\boldsymbol{s}(\boldsymbol{\xi}, \dot{\boldsymbol{\xi}})$ is an arbitrary nonlinear vector function; and $\boldsymbol{w}(t) = [w_1, \dots, w_m]^T$ is a white noise stochastic vector process with $\mathbb{E}[\boldsymbol{w}(t_l)] = \boldsymbol{0}$ and $\mathbb{E}[\boldsymbol{w}(t_l)\boldsymbol{w}^T(t_l - t_{l+1})] = \boldsymbol{S}_{\boldsymbol{w}}\delta(t_l - t_{l+1})$, where $\boldsymbol{S}_{\boldsymbol{w}} \in \mathbb{R}^{m\times m}$ is a deterministic parameter matrix and t_l, t_{l+1} are two arbitrary time instants (see also [154]). Note that various non-white excitation processes, commonly utilized in engineering dynamics (e.g., the Kanai-Tajimi excitation process in earthquake engineering [93, 183]), can be described by the filter Eq. (2.68). In fact, Eq. (2.68) can be construed as the time-domain representation of such excitation processes that are typically described in the frequency domain via power spectra [112]. In addition, even in cases where the excitation power spectrum cannot be represented in the time domain as the response of a filter, it has been shown [20, 174] that a filter approximation of the form of Eq. (2.68) exhibits, in general, satisfactory accuracy for practical applications. Further, Eq. (2.68) can also account for non-Gaussian excitation modeling via the nonlinear function $\boldsymbol{s}(\boldsymbol{\xi}, \dot{\boldsymbol{\xi}})$.

Next, differentiating Eq. (2.66) and substituting into Eqs. (2.67)-(2.68) yields the 4^{th}-order SDE

$$\boldsymbol{\Lambda}_4\boldsymbol{x}^{(4)} + \boldsymbol{\Lambda}_3\boldsymbol{x}^{(3)} + \boldsymbol{\Lambda}_2\ddot{\boldsymbol{x}} + \boldsymbol{\Lambda}_1\dot{\boldsymbol{x}} + \boldsymbol{\Lambda}_0\boldsymbol{x} + \boldsymbol{\kappa}(\boldsymbol{x}, \dot{\boldsymbol{x}}, \ddot{\boldsymbol{x}}, \boldsymbol{x}^{(3)}) = \boldsymbol{w}(t) \tag{2.69}$$

where

$$\left.\begin{aligned}
\boldsymbol{\Lambda}_4 &= \boldsymbol{P}\boldsymbol{\Gamma}^{-1}\boldsymbol{M} \\
\boldsymbol{\Lambda}_3 &= \boldsymbol{P}\boldsymbol{\Gamma}^{-1}\left[-2\dot{\boldsymbol{\Gamma}}\boldsymbol{\Gamma}^{-1}\boldsymbol{M}+\boldsymbol{C}\right]+\boldsymbol{Q}\boldsymbol{\Gamma}^{-1}\boldsymbol{M} \\
\boldsymbol{\Lambda}_2 &= \boldsymbol{P}\boldsymbol{\Gamma}^{-1}\left[\left(2\dot{\boldsymbol{\Gamma}}\boldsymbol{\Gamma}^{-1}\dot{\boldsymbol{\Gamma}}\boldsymbol{\Gamma}^{-1}-\ddot{\boldsymbol{\Gamma}}\boldsymbol{\Gamma}^{-1}\right)\boldsymbol{M}-2\dot{\boldsymbol{\Gamma}}\boldsymbol{\Gamma}^{-1}\boldsymbol{C}+\boldsymbol{K}\right] \\
&\quad +\boldsymbol{Q}\boldsymbol{\Gamma}^{-1}\left(-\dot{\boldsymbol{\Gamma}}\boldsymbol{\Gamma}^{-1}\boldsymbol{M}+\boldsymbol{C}\right)+\boldsymbol{R}\boldsymbol{\Gamma}^{-1}\boldsymbol{M} \\
\boldsymbol{\Lambda}_1 &= \boldsymbol{P}\boldsymbol{\Gamma}^{-1}\left[\left(2\dot{\boldsymbol{\Gamma}}\boldsymbol{\Gamma}^{-1}\dot{\boldsymbol{\Gamma}}\boldsymbol{\Gamma}^{-1}-\ddot{\boldsymbol{\Gamma}}\boldsymbol{\Gamma}^{-1}\right)\boldsymbol{C}-2\dot{\boldsymbol{\Gamma}}\boldsymbol{\Gamma}^{-1}\boldsymbol{K}\right] \\
&\quad +\boldsymbol{Q}\boldsymbol{\Gamma}^{-1}\left(-\dot{\boldsymbol{\Gamma}}\boldsymbol{\Gamma}^{-1}\boldsymbol{C}+\boldsymbol{K}\right)+\boldsymbol{R}\boldsymbol{\Gamma}^{-1}\boldsymbol{C} \\
\boldsymbol{\Lambda}_0 &= \boldsymbol{P}\boldsymbol{\Gamma}^{-1}\left(2\dot{\boldsymbol{\Gamma}}\boldsymbol{\Gamma}^{-1}\dot{\boldsymbol{\Gamma}}\boldsymbol{\Gamma}^{-1}-\ddot{\boldsymbol{\Gamma}}\boldsymbol{\Gamma}^{-1}\right)\boldsymbol{K} \\
&\quad -\boldsymbol{Q}\boldsymbol{\Gamma}^{-1}\dot{\boldsymbol{\Gamma}}\boldsymbol{\Gamma}^{-1}\boldsymbol{K}+\boldsymbol{R}\boldsymbol{\Gamma}^{-1}\boldsymbol{K}
\end{aligned}\right\} \tag{2.70}$$

and

$$\begin{aligned}
\boldsymbol{\kappa}(\boldsymbol{x},\dot{\boldsymbol{x}},\ddot{\boldsymbol{x}},\boldsymbol{x}^{(3)}) &= \boldsymbol{P}\boldsymbol{\Gamma}^{-1}\ddot{\boldsymbol{g}}(\boldsymbol{x},\dot{\boldsymbol{x}}) \\
&\quad +\left(-2\boldsymbol{P}\boldsymbol{\Gamma}^{-1}\dot{\boldsymbol{\Gamma}}\boldsymbol{\Gamma}^{-1}+\boldsymbol{Q}\boldsymbol{\Gamma}^{-1}\right)\dot{\boldsymbol{g}}(\boldsymbol{x},\dot{\boldsymbol{x}}) \\
&\quad +\left[\boldsymbol{P}\boldsymbol{\Gamma}^{-1}\left(2\dot{\boldsymbol{\Gamma}}\boldsymbol{\Gamma}^{-1}\dot{\boldsymbol{\Gamma}}\boldsymbol{\Gamma}^{-1}-\ddot{\boldsymbol{\Gamma}}\boldsymbol{\Gamma}^{-1}\right)\right. \\
&\quad \left.-\boldsymbol{Q}\boldsymbol{\Gamma}^{-1}\dot{\boldsymbol{\Gamma}}\boldsymbol{\Gamma}^{-1}+\boldsymbol{R}\boldsymbol{\Gamma}^{-1}\right]\boldsymbol{g}(\boldsymbol{x},\dot{\boldsymbol{x}})+\boldsymbol{s}(\boldsymbol{x},\dot{\boldsymbol{x}},\ddot{\boldsymbol{x}},\boldsymbol{x}^{(3)})
\end{aligned} \tag{2.71}$$

Notice that the differentiation of Eq. (2.66) yields time derivatives of order higher than 2 in Eqs. (2.69)-(2.71); i.e., $\boldsymbol{x}^{(3)}$ and $\boldsymbol{x}^{(4)}$ denoting the 3^{rd}- and 4^{th}-order derivatives of of $\boldsymbol{x}(t)$, respectively. As in Section 2.4.1, Eq. (2.69) can be cast in a state variable formulation (e.g., [152]), and take the form of Eq. (2.7), where

$$\boldsymbol{\alpha}=\begin{bmatrix}\boldsymbol{x}\\ \dot{\boldsymbol{x}}\\ \ddot{\boldsymbol{x}}\\ \boldsymbol{x}^{(3)}\end{bmatrix}=\begin{bmatrix}\boldsymbol{\alpha}_1\\ \boldsymbol{\alpha}_2\\ \boldsymbol{\alpha}_3\\ \boldsymbol{\alpha}_4\end{bmatrix} \tag{2.72}$$

$$\boldsymbol{A}(\boldsymbol{\alpha},t)=\begin{bmatrix}\boldsymbol{\alpha}_2\\ \boldsymbol{\alpha}_3\\ \boldsymbol{\alpha}_4\\ \boldsymbol{\Lambda}_4^{-1}\left(-\boldsymbol{\Lambda}_3\boldsymbol{\alpha}_4-\boldsymbol{\Lambda}_2\boldsymbol{\alpha}_3-\boldsymbol{\Lambda}_1\boldsymbol{\alpha}_2-\boldsymbol{\Lambda}_0\boldsymbol{\alpha}_1-\boldsymbol{\kappa}(\boldsymbol{\alpha}_1,\boldsymbol{\alpha}_2,\boldsymbol{\alpha}_3,\boldsymbol{\alpha}_4)\right)\end{bmatrix}=\begin{bmatrix}\boldsymbol{A}_1\\ \boldsymbol{A}_2\\ \boldsymbol{A}_3\\ \boldsymbol{A}_4\end{bmatrix} \tag{2.73}$$

and

$$\boldsymbol{B}(\boldsymbol{\alpha},t)=\begin{bmatrix}\boldsymbol{0}_{3m\times 3m} & \boldsymbol{0}_{3m\times m}\\ \boldsymbol{0}_{m\times 3m} & \boldsymbol{\Lambda}_4^{-1}\sqrt{\boldsymbol{S_w}}\end{bmatrix} \tag{2.74}$$

Therefore, the m-dimensional fourth-order SDE of Eq. (2.69) becomes a $4m$-dimensional first-order SDE for the process $\boldsymbol{\alpha}=[\boldsymbol{x},\dot{\boldsymbol{x}},\ddot{\boldsymbol{x}},\boldsymbol{x}^{(3)}]^T=[\boldsymbol{\alpha}_1,\boldsymbol{\alpha}_2,\boldsymbol{\alpha}_3,\boldsymbol{\alpha}_4]^T$.

As in Section 2.4.1 the diffusion matrix $\boldsymbol{B}(\boldsymbol{\alpha},t)$ (as well as $\widetilde{\boldsymbol{B}}(\boldsymbol{\alpha},t)=\boldsymbol{B}(\boldsymbol{\alpha},t)\boldsymbol{B}^T(\boldsymbol{\alpha},t)$) in Eq. (2.74) is singular, and thus, the singularity is bypassed by employing delta-functionals in the path integral formulation, which enforce the compatibility equations ($\dot{\boldsymbol{\alpha}}_1=\boldsymbol{\alpha}_2;\dot{\boldsymbol{\alpha}}_2=\boldsymbol{\alpha}_3;\dot{\boldsymbol{\alpha}}_3=\boldsymbol{\alpha}_4$). In this respect, the transition PDF of $\boldsymbol{\alpha}$ can be written in the form of Eq. (2.17) with

$$\mathcal{L}\left[\boldsymbol{\alpha},\dot{\boldsymbol{\alpha}}\right]=\frac{1}{2}\left[\dot{\boldsymbol{\alpha}}_4-\boldsymbol{A}_4\right]^T\left[\widetilde{\boldsymbol{B}}_{ns}\right]^{-1}\left[\dot{\boldsymbol{\alpha}}_4-\boldsymbol{A}_4\right] \tag{2.75}$$

where $\widetilde{\boldsymbol{B}}_{ns}$ is the non-singular part of $\widetilde{\boldsymbol{B}}$ given by

$$\widetilde{\boldsymbol{B}}_{ns}=\boldsymbol{\Lambda}_4^{-1}\sqrt{\boldsymbol{S_w}}\left[\boldsymbol{\Lambda}_4^{-1}\sqrt{\boldsymbol{S_w}}\right]^T=\boldsymbol{\Lambda}_4^{-1}\boldsymbol{S_w}\left[\boldsymbol{\Lambda}_4^T\right]^{-1} \tag{2.76}$$

Eq. (2.75) can be simplified as

$$\begin{aligned}\mathcal{L}\left[\boldsymbol{\alpha},\dot{\boldsymbol{\alpha}}\right]=\frac{1}{2}&\left[\boldsymbol{\Lambda}_4\dot{\boldsymbol{\alpha}}_4+\boldsymbol{\Lambda}_3\boldsymbol{\alpha}_4+\boldsymbol{\Lambda}_2\boldsymbol{\alpha}_3+\boldsymbol{\Lambda}_1\boldsymbol{\alpha}_2+\boldsymbol{\Lambda}_0\boldsymbol{\alpha}_1+\boldsymbol{\kappa}(\boldsymbol{\alpha}_1,\boldsymbol{\alpha}_2,\boldsymbol{\alpha}_3,\boldsymbol{\alpha}_4)\right]^T\boldsymbol{S_w}^{-1}\\ &\times\left[\boldsymbol{\Lambda}_4\dot{\boldsymbol{\alpha}}_4+\boldsymbol{\Lambda}_3\boldsymbol{\alpha}_4+\boldsymbol{\Lambda}_2\boldsymbol{\alpha}_3+\boldsymbol{\Lambda}_1\boldsymbol{\alpha}_2+\boldsymbol{\Lambda}_0\boldsymbol{\alpha}_1+\boldsymbol{\kappa}(\boldsymbol{\alpha}_1,\boldsymbol{\alpha}_2,\boldsymbol{\alpha}_3,\boldsymbol{\alpha}_4)\right]\end{aligned} \tag{2.77}$$

Following integration over paths $\boldsymbol{\alpha}_2(t)$,$\boldsymbol{\alpha}_3(t)$, and $\boldsymbol{\alpha}_4(t)$ by using the delta functionals [193],

the transition PDF of $\boldsymbol{\alpha}$ is given by Eq. (2.56), which for the case of non-white and non-Gaussian excitation is written as

$$\begin{aligned} p\left(\boldsymbol{x}_f, \dot{\boldsymbol{x}}_f, \ddot{\boldsymbol{x}}_f, \boldsymbol{x}_f^{(3)}, t_f | \boldsymbol{x}_i, \dot{\boldsymbol{x}}_i, \ddot{\boldsymbol{x}}_i, \boldsymbol{x}_i^{(3)}, t_i\right) \\ = \int_{\mathcal{C}\{\boldsymbol{x}_i, \dot{\boldsymbol{x}}_i, \ddot{\boldsymbol{x}}_i, \boldsymbol{x}_i^{(3)}, t_i; \boldsymbol{x}_f, \dot{\boldsymbol{x}}_f, \ddot{\boldsymbol{x}}_f, \boldsymbol{x}_f^{(3)}, t_f\}} \exp\left(-\mathcal{S}\left[\boldsymbol{x}, \dot{\boldsymbol{x}}, \ddot{\boldsymbol{x}}, \boldsymbol{x}^{(3)}, \boldsymbol{x}^{(4)}\right]\right) \\ \times \prod_{j=1}^{m} \delta(\dot{x}_j(t_i) - \dot{x}_{i,j}) \prod_{j=1}^{m} \delta(\ddot{x}_j(t_i) - \ddot{x}_{i,j}) \prod_{j=1}^{m} \delta(x_j^{(3)}(t_i) - x_{i,j}^{(3)}) \widetilde{\mathcal{D}}[\boldsymbol{x}(t)] \end{aligned} \tag{2.78}$$

where

$$\mathcal{S}\left[\boldsymbol{x}, \dot{\boldsymbol{x}}, \ddot{\boldsymbol{x}}, \boldsymbol{x}^{(3)}, \boldsymbol{x}^{(4)}\right] = \int_{t_i}^{t_f} \mathcal{L}\left[\boldsymbol{x}, \dot{\boldsymbol{x}}, \ddot{\boldsymbol{x}}, \boldsymbol{x}^{(3)}, \boldsymbol{x}^{(4)}\right] \mathrm{d}t \tag{2.79}$$

the Lagrangian with respect to the process $\boldsymbol{x}$ is given by

$$\begin{aligned} \mathcal{L}\left[\boldsymbol{x}, \dot{\boldsymbol{x}}, \ddot{\boldsymbol{x}}, \boldsymbol{x}^{(3)}, \boldsymbol{x}^{(4)}\right] \\ = \frac{1}{2}\left[\boldsymbol{\Lambda}_4 \boldsymbol{x}^{(4)} + \boldsymbol{\Lambda}_3 \boldsymbol{x}^{(3)} + \boldsymbol{\Lambda}_2 \ddot{\boldsymbol{x}} + \boldsymbol{\Lambda}_1 \dot{\boldsymbol{x}} + \boldsymbol{\Lambda}_0 \boldsymbol{x} + \boldsymbol{\kappa}(\boldsymbol{x}, \dot{\boldsymbol{x}}, \ddot{\boldsymbol{x}}, \boldsymbol{x}^{(3)})\right]^T \boldsymbol{S_w}^{-1} \\ \times \left[\boldsymbol{\Lambda}_4 \boldsymbol{x}^{(4)} + \boldsymbol{\Lambda}_3 \boldsymbol{x}^{(3)} + \boldsymbol{\Lambda}_2 \ddot{\boldsymbol{x}} + \boldsymbol{\Lambda}_1 \dot{\boldsymbol{x}} + \boldsymbol{\Lambda}_0 \boldsymbol{x} + \boldsymbol{\kappa}(\boldsymbol{x}, \dot{\boldsymbol{x}}, \ddot{\boldsymbol{x}}, \boldsymbol{x}^{(3)})\right] \end{aligned} \tag{2.80}$$

and

$$\widetilde{\mathcal{D}}[\boldsymbol{x}(t)] = \prod_{j=1}^{m} \prod_{t=t_i}^{t_f} \frac{\mathrm{d}x_j(t)}{\sqrt{2\pi \left(\det\left[\widetilde{\boldsymbol{B}}_{ns}\right]\right)^{1/m} (\mathrm{d}t)^7}} \tag{2.81}$$

Further, the extremality condition of Eq. (2.27) yields the EL equations

$$\frac{\partial \mathcal{L}}{\partial x_{c,j}} - \frac{\mathrm{d}}{\mathrm{d}t}\frac{\partial \mathcal{L}}{\partial \dot{x}_{c,j}} + \frac{\mathrm{d}^2}{\mathrm{d}t^2}\frac{\partial \mathcal{L}}{\partial \ddot{x}_{c,j}} - \frac{\mathrm{d}^3}{\mathrm{d}t^3}\frac{\partial \mathcal{L}}{\partial x_{c,j}^{(3)}} + \frac{\mathrm{d}^4}{\mathrm{d}t^4}\frac{\partial \mathcal{L}}{\partial x_{c,j}^{(4)}} = 0, \quad \text{for } j = 1, \ldots, m \tag{2.82}$$

together with $8 \times m$ boundary conditions

$$\left.\begin{aligned} x_{c,j}(t_i) &= x_{i,j} \\ \dot{x}_{c,j}(t_i) &= \dot{x}_{i,j} \\ \ddot{x}_{c,j}(t_i) &= \ddot{x}_{i,j} \\ x^{(3)}_{c,j}(t_i) &= x^{(3)}_{i,j} \\ x_{c,j}(t_f) &= x_{f,j} \\ \dot{x}_{c,j}(t_f) &= \dot{x}_{f,j} \\ \ddot{x}_{c,j}(t_f) &= \ddot{x}_{f,j} \\ x^{(3)}_{c,j}(t_f) &= x^{(3)}_{f,j} \end{aligned}\right\} \quad \text{for } j = 1, \ldots, m \tag{2.83}$$

Next, solving the BVP of Eqs. (2.82) and (2.83) yields the most probable path $\boldsymbol{x}_c(t)$ (m-dimensional), and the transition PDF from the initial state $\{\boldsymbol{x}_i, \dot{\boldsymbol{x}}_i, \ddot{\boldsymbol{x}}_i, \boldsymbol{x}^{(3)}_i, t_i\}$ to the final state $\{\boldsymbol{x}_f, \dot{\boldsymbol{x}}_f, \ddot{\boldsymbol{x}}_f, \boldsymbol{x}^{(3)}_f, t_f\}$ is determined as

$$p\left(\boldsymbol{x}_f, \dot{\boldsymbol{x}}_f, \ddot{\boldsymbol{x}}_f, \boldsymbol{x}^{(3)}_f, t_f | \boldsymbol{x}_i, \dot{\boldsymbol{x}}_i, \ddot{\boldsymbol{x}}_i, \boldsymbol{x}^{(3)}_i, t_i\right) = C \exp\left(-\mathcal{S}\left[\boldsymbol{x}_c, \dot{\boldsymbol{x}}_c, \ddot{\boldsymbol{x}}_c, \boldsymbol{x}^{(3)}_c, \boldsymbol{x}^{(4)}_c\right]\right) \tag{2.84}$$

where the normalization constant C is evaluated based on the condition

$$\int_{-\infty}^{\infty} \cdots \int_{-\infty}^{\infty} p\left(\boldsymbol{x}_f, \dot{\boldsymbol{x}}_f, \ddot{\boldsymbol{x}}_f, \boldsymbol{x}^{(3)}_f, t_f | \boldsymbol{x}_i, \dot{\boldsymbol{x}}_i, \ddot{\boldsymbol{x}}_i, \boldsymbol{x}^{(3)}_i, t_i\right) \mathrm{d}\boldsymbol{x}_f \ldots \mathrm{d}\boldsymbol{x}^{(3)}_f = 1 \tag{2.85}$$

2.4.3 Numerical implementation aspects

Although the BVP of Eqs. (2.61)-(2.62) is amenable to a closed-form analytical solution for a linear dynamical system, i.e., $\boldsymbol{g}(\boldsymbol{x}, \dot{\boldsymbol{x}}) = \boldsymbol{0}$, unfortunately this is not the case, in general, for nonlinear systems. Similarly, for systems subject to non-stationary, non-white and non-Gaussian excitation processes, analytical solutions to the BVP of Eqs. (2.82)-(2.83) can only be obtained for cases when $\boldsymbol{\kappa}(\boldsymbol{x}, \dot{\boldsymbol{x}}, \ddot{\boldsymbol{x}}, \boldsymbol{x}^{(3)})$ given by Eq. (2.71) is zero. There-

fore, a numerical solution scheme needs to be implemented. In this regard, without loss of generality and considering fixed initial conditions, the only variables describing the PDF $p(\boldsymbol{x}_f, \dot{\boldsymbol{x}}_f, t_f|\boldsymbol{x}_i, \dot{\boldsymbol{x}}_i, t_i)$ at a time instant t_f are $\boldsymbol{x}_f$ and $\dot{\boldsymbol{x}}_f$ (or $\boldsymbol{x}_f$, $\dot{\boldsymbol{x}}_f$, $\ddot{\boldsymbol{x}}_f$, and $\boldsymbol{x}_f^{(3)}$ for describing $p(\boldsymbol{x}_f, \dot{\boldsymbol{x}}_f, \ddot{\boldsymbol{x}}_f, \boldsymbol{x}_f^{(3)}, t_f|\boldsymbol{x}_i, \dot{\boldsymbol{x}}_i, \ddot{\boldsymbol{x}}_i, \boldsymbol{x}_i^{(3)}, t_i)$ for the case of non-stationary, non-white and non-Gaussian excitation processes). Next, adopting a brute force numerical solution approach, for each time instant t_f an effective domain of values is considered for the joint response PDF and following the discretization of the effective domain using N_s points in each dimension, the joint response PDF values corresponding to the points of the mesh are obtained by solving the BVP of Eqs. (2.61)-(2.62) (or of Eqs. (2.82)-(2.83)). Specifically, for a given t_f and for an m-DOF system subject to Gaussian white noise excitation the resulting number of BVPs to be solved is $N_{bf} = N_s^{2m}$, where $2m$ is the number of stochastic dimensions (m displacements and m velocities). Accordingly, for an m-DOF system subject to non-stationary, non-white, and non-Gaussian excitation with Eqs. (2.66)-(2.68) governing its dynamics, $N_{bf} = N_s^{4m}$ BVPs are solved, where $4m$ is the number of stochastic dimensions. Further, in cases where the determination of the complete time-dependent non-stationary response PDF is of interest, the procedure should be applied for each and every time instant. Specifically, employing a brute-force discretization of the time domain (temporal dimension) into N_t points, the required number of BVPs to be solved becomes $N_{bf} = N_t N_s^{2m}$ and $N_{bf} = N_t N_s^{4m}$ for m-DOF systems subject to white and non-white noise excitation processes, respectively. Clearly, this demonstrates the high computational cost related to a brute force solution scheme implementation, especially for high-dimensional systems.

To address the above computational limitations, Kougioumtzoglou *et al.* [104] employed a polynomial expansion for the joint response PDF at specific time instants (i.e., $N_t = 1$); thus, yielding the required number of PDF measurements equal to the number of the expansion coefficients. Further, it was shown that the computational cost follows a power-law function of the form $\sim (2m)^{l_s}/l_s!$ (where l_s is the degree of the polynomial), which can be orders of magnitude smaller than $N_{bf} = N_s^{2m}$. Indicatively, the joint response PDF of a 10-DOF

nonlinear dynamical system can be obtained with only 10,626 measurements by utilizing the polynomial approximation, whereas a brute force PDF domain discretization scheme would require 30^{20} measurements (for $N_s = 30$). However, even with the enhancement in computational efficiency proposed in [104], the related computational cost as a power-law function of the number of stochastic dimensions still restricts the applicability of the methodology to relatively low-dimensional systems. Further, the enhancement in [104] relates to determining the joint response PDF at a specific fixed final time instant t_f. In other words, in cases where the determination of the complete time-dependent non-stationary response PDF is of interest, the procedure should be applied for each and every time instant. Indicatively, for the determination of the joint response PDF of a 10-DOF system a brute-force discretization of the time domain (temporal dimension) into $N_t = 1{,}000$ points, for instance, would still require 3.2×10^6 PDF measurements. Nevertheless, in Chapter 4, motivated by the aforementioned challenge, the computational efficiency of the WPI is further increased by resorting to expansions based on Kronecker products of basis matrices (Section 4.2.1) and on positive definite functions (Section 4.2.2). In addition, further enhancement in the computational efficiency of the WPI technique is achieved by employing sparse representations for the response PDF in conjunction with appropriate optimization algorithms.

Chapter 3

Extension of the Wiener path integral technique to account for excitations modeled via fractional-order filters

3.1 Introduction

Classical continuum mechanics theories have been traditionally used in engineering dynamics for modeling the governing equations of motion of the oscillator under consideration. Nevertheless, the need for more accurate media behavior modeling has led recently to advanced mathematical tools such as fractional calculus (e.g., [139, 155, 156]). Besides the fact that fractional calculus can be construed as a generalization of classical calculus (and thus, provides with enhanced modeling flexibility), it has been successfully employed in theoretical and applied mechanics for developing non-local continuum mechanics theories (e.g., [40, 184]), as well as for viscoelastic material modeling. Indeed, experimental viscoelastic response data obtained via creep and relaxation tests agree extremely well with such kind of modeling (e.g., [39]). Indicative applications in structural engineering, where theoretical developments are in agreement with experimental data, include modeling of viscoelastic

dampers used for vibration control, or for seismic isolation purposes (e.g., [99, 111]).

From a mathematics perspective, the equation of motion typically takes the form of a fractional differential equation to be solved for the oscillator response. In many cases, the above modeling is also coupled with complex nonlinearities and hysteresis; thus, rendering even the deterministic solution of such equations an open issue and an active research topic. Clearly, solving the stochastic counterparts of these equations becomes significantly more challenging. Therefore, there is a need for developing efficient solution schemes for determining the stochastic response and assessing the reliability of dynamic systems endowed with fractional derivative terms. Indicative solution techniques for linear and nonlinear (continuous or discretized) oscillators with fractional derivative terms can be found in [3, 4, 22, 36, 37, 41, 57, 87, 113, 164, 175, 176, 178, 180].

Moreover, the need for increasingly sophisticated modeling of excitations has led recently to the use of fractional-order filters for describing stochastic loads acting on structural systems. For instance, the widely used in earthquake engineering Kanai-Tajimi power spectrum has been recently enhanced by utilizing a fractional-order filter for circumventing certain limitations of the original standard model [6, 93, 183]. In this regard, the recently developed WPI technique that is presented in Chapter 2 is extended in this chapter to account for stochastic excitations modeled via fractional-order filters. Overall, the herein developed technique increases significantly the versatility of the WPI and renders the approach a powerful tool for determining the stochastic response of nonlinear oscillators subject to an extended range of excitation processes. An indicative numerical example is considered, while comparisons with relevant MCS data demonstrate the reliability of the technique.

3.2 WPI technique generalization: excitations modeled via fractional-order filters

In this chapter the WPI technique is generalized for addressing dynamical systems subject to stochastic excitations modeled via fractional-order filters; i.e, filters that involve fractional-order derivative terms of the form

$$D^{\beta}[x(t)] = \frac{1}{\Gamma(1-\beta)} \int_{t_i}^{t} \frac{\dot{x}(\tau)}{(t-\tau)^{\beta}} \mathrm{d}\tau \tag{3.1}$$

Eq. (3.1) represents a Caputo fractional derivative of order $0 < \beta < 1$ (see also [139] for alternative fractional derivative definitions). In this regard, consider a more general version of the system governing Eq. (2.34) given as

$$\boldsymbol{M}\ddot{\boldsymbol{x}} + \boldsymbol{g}(\boldsymbol{x}, D^{\boldsymbol{\beta}_1}\boldsymbol{x}, \dot{\boldsymbol{x}}) = \boldsymbol{f}\left[\boldsymbol{w}, \boldsymbol{\xi}\right] \tag{3.2}$$

where $\boldsymbol{f}\left[\cdot,\cdot\right]$ is an arbitrary nonlinear operator; $D^{\boldsymbol{\beta}_1}$ is a differential operator of fractional orders $\boldsymbol{\beta}_1$; and $\boldsymbol{\xi}$ is modeled as the output of the filter

$$\boldsymbol{P}\ddot{\boldsymbol{\xi}} + \boldsymbol{s}(\boldsymbol{\xi}, D^{\boldsymbol{\beta}_2}\boldsymbol{\xi}, \dot{\boldsymbol{\xi}}) = \boldsymbol{w} \tag{3.3}$$

where $\boldsymbol{P}$ is a deterministic parameters matrix; $\boldsymbol{s}$ is an arbitrary function; and $\boldsymbol{\beta}_2$ is another set of fractional orders for the differential operator $D^{\boldsymbol{\beta}_2}$. Eqs. (3.2) and (3.3) are generally called multi-term fractional SDEs, whose analytical or numerical solution (depending on the modeling parameters and operators $\boldsymbol{g}, \boldsymbol{s}, \boldsymbol{\beta}_1, \boldsymbol{\beta}_2$, and $\boldsymbol{f}\left[\cdot,\cdot\right]$) has been a rather challenging task and an active area of research [156]. In this paper two broad classes of problems are addressed; namely, *Case 1* where $\boldsymbol{f}\left[\boldsymbol{w}, \boldsymbol{\xi}\right] = \boldsymbol{\xi}$ (i.e., the output of the filter Eq. (3.3) is the input to the system Eq. (3.2)) and *Case 2* where $\boldsymbol{f}\left[\boldsymbol{w}, \boldsymbol{\xi}\right] = \boldsymbol{w} + \hat{\mathbf{f}}\left[\boldsymbol{\xi}\right]$, where $\hat{\mathbf{f}}\left[\cdot\right]$ is an arbitrary operator acting on $\boldsymbol{\xi}$.

Considering $\boldsymbol{f}\left[\boldsymbol{w},\boldsymbol{\xi}\right]=\boldsymbol{\xi}$, differentiating Eq. (3.2) and substituting into Eq. (3.3) yields the 4^{th}-order fractional SDE

$$\boldsymbol{\Lambda}_4\boldsymbol{x}^{(4)}+\boldsymbol{\kappa}\left(\boldsymbol{x},D^{\boldsymbol{\beta}_3}\boldsymbol{x},\ldots,\boldsymbol{x}^{(3)}\right)=\boldsymbol{w}\Big\}\ \ \textit{Case 1} \tag{3.4}$$

where $\boldsymbol{\Lambda}_4=\boldsymbol{PM}$; $\boldsymbol{\kappa}$ is a function that depends on the functions $\boldsymbol{g}$ and $\boldsymbol{s}$; and $\boldsymbol{\beta}_3$ is another set of fractional orders that arise from the differentiation and substitution of Eq. (3.2) into Eq. (3.3) and the fact that $D^{\beta_1}D^{\beta_2}x(t)=D^{\beta_1+\beta_2}x(t)$ for two arbitrary derivative orders β_1 and β_2. Next, extending the formulation of Section 2.4.2, the joint transition PDF of the process $\boldsymbol{\alpha}=\left[\boldsymbol{x},\dot{\boldsymbol{x}},\ddot{\boldsymbol{x}},\boldsymbol{x}^{(3)}\right]^T$ takes the form of Eq. (2.78) with $\mathcal{S}\left[\boldsymbol{x},D^{\boldsymbol{\beta}_3}\boldsymbol{x},\ldots,\boldsymbol{x}^{(4)}\right]$ given by Eq. (2.79) with

$$\mathcal{S}\left[\boldsymbol{x},D^{\boldsymbol{\beta}_3}\boldsymbol{x},\ldots,\boldsymbol{x}^{(4)}\right]=\int_{t_i}^{t_f}\mathcal{L}\left[\boldsymbol{x},D^{\boldsymbol{\beta}_3}\boldsymbol{x},\ldots,\boldsymbol{x}^{(4)}\right]\mathrm{d}t \tag{3.5}$$

and

$$\begin{aligned}\mathcal{L}\left[\boldsymbol{x},D^{\boldsymbol{\beta}_3}\boldsymbol{x},\ldots,\boldsymbol{x}^{(4)}\right]=\frac{1}{2}\left[\boldsymbol{\Lambda}_4\boldsymbol{x}^{(4)}+\boldsymbol{\kappa}\left(\boldsymbol{x},D^{\boldsymbol{\beta}_3}\boldsymbol{x},\ldots,\boldsymbol{x}^{(3)}\right)\right]^T\\ \times\boldsymbol{S_w}^{-1}\left[\boldsymbol{\Lambda}_4\boldsymbol{x}^{(4)}+\boldsymbol{\kappa}\left(\boldsymbol{x},D^{\boldsymbol{\beta}_3}\boldsymbol{x},\ldots,\boldsymbol{x}^{(3)}\right)\right]\end{aligned} \tag{3.6}$$

Further, the extremality condition of Eq. (2.27) becomes

$$\delta\mathcal{S}\left[\boldsymbol{x},D^{\boldsymbol{\beta}_3}\boldsymbol{x},\ldots,\boldsymbol{x}^{(4)}\right]=0 \tag{3.7}$$

which yields a fractional variational problem and leads to the respective fractional EL equations (see also [1, 37])

$$\frac{\partial\mathcal{L}}{\partial x_{c,j}}+{}^{RL}_{t}D^{\beta}\frac{\partial\mathcal{L}}{\partial D^{\beta}x_{c,j}}+\cdots+\frac{\mathrm{d}^4}{\mathrm{d}t^4}\frac{\partial\mathcal{L}}{\partial x^{(4)}_{c,j}}=0,\quad j=1,...,m \tag{3.8}$$

The fractional EL Eq. (3.8) accompanied by the initial and final conditions of Eq. (2.83) defines a nonlinear fractional BVP to be solved for the determination of the most probable path $\boldsymbol{x}_c(t)$. In a similar manner as for the standard BVP of Eqs. (2.82)-(2.83), analytical solutions of the fractional BVP of Eqs. (3.8) and (2.83) exist only for rather simple forms of functions $\boldsymbol{\kappa}$ in Eq. (3.4). In this regard, a numerical solution technique can be employed (e.g., [42]), which can be readily coupled with the brute-force numerical implementation delineated in Section 2.4.3 or the efficient implementations proposed in Chapter 4 for obtaining the joint transition PDF $p\left(\boldsymbol{\alpha}_f, t_f | \boldsymbol{\alpha}_i, t_i\right)$.

For the case where $\boldsymbol{f}\left[\boldsymbol{w}, \boldsymbol{\xi}\right] = \boldsymbol{w} + \hat{\mathbf{f}}\left[\boldsymbol{\xi}\right]$ in Eq. (3.2), Eqs. (3.2)-(3.3) are written as

$$\left.\begin{aligned} \boldsymbol{M}\ddot{\boldsymbol{x}} + \boldsymbol{g}(\boldsymbol{x}, D^{\boldsymbol{\beta}_1}\boldsymbol{x}, \dot{\boldsymbol{x}}) - \hat{\mathbf{f}}\left[\boldsymbol{\xi}\right] &= \boldsymbol{w} \\ \boldsymbol{P}\ddot{\boldsymbol{\xi}} + \boldsymbol{s}(\boldsymbol{\xi}, D^{\boldsymbol{\beta}_2}\boldsymbol{\xi}, \dot{\boldsymbol{\xi}}) &= \boldsymbol{w} \end{aligned}\right\} \ \textit{Case 2} \tag{3.9}$$

which is a system of fractional SDEs with a singular diffusion matrix (see also [144] for a system with standard integer-order derivatives with the same right-hand side excitation terms). Although this generally poses a challenge for the WPI technique [144] Eq. (3.9) can be multiplied by the non-singular block matrix

$$\boldsymbol{J} = \begin{bmatrix} \boldsymbol{I}_{m\times m} & \boldsymbol{0}_{m\times m} \\ -\boldsymbol{I}_{m\times m} & \boldsymbol{I}_{m\times m} \end{bmatrix} \tag{3.10}$$

and become

$$\boldsymbol{M}\ddot{\boldsymbol{x}} + \boldsymbol{g}(\boldsymbol{x}, D^{\boldsymbol{\beta}_1}\boldsymbol{x}, \dot{\boldsymbol{x}}) - \hat{\mathbf{f}}\left[\boldsymbol{\xi}\right] = \boldsymbol{w} \tag{3.11a}$$

$$\boldsymbol{P}\ddot{\boldsymbol{\xi}} + \boldsymbol{s}(\boldsymbol{\xi}, D^{\boldsymbol{\beta}_2}\boldsymbol{\xi}, \dot{\boldsymbol{\xi}}) - \boldsymbol{M}\ddot{\boldsymbol{x}} - \boldsymbol{g}(\boldsymbol{x}, D^{\boldsymbol{\beta}_1}\boldsymbol{x}, \dot{\boldsymbol{x}}) + \hat{\mathbf{f}}\left[\boldsymbol{\xi}\right] = \boldsymbol{0} \tag{3.11b}$$

Therefore, Eq. (3.11a) takes the form of Eq. (2.34) with the difference that it also involves the process $\boldsymbol{\xi}$ (and its derivatives) and that the condition of Eq. (3.11b) needs to be satisfied at all times. Next, the joint transition PDF of the augmented process $\boldsymbol{\alpha} = \left[\boldsymbol{x}, \boldsymbol{\xi}, \dot{\boldsymbol{x}}, \dot{\boldsymbol{\xi}}\right]^T$ is

given by Eq. (2.56) which for this case is written as

$$p\left(\boldsymbol{\alpha}_f, t_f|\boldsymbol{\alpha}_i, t_i\right) = \int_{\mathcal{C}\{\boldsymbol{\alpha}_i,t_i;\boldsymbol{\alpha}_f,t_f|\boldsymbol{\phi}=\mathbf{0}\}} \exp\left(-\mathcal{S}\left[\boldsymbol{x}, \boldsymbol{\xi}, \ldots, \ddot{\boldsymbol{\xi}}\right]\right) \widetilde{\mathcal{D}}[\boldsymbol{x}(t)]\widetilde{\mathcal{D}}[\boldsymbol{\xi}(t)] \tag{3.12}$$

where $\mathcal{S}\left[\boldsymbol{x}, \boldsymbol{\xi}, \ldots, \ddot{\boldsymbol{\xi}}\right]$ is given by Eq. (2.20) with

$$\mathcal{L}\left[\boldsymbol{x}, \boldsymbol{\xi}, \ldots, \ddot{\boldsymbol{\xi}}\right] = \frac{1}{2}\left[\boldsymbol{M}\ddot{\boldsymbol{x}} + \boldsymbol{g}(\boldsymbol{x}, D^{\boldsymbol{\beta}_1}\boldsymbol{x}, \dot{\boldsymbol{x}}) - \hat{\mathbf{f}}\left[\boldsymbol{\xi}\right]\right]^T \times \boldsymbol{S_w}^{-1}\left[\boldsymbol{M}\ddot{\boldsymbol{x}} + \boldsymbol{g}(\boldsymbol{x}, D^{\boldsymbol{\beta}_1}\boldsymbol{x}, \dot{\boldsymbol{x}}) - \hat{\mathbf{f}}\left[\boldsymbol{\xi}\right]\right] \tag{3.13}$$

In Eq. (3.12) $\mathcal{C}\{\boldsymbol{\alpha}_i, t_i; \boldsymbol{\alpha}_f, t_f|\boldsymbol{\phi} = \mathbf{0}\}$ represents the set of all paths that satisfy the initial and final conditions $\boldsymbol{\alpha}_i = \left[\boldsymbol{x}_i, \boldsymbol{\xi}_i, \dot{\boldsymbol{x}}_i, \dot{\boldsymbol{\xi}}_i\right]^T$ at time t_i and $\boldsymbol{\alpha}_f = \left[\boldsymbol{x}_f, \boldsymbol{\xi}_f, \dot{\boldsymbol{x}}_f, \dot{\boldsymbol{\xi}}_f\right]^T$ at time t_f, respectively, as well as the condition $\boldsymbol{\phi} = \mathbf{0}$ that corresponds to Eq. (3.11b).

Further, the variational problem of Eq. (2.26) for the determination of $\boldsymbol{\alpha}_c = [\boldsymbol{x}_c, \boldsymbol{\xi}_c]^T$ becomes

$$\textit{minimize } \mathcal{S}\left[\boldsymbol{\alpha}_c\right], \textit{ subject to } \boldsymbol{\alpha}_c \in \mathcal{C}\{\boldsymbol{\alpha}_i, t_i; \boldsymbol{\alpha}_f, t_f|\boldsymbol{\phi} = \mathbf{0}\} \tag{3.14}$$

Eq. (3.14) can be construed also as a fractional-order optimal control problem (e.g., [3, 117]), where the most probable path (i.e., the optimal solution) $\boldsymbol{\alpha}_c = [\boldsymbol{x}_c, \boldsymbol{\xi}_c]^T$ that minimizes $\mathcal{S}\left[\boldsymbol{x}, \boldsymbol{\xi}, \ldots, \ddot{\boldsymbol{\xi}}\right]$ (i.e., the performance index) is required to satisfy the constraints $\boldsymbol{\phi} = \mathbf{0}$ of Eq. (3.11b) that involve fractional derivative terms. In this regard, the standard Rayleigh-Ritz solution technique (e.g., [116]) is combined herein with an algorithm for solving constrained optimization problems (e.g., of the type of Sequential Quadratic Programming; see [144] for more details). Following the determination of the most probable path $[\boldsymbol{x}_c, \boldsymbol{\xi}_c]^T$, the joint transition PDF $p\left(\boldsymbol{\alpha}_f, t_f|\boldsymbol{\alpha}_i, t_i\right)$ is approximated by Eqs. (2.63)-(2.65). Similarly to *Case 1*, the problem of solving the fractional SDEs of Eq. (3.9) has been reduced to a set of deterministic problems given by Eq. (3.14), which can be combined with the brute-force implementation of Section 2.4.3 or more computationally efficient implementations that are proposed in Chapter 4.

3.3 Numerical example

A widely utilized earthquake excitation model relates to the Kanai-Tajimi power spectrum introduced in [93, 183] and further generalized and enhanced in [6] by exploiting the modeling capabilities of fractional derivatives. In this regard, the bedrock acceleration can be approximated as a white noise process filtered through the soil deposit, which is modeled as a single-degree-of-freedom oscillator (SDOF) with a fractional derivative term, i.e.,

$$\ddot{\xi} + 2\bar{\zeta}_g \omega_g D^{\beta} \xi + \omega_g^2 \xi = -w(t) \tag{3.15}$$

where ξ is the ground displacement relative to the bedrock; and $w(t)$ is a scalar white noise process with $S_w = 2\pi S_0$ (see Section 2.4.1). Note that the order of the fractional derivative β, as well as the damping $\bar{\zeta}_g$ [6] and the natural frequency ω_g coefficients in Eq. (3.15) can be obtained by experimental shear creep tests on ground samples. Next, by expressing the absolute ground acceleration as

$$\ddot{x}_g(t) = \ddot{\xi}(t) + w(t) \tag{3.16}$$

(see [6] for the corresponding power spectrum) the equation of motion of a nonlinear Duffing SDOF oscillator with mass, damping, and stiffness coefficients m_0, c_0, and k_0, respectively, takes the form

$$\ddot{x} + \frac{c_0}{m_0}\dot{x} + \frac{k_0}{m_0}x + \epsilon_0 x^3 = -\ddot{x}_g(t) \tag{3.17}$$

where ϵ_0 is the magnitude of the nonlinearity. By combining Eqs. (3.15)-(3.17) it is clear that this example corresponds to *Case 2* defined by Eq. (3.9) and thus, Eqs. (3.11a)-(3.11b)

become

$$-\ddot{x} - \frac{c_0}{m_0}\dot{x} - \frac{k_0}{m_0}x - \epsilon_0 x^3 - \ddot{\xi} = w \tag{3.18a}$$

$$2\bar{\zeta}_g\omega_g D^\beta \xi + \omega_g^2 \xi - \ddot{x} - \frac{c_0}{m_0}\dot{x} - \frac{k_0}{m_0}x - \epsilon_0 x^3 = 0 \tag{3.18b}$$

and the Lagrangian of the system of Eq. (3.18a) is given by Eq. (3.13) as

$$\mathcal{L}\left[x, \xi, \ldots, \ddot{\xi}\right] = \frac{1}{4\pi S_0}\left[\ddot{x} + \frac{c_0}{m_0}\dot{x} + \frac{k_0}{m_0}x + \epsilon_0 x^3 + \ddot{\xi}\right]^2 \tag{3.19}$$

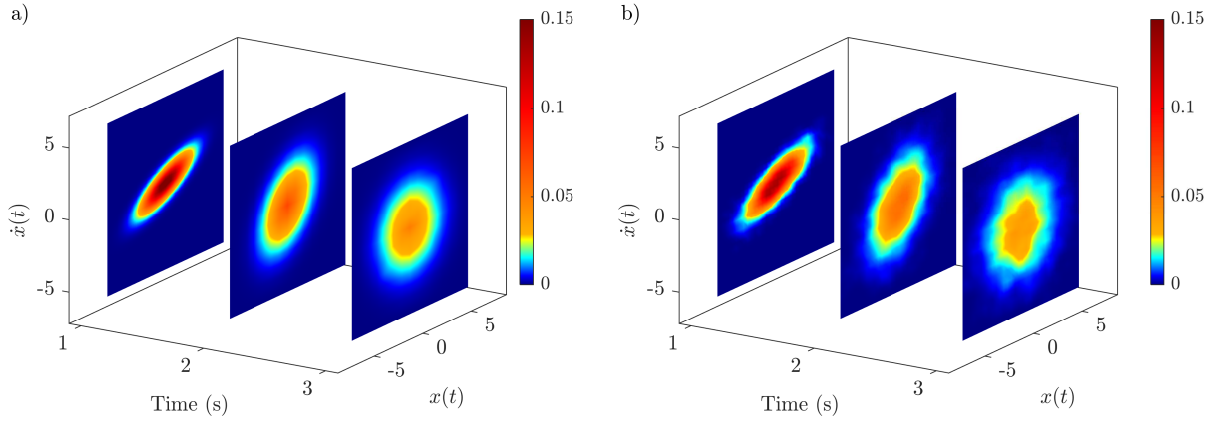

Figure 3.1: Non-stationary joint response PDF of an SDOF Duffing oscillator governed by Eq. (3.17) subject to external excitation modeled by Eqs. (3.15)-(3.16), with parameter values ($m_0 = 1$, $c_0 = 0.2$, $k_0 = 1$, $\epsilon_0 = 1$, $\bar{\zeta}_g = 0.6$, $\beta = 0.5$,$\omega_g = 5\pi$, and $S_0 = 0.5$), as obtained via the WPI technique (a); comparisons with MSC data - 10,000 realizations (b).

Finally, for obtaining the joint transition PDF of the augmented process $\boldsymbol{\alpha} = \left[x, \xi, \dot{x}, \dot{\xi}\right]^T$ the efficient numerical implementation of [147] is employed and thus, only a few fractional-order optimal control problems of the form of Eq. (3.14) are solved for various values of final conditions t_f and $\boldsymbol{\alpha}_f$ (see also Section 2.4.3 and Chapter 4). In Figs. 3.1-3.2 the joint response PDF $p(x, \dot{x}, t)$ and the marginal PDFs $p(x, t)$ and $p(\dot{x}, t)$ obtained by the herein generalized WPI technique are plotted for parameter values ($m_0 = 1$, $c_0 = 0.2$, $k_0 = 1$, $\epsilon_0 = 1$, $\bar{\zeta}_g = 0.6$, $\beta = 0.5$, $\omega_g = 5\pi$, and $S_0 = 0.5$) and for several time instants. Comparisons with pertinent

MCS data (10,000 realizations) demonstrate a relatively high accuracy degree.

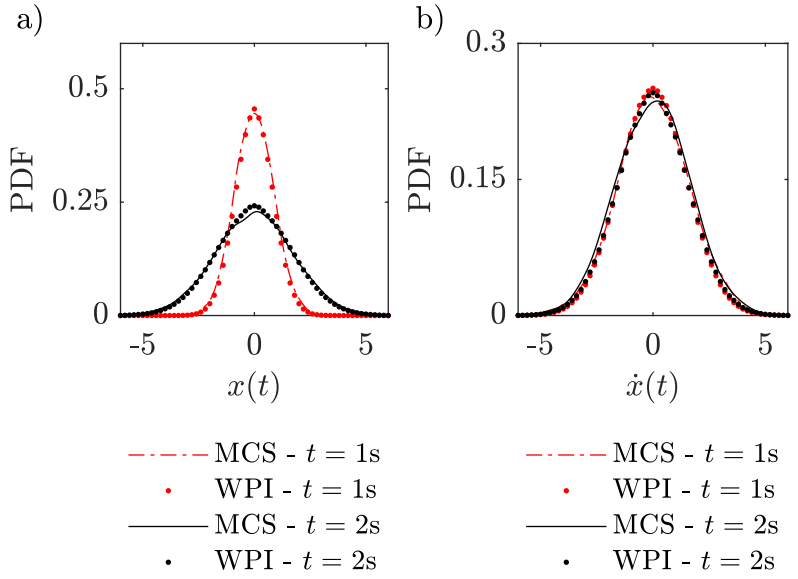

Figure 3.2: Marginal PDFs of the displacement (a) and the velocity (b) of an SDOF Duffing oscillator with equation of motion given by Eq. (3.17) subject to external excitation modeled by Eqs. (3.15)-(3.16), with parameter values ($m_0 = 1$, $c_0 = 0.2$, $k_0 = 1$, $\epsilon_0 = 1$, $\bar{\zeta}_g = 0.6$, $\beta = 0.5$, $\omega_g = 5\pi$, and $S_0 = 0.5$); comparisons with MSC data - 10,000 realizations.

3.4 Concluding remarks

A generalization of the WPI technique has been developed in this chapter to account for a broad class of excitation processes modeled via (nonlinear) fractional filters. It has been shown that by utilizing the herein proposed generalization the original problem of solving a system of multi-term fractional SDEs degenerates either to a set of deterministic fractional BVPs (*Case 1*) or to a set of deterministic fractional-order optimal control problems (*Case 2*). Regarding the computational cost, it has been shown that the technique can be readily coupled with recently developed computationally efficient implementations (e.g., [147]) for obtaining the joint transition PDF by solving a minimal number of deterministic problems. Overall, the developments in this chapter increase significantly the versatility of the WPI technique and render it a potent tool for determining, in a computationally efficient manner, the stochastic response of nonlinear oscillators subject to an extended range of excitation

processes. Finally, via a numerical example involving a fractional-order Kanai-Tajimi filter, it has been shown that the herein generalized WPI technique exhibits satisfactory accuracy in determining the joint transition PDF as compared with pertinent MCS data.

Chapter 4

Sparse representations and multi-dimensional global bases for enhancing the computational efficiency of the Wiener path integral technique

4.1 Introduction

In Section 2.4.3 the high computational cost of a brute-force implementation of the WPI technique, especially for high-dimensional systems, has been highlighted. Further, it has been argued that even with the enhancement in computational efficiency proposed by Kougioumtzoglou *et al.* [104], the related computational cost as a power law function of the number of stochastic dimensions still limits the applicability of the methodology to relatively low-dimensional systems. In this regard, the objective of this chapter relates to generalizing the WPI technique and further enhancing its computational efficiency by con-

structing time-dependent bases for determining the non-stationary response PDF directly, based on knowledge of relatively few PDF points in the joint space-time domain. In addition, compressive sampling procedures are employed in conjunction with group sparsity concepts and appropriate optimization algorithms for decreasing even further the computational cost associated with determining the system response PDF.

Evaluating the PDF of a stochastic process given partial information is a typical problem in a wide range of research fields [69, 91]. In stochastic dynamics, PDF expansions have been utilized for solving the Fokker-Planck and the Backward Kolmogorov equations [50, 169], or other alternative equations governing the stochastic response of a dynamical system [157]. Indicatively, PDF expansions have been coupled with weighted residual methodologies [38, 85, 124, 127], where the approximate PDF is substituted into the Fokker-Planck equation and the residual error is minimized; with moment closure schemes [30, 55, 81, 92, 115], which yield a finite set of moment equations to be solved for approximating the response PDF; with finite element method direct numerical solution schemes [106, 130]; with discretized Chapman-Kolmogorov equation schemes propagating the response PDF in short time steps [128, 129, 131, 196]; and with solution schemes based on the maximum entropy principle [12, 165].

Typical PDF expansions and approximation schemes utilize truncated Gram-Charlier or Edgeworth series [30, 50, 85, 115, 127], Hermite or other polynomials [38, 55, 81, 106, 131, 200], Gaussian distributions with varying mean and variance [84], kernel density functions [157] and B-splines or piecewise linear functions [128, 196]. Further, [124] employed Shannon wavelets for approximating the PDF within the context of the weighted residual method. Moreover, radial basis functions (RBFs) demonstrated accurate results in the context of numerically solving the Fokker-Planck equation [35, 94].

In this chapter an approximation scheme based on the WPI technique is developed for efficiently determining the non-stationary joint response PDF of stochastically excited MDOF dynamical systems. To this aim, two distinct expansions are proposed for the PDF; the first

is based on Kronecker products of bases such as wavelets, and the second is based on positive definite functions, which is a more general class of functions than RBFs. As a result, the WPI technique is generalized herein to account explicitly for the time dimension in its formulation and implementation. An additional objective of this chapter is to further enhance the computational efficiency of the WPI technique by exploiting recent developments in the area of sparse representations. Indicatively, sparse expansions of multivariate polynomials have been recently used for numerically solving stochastic (partial) differential equations [25, 46, 197]. It is shown that the herein developed enhancement renders the technique capable of treating readily relatively high-dimensional stochastic systems.

4.2 Non-stationary joint response PDF approximation

As explained in Chapter 2 the WPI technique can be utilized for treating MDOF nonlinear oscillators subject to external non-stationary, non-Gaussian, and non-white excitation processes. Further, as Kougioumtzoglou [101] has recently shown, the WPI technique can address not only problems subject to stochastic excitation $\boldsymbol{w}(t)$, but also a certain class of one-dimensional mechanics problems with stochastic media properties; that is, stochasticity is embedded in the operator $\mathcal{F}[.]$ of Eq. (1.1). However, for the purpose of this chapter, and without loss of generality, the m-DOF nonlinear dynamical system with stochastic external excitation of Eq. (2.34) is considered hereinafter. In this regard, without loss of generality and considering fixed initial conditions, the only variables describing the PDF $p(\boldsymbol{x}_f, \dot{\boldsymbol{x}}_f, t_f | \boldsymbol{x}_i, \dot{\boldsymbol{x}}_i, t_i)$ at a time instant t_f are $\boldsymbol{x}_f$ and $\dot{\boldsymbol{x}}_f$; thus, it can be written as $p(\boldsymbol{x}, \dot{\boldsymbol{x}}, t)$. Further, determining a single point of the joint response PDF $p(\boldsymbol{x}, \dot{\boldsymbol{x}}, t)$ amounts to solving a deterministic variational problem of the form of Eqs. (2.61)-(2.62). In the ensuing analysis, adopting a data analysis perspective, this procedure will be referred to as obtaining a measurement of the joint response PDF.

Next, $p(\boldsymbol{x}, \dot{\boldsymbol{x}}, t)$ can be approximated as

$$p(\boldsymbol{x}, \dot{\boldsymbol{x}}, t) \approx \exp\left(\mu\left(\boldsymbol{x}, \dot{\boldsymbol{x}}, t\right)\right) \tag{4.1}$$

or, alternatively, as

$$p(\boldsymbol{x}, \dot{\boldsymbol{x}}, t) \approx \nu\left(\boldsymbol{x}, \dot{\boldsymbol{x}}, t\right) \tag{4.2}$$

where $\mu\left(\boldsymbol{x}, \dot{\boldsymbol{x}}, t\right)$ and $\nu\left(\boldsymbol{x}, \dot{\boldsymbol{x}}, t\right)$ are approximating functions. Therefore, depending on whether Eq. (4.1) or Eq. (4.2) is used, a measurement of the response PDF at a specific location $(\boldsymbol{x}, \dot{\boldsymbol{x}}, t)$ via the WPI technique refers to either the exponent or the exponential function of Eq. (2.63), respectively.

Further, following the selection of N locations to perform the approximation, Eqs. (4.1)-(4.2) take the form of a linear system of N equations, i.e.,

$$\boldsymbol{y}_0 = \boldsymbol{D}\boldsymbol{c} \tag{4.3}$$

where $\boldsymbol{y}_0 \in \mathbb{R}^{N\times 1}$ is a vector of N measurements of $\log\left(p(\boldsymbol{x}, \dot{\boldsymbol{x}}, t)\right)$ (or of $p(\boldsymbol{x}, \dot{\boldsymbol{x}}, t)$ if Eq. (4.2) is used), $\boldsymbol{D} \in \mathbb{R}^{N\times N}$ is the basis matrix and $\boldsymbol{c} = [c_1, \ldots, c_N]^T \in \mathbb{R}^{N\times 1}$ is the expansion coefficient vector. A WPI solution approach coupled with Eq. (4.3) has proven to drastically increase the computational efficiency of the WPI technique [104], as only $N \ll N_{bf}$ BVPs of the form of Eqs. (2.61)-(2.62) need to be solved for determining the joint response PDF for a fixed value of t.

Nevertheless, it is demonstrated herein that further significant decrease in the computational cost is possible, if the response PDF is considered as a function of time explicitly. Moreover, if only $R \ll N$ measurements (or, in other words, deterministic variational problems to be solved) are utilized in Eq. (4.3) the computational cost can be reduced even further.

First, in Section 4.2.1, a separable basis is constructed for approximating the non-

stationary PDF by combining the bases/structures selected for each dimension [49]. Such a basis proves, in general, capable of handling the anisotropic features of multivariate functions and appears a natural choice for approximating the response PDF. Next, an alternative approach is followed in Section 4.2.2, where the approximation takes the form of a scattered data fitting problem [60]. The non-stationary PDF is sampled at various locations in the spatio-temporal domain and a fit to the dataset based on positive definite functions (which can be construed as a generalization of the widely used RBFs [60]) is sought for. Also, it is noted that positive definite functions have been deliberately selected over RBFs for better coping with the potentially anisotropic features of the non-stationary PDF [60]. Finally, in Section 4.2.4, $R \ll N$ measurements are utilized in Eq. (4.3), which yields an underdetermined system of equations that can be solved by relying on potent sparse representation concepts and tools [148].

4.2.1 Kronecker product approach

4.2.1.1 Kronecker product bases

Various multivariate bases have been developed based on Kronecker products [16]. Remarkably, the applications of Kronecker structure range from image/video processing [28] and distributed sensing [49] to pre-conditioning for linear system solution [187] and matrix approximation [108].

Specifically, the Kronecker product $\boldsymbol{H} \otimes \boldsymbol{J}$ of two matrices $\boldsymbol{H} \in \mathbb{R}^{H_1 \times H_2}$ and $\boldsymbol{J} \in \mathbb{R}^{J_1 \times J_2}$ is a matrix of size $H_1 J_1 \times H_2 J_2$ defined by (e.g., [16])

$$\boldsymbol{H} \otimes \boldsymbol{J} = \begin{bmatrix} h_{11}\boldsymbol{J} & \dots & h_{1H_2}\boldsymbol{J} \\ \vdots & \ddots & \vdots \\ h_{H_11}\boldsymbol{J} & \dots & h_{H_1H_2}\boldsymbol{J} \end{bmatrix} \tag{4.4}$$

Further, given the basis matrices $\boldsymbol{D}_1 \in \mathbb{R}^{n_1 \times n_1}$ and $\boldsymbol{D}_2 \in \mathbb{R}^{n_2 \times n_2}$, consider a transform

applied to a data matrix $\boldsymbol{Y}_0 \in \mathbb{R}^{n_1 \times n_2}$ by using the separable basis constructed by their Kronecker product. Vectorizing matrix $\boldsymbol{Y}_0$, i.e., concatenating its columns vertically, so that $\boldsymbol{y}_0 = vec(\boldsymbol{Y}_0) \in \mathbb{R}^{n_1 n_2}$, the data vector can be written as (e.g., [16])

$$\boldsymbol{y}_0 = (\boldsymbol{D}_2 \otimes \boldsymbol{D}_1)\, \boldsymbol{c} \tag{4.5}$$

where $\boldsymbol{c}$ denotes the coefficient matrix in vectorized form. Generalizing, consider P dimensions in total and $n_1 n_2 \dots n_P$ measurements taken from a multivariate function $y_0(\boldsymbol{q})$, where $\boldsymbol{q} \in \mathbb{R}^P$. The measurement tensor $\boldsymbol{Y}_0 \in \mathbb{R}^{n_1 \times n_2 \times \cdots \times n_P}$ admits a Kronecker expansion of the form of Eq. (4.5) expressed as

$$\boldsymbol{y}_0 = (\boldsymbol{D}_P \otimes \cdots \otimes \boldsymbol{D}_2 \otimes \boldsymbol{D}_1)\, \boldsymbol{c} \tag{4.6}$$

where $\boldsymbol{y}_0, \boldsymbol{c} \in \mathbb{R}^{n_1 n_2 \cdots n_P}$. Therefore, after collecting $N = n_1 n_2 \dots n_P$ measurements from the P-dimensional space and selecting a basis in each dimension $(\boldsymbol{D}_1, \dots, \boldsymbol{D}_P)$ the coefficients of the Kronecker expansion can be obtained by solving the linear system of Eq. (4.6). It is noted that the columns of the basis matrices $\boldsymbol{D}_1, \dots, \boldsymbol{D}_P$ in Eq. (4.6) are the basis functions selected for each dimension discretized into $n_1, \dots, n_P$ points, respectively.

4.2.1.2 Multi-dimensional basis construction for approximating the non-stationary joint response PDF

Following the procedure outlined in Section 4.2.1.1 it is rather straightforward to construct a multi-dimensional basis for approximating the non-stationary response PDF by employing Eqs. (4.2) and (4.6). Specifically, the response PDF is a function of $(\boldsymbol{x}, \dot{\boldsymbol{x}}, t)$, which is of size $P = 2m + 1$; that is, $2m$ spatial dimensions and 1 temporal dimension. In this regard, various (potentially different) bases can be chosen for the approximation in each dimension in conjunction with the numbers n_p, where $p \in \{1, \dots, 2m+1\}$. Next, the expansion coefficients vector $\boldsymbol{c}$ is determined by solving the linear system of Eq. (4.6), where $\boldsymbol{y}_0$ is the

vector containing $n_1 \dots n_{2m+1}$ measurements of $p(\boldsymbol{x}, \dot{\boldsymbol{x}}, t)$ determined via WPI and employing a uniform mesh. In the following, and without loss of generality, two distinct approaches are pursued in choosing the bases to be utilized in Eq. (4.6).

First, the same one-dimensional wavelet basis is used for each and every dimension. In particular, an arbitrary function $f(t)$ can be expressed as

$$f(t) = \sum_{h=-\infty}^{\infty} \sum_{r=-\infty}^{\infty} c_{hr} \psi_{hr}(t) \tag{4.7}$$

where c are the expansion coefficients to be determined, h and r denote the different scales and translation levels, respectively, and $\psi_{hr}(t) = \frac{1}{2^h}\psi(\frac{t}{2^h} - r)$, with $\psi(t)$ the wavelet family to be chosen. Alternatively, Eq. (4.7) can be expressed via the associated scaling function $\phi(t)$ as

$$f_N(t) = \sum_{r=0}^{N-1} c_r \phi_{Hr}(t) \tag{4.8}$$

where $f_N(t)$ denotes the N-term approximation of the function $f(t)$ with only $N = 2^{-H}$ scaling functions, given as $\phi_{Hr}(t) = \frac{1}{2^H}\phi(\frac{t}{2^H} - r)$, and H denotes the selected scale, or equivalently the approximation level. A detailed presentation of wavelet theory can be found in several books, such as [120]. Obviously, the efficacy of the chosen wavelet family is application-dependent. Thus, various both discrete and continuous wavelets have been developed over the past decades [120], as well as generalizations with additional parameters such as harmonic wavelets (e.g., [102, 133, 179]) and chirplets (e.g., [121]); see also the review paper by Spanos & Failla [177] for diverse wavelet applications in engineering dynamics. In the ensuing analysis, the Meyer wavelet (e.g., [120]) is used in the related expansions.

Second, an alternative approach is pursued, which exploits the flexibility of the herein proposed framework to use different bases. In this regard, and considering Eq. (4.1), a multivariate polynomial can be employed for the spatial dimensions, as in [104], and a wavelet basis for the temporal dimension. Therefore, the linear system of Eq. (4.5) becomes

$$\boldsymbol{y}_0 = (\boldsymbol{D}_w \otimes \boldsymbol{D}_s)\, \boldsymbol{c} \tag{4.9}$$

where $\boldsymbol{y}_0$ contains the measurements of $\log\left(p(\boldsymbol{x}, \dot{\boldsymbol{x}}, t)\right)$ determined via the WPI, $\boldsymbol{D}_w$ denotes the one-dimensional wavelet basis, $\boldsymbol{D}_s$ the monomial basis (e.g., [140]) and $\boldsymbol{c}$ the coefficient vector. Specifically, $\boldsymbol{D}_s$ is an $n_s \times n_s$ matrix, where $n_s = \binom{l_s+2m}{2m}$ for a polynomial of degree l_s, and $\boldsymbol{D}_w$ is an $n_t \times n_t$ matrix. Therefore, $N = n_s n_t$ measurements of the joint response PDF via the WPI technique are required.

Overall, it is readily seen that utilizing a Kronecker product formulation is a conceptually simple approach for higher-dimensional approximations by combining several lower-dimensional approximations in a straightforward manner. This yields enhanced flexibility in the implementation of the approach as various, potentially different, bases can be used, which have already proven to be well-suited for the respective lower-dimensional problems. For instance, the monomial basis has exhibited significant accuracy in approximating the spatial dimensions of a class of problems in [104] and in [145]. Thus, under the Kronecker product formulation, it can be directly used in conjunction with an additional basis related to the temporal dimension. Nevertheless, the lower-dimensional bases and the respective number of measurements need to be selected a priori, while as noted in [145], the monomial basis is prone to ill-conditioning, and, hence, the points of the mesh should be selected based on certain optimality criteria for enhanced robustness and accuracy of the approximation (see for instance [186]). If, alternatively, only one-dimensional wavelet bases are used for constructing the multi-dimensional basis via Eq. (4.6), the associated computational cost increases exponentially with increasing number of dimensions and becomes eventually prohibitive for relatively high-dimensional problems.

To address the above points, a mesh-free approximation scheme is developed in Section 4.2.2 by utilizing positive definite functions. The advantages of such an approach pertain mainly to the fact that the basis functions depend on the measurement locations, and thus, are not selected a priori. Therefore, as explained in detail in Section 4.2.2, the result-

ing interpolation matrix is well-conditioned yielding a robust and accurate approximation. Overall, positive definite functions appear more general and suitable for higher-dimensional systems, whereas Kronecker product bases perform better for lower-dimensional systems, especially when there is some available information regarding the response PDF.

4.2.2 Positive definite functions approach

4.2.2.1 Positive definite functions aspects

In this section, the multivariate (P-dimensional) approximation problem is formulated as a scattered data fitting problem, which is a fundamental problem in approximation theory and is summarized in the following [60]: Given a set of measurements $(\boldsymbol{q}_r, y_{0,r})$ from a function $y_0(\boldsymbol{q})$, where $r \in \{1, \ldots, N\}$; $\boldsymbol{q}$, $\boldsymbol{q}_r \in \mathbb{R}^P$; and $y_{0,r} \in \mathbb{R}$, determine a function $\mu(\boldsymbol{q})$ such that

$$\mu(\boldsymbol{q}_r) = y_{0,r} \tag{4.10}$$

$\forall\ r \in \{1, \ldots, N\}$. Even though in the univariate case (i.e., $P = 1$) this meshfree problem has a unique solution using N distinct measurements and a polynomial of order $N - 1$, the multivariate case is more complex leading to ill-conditioned interpolation matrices [59]. According to the Mairhuber-Curtis theorem (e.g., [13]), for the problem to be well-posed, i.e., for a solution to exist and be unique, the basis functions cannot be fixed a priori.

The above challenge has led mathematicians to introduce data-dependent bases, which are bases created following the selection of the sampling locations. In this direction, positive definite functions (or kernels more generally) have been commonly used in approximation theory [58, 60]. Following [59], a complex-valued continuous function $d : \mathbb{R}^P \to \mathbb{C}$ is called positive definite on $\mathbb{R}^P$ if

$$\sum_{h=1}^{N} \sum_{r=1}^{N} c_h \bar{c}_r d(\boldsymbol{q}_h - \boldsymbol{q}_r) \geq 0 \tag{4.11}$$

for any N pairwise different points $\boldsymbol{q}_1, \ldots, \boldsymbol{q}_N \in \mathbb{R}^P$ and $\boldsymbol{c} = [c_1, \ldots, c_N]^T \in \mathbb{C}^N$. Among the

most widely used positive definite functions is the Gaussian function, i.e., $d(\boldsymbol{q}) = e^{-\epsilon_1^2\|\boldsymbol{q}\|_2^2}$, with $\boldsymbol{q} \in \mathbb{R}^P$ and a shape parameter $\epsilon_1 > 0$. The widespread utilization of positive definite functions in the approximation field can be attributed, at least partly, to their connection with the scattered data fitting problem of Eq. (4.10), and to the existence of well-behaved (i.e., non-singular) interpolation matrices (e.g., [125]). Further, there are constantly new classes of positive definite functions being introduced in conjunction with related theoretical work on error bounds [59]. Finally, it is worth noting that the numerical implementation of positive definite functions is amenable to high-performance computing [198], while their applications range from meshfree interpolation and solution of partial differential equations [64] to simulation of stochastic processes [136] and machine learning [159].

4.2.2.2 Multi-dimensional basis construction for approximating the non-stationary joint response PDF

As mentioned in Section 4.2.2.1, given the measurements $(\boldsymbol{q}_r, y_{0,r})$ the objective is to determine an interpolating function $\mu(\boldsymbol{q})$, expressed as

$$\mu(\boldsymbol{q}) = \sum_{r=1}^{N} c_r d_r(\boldsymbol{q}) \tag{4.12}$$

where the basis functions d_r, for $r \in \{1, \ldots, N\}$, are positive definite and $\boldsymbol{c} = [c_1, \ldots, c_N]^T \in \mathbb{R}^N$ denotes the expansion coefficient vector. Clearly, the choice of the specific basis functions is problem-dependent, with RBFs being among the most popular choices [15]. RBFs are rotationally and translationally invariant and are commonly used in engineering problems. For RBF interpolation the basis functions are expressed as a function of $\|\boldsymbol{q} - \boldsymbol{q}_r\|$, where $\boldsymbol{q}_r$, for $r \in \{1, \ldots, N\}$, corresponds to the sampling locations.

Alternative choices include, but are not limited to, multiscale kernels [141], which are defined as linear combinations of shifted and scaled versions of a single function and exhibit properties similar to wavelets, and translationally invariant functions [60]. The latter are

constructed by relaxing the rotational invariance property of RBFs and have been found to provide further flexibility in the interpolation and to improve the condition number of the interpolation matrix [60]. A typical example that is also adopted in the ensuing analysis is the anisotropic multivariate Gaussian function

$$d_r(\boldsymbol{q}) = \exp\left(-\sum_{p=1}^{P} \epsilon_p^2 \left(q_p - q_{r,p}\right)^2\right) \tag{4.13}$$

where ϵ_p, for $p \in \{1, \ldots, P\}$, denotes the shape parameter for the p-th dimension, while q_p and $q_{r,p}$ denote the p-th component of $\boldsymbol{q}$ and $\boldsymbol{q}_r$, respectively. The basis then becomes a collection of functions of the form of Eq. (4.13), i.e.,

$$\{d_1(\boldsymbol{q}), \ldots, d_N(\boldsymbol{q})\} \tag{4.14}$$

Next, considering $\boldsymbol{q} = (\boldsymbol{x}, \dot{\boldsymbol{x}}, t)$ yields $P = 2m+1$ dimensions, while the same shape parameter value ϵ_s is used for all the spatial dimensions and the value ϵ_t for the temporal dimension. In this regard, by employing anisotropic Gaussian functions, Eq. (4.1) becomes

$$p(\boldsymbol{x}, \dot{\boldsymbol{x}}, t) \approx \exp\left[\sum_{r=1}^{N} c_r \exp\left(-\sum_{j=1}^{m} \epsilon_s^2 \left(x_j - x_{r,j}\right)^2 - \sum_{j=1}^{m} \epsilon_s^2 \left(\dot{x}_j - \dot{x}_{r,j}\right)^2 - \epsilon_t^2 \left(t - t_r\right)^2\right)\right] \tag{4.15}$$

Note that the N sampling locations need to be well-distributed in the $(2m+1)$-space. To this aim, the Halton sequence is used [82], which is also frequently employed in quasi-Monte Carlo methods for multi-dimensional integration; see also the papers by Bratley *et al.* [14] and by De Marchi *et al.* [34] for some alternative sampling strategies. Further, it is desirable in many cases to have an interpolant that exactly reconstructs a polynomial of a given order; see, for instance, the "patch test" in finite elements (e.g., [203]). To this aim, the basis of Eq. (4.14) can be augmented by including monomials to a given order; that is

$$\{d_1(\boldsymbol{q}), \ldots, d_N(\boldsymbol{q}), 1, q_1, q_2, \ldots, q_1^2, 2q_1q_2, \ldots\} \tag{4.16}$$

Therefore, the size of the basis of Eq. (4.16) becomes $N + n_s$, where N is the number of measurements, and $n_s = \binom{l_s+2m+1}{2m+1}$ is the number of monomials $d_{s,u}(\boldsymbol{q})$, $u \in \{1, \ldots, n_s\}$, for a polynomial of degree l_s. In the following, a 4^{th}-degree polynomial is considered in the augmented basis of Eq. (4.16). The rationale for selecting the above basis relates to the fact that for problems of the form of Eq. (2.34), the joint response PDF is Gaussian for $\boldsymbol{g}(\boldsymbol{x}, \dot{\boldsymbol{x}}) = 0$; thus, it is represented exactly by a 2^{nd}-degree polynomial. The nonlinear system joint response PDF can be construed as a perturbation (not necessarily small) from the Gaussian, and it can be approximated by higher-order polynomials. In several examples, including rather challenging cases of bimodal response PDFs [145], it has been demonstrated that the choice of a 4^{th}-degree polynomial reflects a reasonable compromise between accuracy and efficiency. In this regard, enforcing the N interpolation conditions of Eq. (4.12) and adding n_s conditions of the form

$$\sum_{r=1}^{N} c_r d_{s,u}(\boldsymbol{q}_r) = 0, \quad \text{for } u \in \{1, \ldots, n_s\} \tag{4.17}$$

leads to the augmented linear system of equations [59]

$$\begin{bmatrix} \boldsymbol{D} & \boldsymbol{D}_s \\ \boldsymbol{D}_s^T & \boldsymbol{0} \end{bmatrix} \begin{bmatrix} \boldsymbol{c} \\ \boldsymbol{c}_s \end{bmatrix} = \begin{bmatrix} \boldsymbol{y}_0 \\ \boldsymbol{0} \end{bmatrix} \tag{4.18}$$

where $\boldsymbol{D} = [d_1(\boldsymbol{q}_r), \ldots, d_n(\boldsymbol{q}_r)]_{N \times N}$, $\boldsymbol{D}_s = [d_{s,u}(\boldsymbol{q}_r)]_{N \times n_s}$, $\boldsymbol{c}$ denotes the expansion coefficients vector, $\boldsymbol{c}_s$ the polynomial coefficients vector, and $\boldsymbol{y}_0$ the measurement vector. It is noted that the conditions of Eq. (4.17) are arbitrary and have been added for obtaining a non-singular interpolation matrix [59]. Once the system of Eq. (4.18) is solved, the coefficient vector $[\boldsymbol{c}\ ; \boldsymbol{c}_s]$ is determined; see also [190] for more details on the conditions to be satisfied for the well-posedness of Eq. (4.18). Note that although the augmented coefficient vector of Eq. (4.18) is of length $N + n_s > N$, the number of measurements required for the approximation remains the same and equal to N. Further, Eq. (4.15) is modified to account

for the augmented basis, and the non-stationary joint response PDF can be approximated as

$$p\left(\boldsymbol{x}, \dot{\boldsymbol{x}}, t\right) \approx \exp\left\{\left(\sum_{r=1}^{N} c_r d_r(\boldsymbol{x}, \dot{\boldsymbol{x}}, t) + \sum_{u=1}^{n_s} c_{s,u} d_{s,u}(\boldsymbol{x}, \dot{\boldsymbol{x}}, t)\right)\right\} \tag{4.19}$$

4.2.2.3 Selection of shape parameters

Positive definite functions have been criticized for producing ill-conditioned interpolation matrices $\boldsymbol{D}$, and thus, causing numerical instability issues [33]. Note, however, that a careful examination of the matter [59] reveals that there is a trade-off between accuracy and stability. Theoretical bounds pertaining to several positive definite functions indicate that by decreasing the values of the shape parameters ϵ_p in Eq. (4.13), or the separation distance between the sampling locations (i.e., by increasing N), the accuracy of the interpolation is improved. Nevertheless, this theoretically attainable accuracy is hard to be reached in practice. This is due to numerical stability issues related to the rapid increase of the interpolation matrix condition number. This trade-off has led researchers to seek for "optimal" shape parameters, which provide high accuracy without compromising numerical stability [126].

The approach adopted in the ensuing analysis was developed in [150] and is based on leave-one-out cross validation. Specifically, for fixed shape parameters ϵ_s and ϵ_t, fitting an interpolant of the form of Eqs. (4.12) and (4.18) to $N-1$ measurements N times (one is left out each time) yields an interpolation error E_r, for $r \in \{1, \ldots, N\}$, by comparing the interpolant with the measurement left out. The error, E, associated with the pair $(\epsilon_s,\, \epsilon_t)$ is then selected to be the maximum of all the errors E_r. Therefore, the error associated with the pair $(\epsilon_s,\, \epsilon_t)$ becomes the cost function in an optimization algorithm that searches for the pair $(\epsilon_s,\, \epsilon_t)$ with the minimum error E. Finally, as stated in Section 4.2.2.2, introducing the anisotropic Gaussian function of Eq. (4.13) also improves the condition number of the interpolation matrix as a "side-effect". Of course, alternative approaches such as preconditioning [59], or exploration of other bases [142], can always be used for addressing cases

of ill-conditioned matrices.

4.2.3 Mechanization of the technique

The mechanization of the Kronecker product approach of Section 4.2.1 involves the following steps:

(a) Select P lower dimensional bases $\boldsymbol{D}_1, \ldots, \boldsymbol{D}_P$.

(b) Create the interpolation matrix $\boldsymbol{D} = \boldsymbol{D}_P \otimes \cdots \otimes \boldsymbol{D}_2 \otimes \boldsymbol{D}_1$.

(c) Obtain $N = n_1 n_2 \ldots n_P$ measurements of the PDF via the WPI by utilizing Eq. (2.63).

(d) Determine the coefficient vector $\boldsymbol{c}$ by solving the linear system of Eq. (4.6).

(e) The complete non-stationary joint response PDF is evaluated by employing the Kronecker product basis and the coefficient vector via Eqs. (4.2) and (4.6).

Further, the mechanization of the positive definite functions approach of Section 4.2.2 involves the following steps:

(a) Select the N basis functions of Eq. (4.16), in conjunction with Eq. (4.13).

(b) Obtain N measurements of the PDF via the WPI by utilizing Eq. (2.63) and by employing the Halton sequence for selecting the locations of the measurements [82].

(c) Determine the coefficient vector $\boldsymbol{c}$ by solving the linear system of Eq. (4.18).

(d) The complete non-stationary joint response PDF is approximated via Eq. (4.19).

4.2.4 Sparse representations and compressive sampling

Compressive sampling (or compressive sensing) procedures are currently revolutionizing the signal processing field [65, 151]. In this section it is shown that by relying on compressive

sampling concepts, and by exploiting additional information regarding $p(\boldsymbol{x}, \dot{\boldsymbol{x}}, t)$, the approximation scheme of Eq. (4.1) can become even more efficient computationally. The rationale of the herein proposed enhancement relates to using the least amount of joint response PDF measurements (i.e., $R \ll N$ measurements obtained using the WPI technique) for computing the coefficient vector $\boldsymbol{c}$.

If only $R < N$ measurements are obtained, Eq. (4.1) takes the form of an underdetermined linear system, which can be written as

$$\boldsymbol{y} = \boldsymbol{\Phi} \boldsymbol{y}_0 = \boldsymbol{\Phi} \boldsymbol{D} \boldsymbol{c} = \boldsymbol{V} \boldsymbol{c} \tag{4.20}$$

In Eq. (4.20) $\boldsymbol{\Phi}$ is an $R \times N$ matrix, also known as compressive sampling matrix [18] as it randomly deletes rows of $\boldsymbol{y}_0$ and $\boldsymbol{D}$. The underdetermined system of Eq. (4.20) has either no solution, or an infinite number of solutions. Nevertheless, in many cases there is additional information available concerning the coefficient vector $\boldsymbol{c}$. For instance, if only a small number of its components, say K out of N components, are nonzero, then the problem can be regularized and there has been extensive research during the past decade on solution procedures [52]. In particular, the sufficiently sparse ($K \ll N$) coefficient vector $\boldsymbol{c}$ is typically referred to as K-sparse. For such cases, searching for the vector $\hat{\boldsymbol{c}}$ with the least amount of elements that satisfies the condition $\boldsymbol{y} = \boldsymbol{V} \hat{\boldsymbol{c}}$ constitutes a non-convex optimization problem. Although this problem has a unique solution if $\boldsymbol{V}$ has certain desired properties and the number of measurements, R, is sufficiently large (e.g., [151]), it is known to be NP-hard (where NP stands for nondeterministic polynomial time), or in other words, there is no known algorithm for solving it efficiently (e.g., [132]).

To address the above challenge, greedy algorithms can be used to find an approximate solution of the original non-convex problem [52]. Alternatively, the regularization constraint can be relaxed. For example, instead of seeking for the solution with the least amount of elements (or in other words, with the minimum ℓ_0-norm), the solution with the minimum

ℓ_1-norm is sought for, alternatively. The problem becomes, therefore, convex and can be readily solved via standard numerical algorithms. However, the price to be paid for such a relaxation approach relates to increasing the number of measurements, R, required for a unique solution [151]; see also [27, 201].

The main question in such problems relates to the properties that $\boldsymbol{V}$ should have in order for the aforementioned minimization problem to have a unique solution. Also, depending on the type of $\boldsymbol{V}$ selected, knowledge of the number of measurements for nearly exact recovery of the coefficient vector $\boldsymbol{c}$ is required in an a priori manner. The latter is known in the sparse representations literature as measurement bound, as a lower bound of R measurements guaranteeing nearly exact recovery of $\boldsymbol{c}$ is sought for; see, e.g., [17] for an introduction to the topic. In this regard, theoretical measurement bounds exist only for certain classes of matrices, e.g., for Gaussian matrices $\boldsymbol{V}$, or random submatrices of bounded orthonormal systems, such as Fourier, Wavelet and Legendre bases (see [65, 148, 181]). These bounds typically show how the order of magnitude of the required number of measurements R changes with increasing dimension N, and sparsity K. Therefore, they are mainly useful for comparing the performances of various optimization algorithms and for providing with an indicative number of measurements. In Section 4.2.7, a more general approach is described, which is often used in practical applications.

4.2.5 Sparse polynomial approximation and group sparsity

As explained in the beginning of Section 4.2 approximating the time-dependent response PDF $p(\boldsymbol{x}, \dot{\boldsymbol{x}}, t)$ leads to the linear system Eq. (4.3). Further, if only $R < N$ measurements are collected the expansion coefficients vector $\boldsymbol{c}$ is obtained by solving the underdetermined system of Eq. (4.20). However, note that approximating the response PDF of any system the form of Eqs. (2.34), (2.66), or even (3.2) would lead to Eq. (4.3) or Eq. (4.20) if N or $R < N$ measurements were collected, respectively. In this regard, without loss of generality, the case of determining the response PDF $p(\boldsymbol{x}, \dot{\boldsymbol{x}}, t)$ of Eq. (4.1) at given time instants is

considered in this section. Thus, the only variables in the approximation are $\boldsymbol{x}$ and $\dot{\boldsymbol{x}}$ and the PDF at a given time instant can be written as $p(\boldsymbol{x}, \dot{\boldsymbol{x}})$.

Although approximation strategies based on univariate functions are considered a well-developed topic, there is still active research in approximation schemes utilizing multivariate polynomials (see for example [68]). In the ensuing analysis and in accordance with the rationale presented in Section 4.2.2.2, the monomial basis (e.g., [140]) is adopted for approximating the exponent of the joint response PDF in Eq. (4.1), and therefore a polynomial approximation is constructed.

Further, to determine the polynomial approximation coefficients, $N = \binom{l_s+2m}{2m}$ points from $\mathbb{R}^{2m}$ need to be chosen, for an l_s-degree polynomial. These are the points at which the joint response PDF is sampled using the WPI technique and can be selected either randomly, or based on some kind of optimality criterion to enhance the robustness and accuracy of the approximation (see, e.g., [186]). As noted by Sommariva & Vianello [170], choosing "optimal" approximation points can, also, overcome certain numerical issues that typically accompany the monomial basis, such as the handling of resulting ill-conditioned Vandermonde matrices.

Next, the monomials are ordered based on the graded lexicographical order, which for a 10-DOF dynamical system, for instance, would take the form

$$1 \prec x_1 \prec \cdots \prec \dot{x}_{10} \prec \underbrace{x_1^2 \prec 2x_1x_2 \prec x_2^2 \prec 2x_1x_3 \prec 2x_2x_3 \prec x_3^2 \cdots \prec \dot{x}_{10}^2}_{\text{monomials of order 2}} \prec \ldots \tag{4.21}$$

Interestingly, this ordering scheme becomes important in the context of sparse polynomial approximation. Numerical examples involving arbitrary nonlinear systems of the form of Eq. (2.34) have demonstrated that the coefficients corresponding to the Gaussian part of the exponent, i.e., monomials of order 2, are always nonzero, whereas only few of the higher order coefficients are nonzero. In particular, the fact that Gaussian coefficients form a group, which is always active, serves as an additional piece of information that can be exploited. In

the framework of sparse representations, this corresponds to group (or structured) sparsity, which is a term describing any kind of structure that the coefficient vector is known to have [90]. For the group sparsity to be considered and exploited, the standard compressive sampling algorithms need to be modified as delineated in the following section. In this regard there are both convex (e.g., [10]) and non-convex approaches (e.g., [86]).

4.2.6 Optimization algorithm

In the ensuing analysis, the StructOMP greedy algorithm proposed by Huang *et al.* [86] is adopted for addressing the original non-convex problem. It can be construed as a generalization of the widely used Orthogonal Matching Pursuit (OMP) algorithm [185] and is preferred in the ensuing numerical examples over alternative convex approaches, such as Group-LASSO [199]. In fact, for various typical stochastic dynamics problems of the form of Eq. (2.34), StructOMP has exhibited superior performance, both in terms of convergence rate and of approximation accuracy.

Specifically, the input to StructOMP is the R-length measurement vector $\boldsymbol{y}$, the $R \times N$ matrix $\boldsymbol{V}$ and the group structure (in the form of blocks) that the coefficient vector is anticipated to exhibit. In the herein considered applications the coefficient vector is separated into blocks, with every block corresponding to a single monomial, except for the second-order monomials that are grouped together. In standard sparse vectors, each component of the coefficient vector is considered to have complexity 1. This means that if this coefficient is active, then the coefficient vector will be less sparse by 1. In group sparse vectors each block is assigned a value that describes its complexity, which depends on its coding length (see the original paper by Huang *et al.* [86] for more details). Obviously, all the single monomials are assigned the same complexity value, whereas the grouped monomials are assigned higher complexity values than the single ones. Additionally, the total complexity of the coefficient vector, S, is the sum of the individual complexities of the blocks used to construct it.

As in Section 4.2.4, $\boldsymbol{c}$ denotes the original coefficient vector that solves the system of

Eq. (4.3) and $\hat{\boldsymbol{c}}$ the estimated one that solves the system of Eq. (4.20) using StructOMP. The algorithm selects which block reduces the approximation error

$$err = \|\boldsymbol{y} - \boldsymbol{V}\hat{\boldsymbol{c}}\|_2 \tag{4.22}$$

per unit increase of complexity the most (this block is considered to provide the maximum progress to the algorithm), and then assigns values to the coefficients of the selected block via least squares regression. Subsequently, the algorithm finds the next block with the maximum progress and terminates either when err becomes smaller than a prescribed threshold or when the complexity of $\hat{\boldsymbol{c}}$ becomes larger than a prescribed value. For the Performance Analysis in Section 4.2.7 the latter is used, because the recovery error is measured for fixed complexity S. On the contrary, in the numerical examples in Section 4.3 the former is used, since the goal is to minimize the recovery error even if a less sparse (or more complex) coefficient vector is used in the expansion.

4.2.7 Performance analysis

As noted in Section 4.2.6, the input to the StructOMP algorithm is the R-length measurement vector $\boldsymbol{y}$, the $R \times N$ matrix $\boldsymbol{V}$ (where $\boldsymbol{V} = \boldsymbol{\Phi}\boldsymbol{D}$) and the group structure that the coefficient vector $\boldsymbol{c}$ is anticipated to have. Thus, a decision has to be made a priori regarding the number R of measurements, the degree of the multivariate polynomial to be used and the group structure provided as input to StructOMP. First, the degree of the polynomial expansion is selected and the basis matrix $\boldsymbol{D}$, and thus, $\boldsymbol{V}$ is constructed. Next, the group structure is formed using the group of second-order monomials, while the remaining monomials are considered separately as single monomials. Based on the rationale explained in Sections 4.2.5 and 4.2.6, since the group of second-order monomials is always active, the complexity of the coefficient vector is directly related only to the number of single monomials (NSM). In addition, given that the more complex the coefficient vector is the more

measurements are needed for its accurate recovery, the number of measurements R depends solely on NSM. Therefore, the anticipated NSM has to be decided a priori and a tool is needed to find the corresponding required number of joint response PDF measurements R.

In the absence of theoretical results, novel algorithms are typically tested with the aid of synthetic data before being used in practical applications [43, 44, 89, 185]. In this regard, based on the experimental set-up described below, empirical measurement bounds are determined, guaranteeing coefficient vector estimates with bounded error. In particular, for a monomial basis, coefficient vectors with synthetic data are created, with varying numbers of single monomials, and hence, with varying total complexity, S. Next, a value is assigned randomly (e.g., from a Gaussian distribution; see [185]) to each nonzero component, and recovery of these vectors is attempted using StructOMP with only $R < N$ measurements and coefficient vector complexity S. Finally, the average recovery error

$$\frac{\|\boldsymbol{c} - \hat{\boldsymbol{c}}\|_2}{\|\boldsymbol{c}\|_2} \tag{4.23}$$

is measured over 100 independent runs of the algorithm for each pair $(R/N,\ S/R)$, and the result is shown in Fig. 4.1. It is observed that for every R/N there is a value of S/R above which sparse approximation becomes relatively inaccurate, or in other words, it changes *phase* (e.g., [44]). This is the reason why the plot in Fig. 4.1, illustrating the transition from highly accurate recovery (blue) to recovery with significant error (red), is commonly called *Phase Diagram* (e.g., [44]).

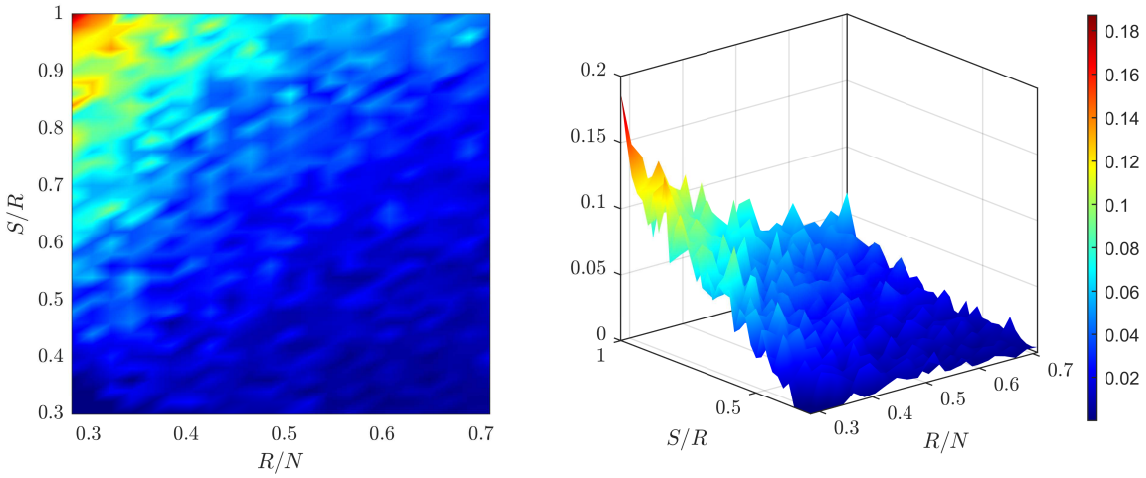

Figure 4.1: Phase Diagram for StructOMP using the Monomial Basis. The z-axis corresponds to the average normalized ℓ_2 recovery error, $\frac{\|\boldsymbol{c}-\hat{\boldsymbol{c}}\|_2}{\|\boldsymbol{c}\|_2}$, over 100 runs; the x-axis corresponds to the ratio showing how much underdetermined the problem is, whereas the y-axis corresponds to the ratio showing the level of complexity of the coefficient vector.

The quantities R/N and S/R in Fig. 4.1 are non-dimensional. Therefore, to use Fig. 4.1 for creating a measurement bounds plot for an m-DOF system, the actual dimension of the coefficient vector, N, is substituted into R/N. In this regard, the x-axis corresponds to the required number of measurements R, while the y-axis corresponds to the NSM of the coefficient vector. Specifically, for a 10-DOF dynamical system of the form of Eq. (2.34) with 20 stochastic dimensions and considering a fourth-order polynomial expansion, N becomes 10,626. Fig. 4.2 shows the estimated measurement bounds for $N = 10{,}626$ with the complexity S represented by the NSM of the coefficient vector. Indicatively, for a 10-DOF linear dynamical system of the form of Eq. (2.34), only the group of second-order monomials is active, because the joint response PDF is Gaussian, and thus, NSM is equal to zero. Therefore, as shown in Fig. 4.2 the coefficient vector for such a system can be recovered with less than $R = 3{,}000$ measurements of the joint response PDF using the WPI technique and with average normalized error less than 3%. For a 10-DOF nonlinear dynamical system of the form of Eq. (2.34), with a non-Gaussian response PDF, NSM is nonzero and as shown in Fig. 4.2 the number of measurements R has to increase accordingly. Further, a significant additional advantage of employing a sparse approximation treatment relates to the a priori

knowledge about the sensitivity of the technique. As shown in Fig. 4.2 an estimate of the expected increase of the error is readily available in case the coefficient vector sparsity is not predicted accurately.

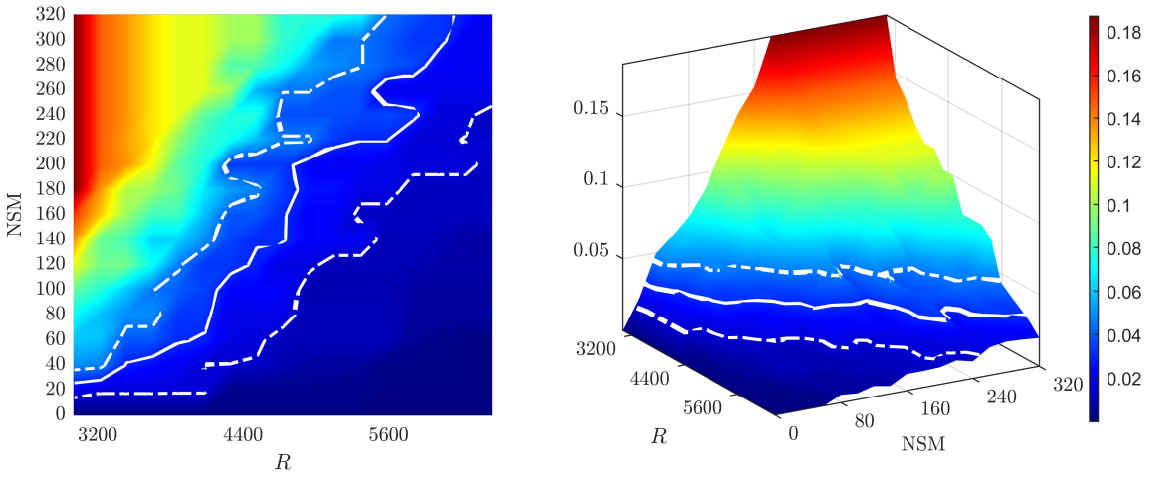

Figure 4.2: Measurement bounds for $N = 10{,}626$, corresponding to $m = 10$ and a fourth-order polynomial approximation using StructOMP. The z-axis corresponds to the average normalized ℓ_2 recovery error, $\frac{\|\boldsymbol{c}-\hat{\boldsymbol{c}}\|_2}{\|\boldsymbol{c}\|_2}$, over 100 runs; the x-axis corresponds to the ratio showing how much underdetermined the problem is, whereas the y-axis corresponds to the ratio showing the level of complexity of the coefficient vector. The white solid line indicates the required number of measurements for the error to be smaller than 3%, while the white dashed lines show the deviation of the error by ±1%.

4.2.8 Wiener path integral computational efficiency enhancement

For any m-DOF system of the form of Eq. (2.34), the joint response PDF can be described by Eq. (4.1) with a length N coefficient vector. Therefore, plots similar to Fig. 4.2 can be constructed for any dimension m. Such plots are useful for deciding on the number of required measurements and for providing an estimate for the coefficient vector complexity. For instance, for an error less than 3% and selecting the number of single monomials to be 10% of the Gaussian coefficients (see Fig. 4.2) the required number of measurements can be found for an arbitrary system of m DOFs. In this regard, Fig. 4.3 shows how the required number of measurements grows with increasing dimension of the system, m. This number is compared with the respective one required for cases where the formulation does not yield an

underdetermined problem; that is, the number of measurements is equal to the number of coefficients in the expansion yielding a power law function of the form $\sim(2m)^{l_s}/l_s!$ (see [104]). Further, the number of coefficients corresponding to a linear system response multivariate Gaussian PDF is included as well. It can be readily seen that the proposed approach can be orders of magnitude more efficient than both a brute-force numerical implementation of the WPI [103], and the approximate technique developed by Kougioumtzoglou *et al.* [104]. Most importantly, as shown in Fig. 4.3, this enhancement in efficiency becomes even more prevalent as the number of DOFs (or equivalently the number of stochastic dimensions) increases; thus, rendering the herein proposed sparse representation approach indispensable, especially for high-dimensional systems. Of course, it is noted that Fig. 4.3 shows an indicative rate of growth of R. Systems with complex nonlinearities may require a larger number R. Thus, it is suggested to terminate the StructOMP algorithm only after the addition of a new block does not cause any further reduction of the approximation error in Eq. (4.22) (see Section 4.2.6 for more details).

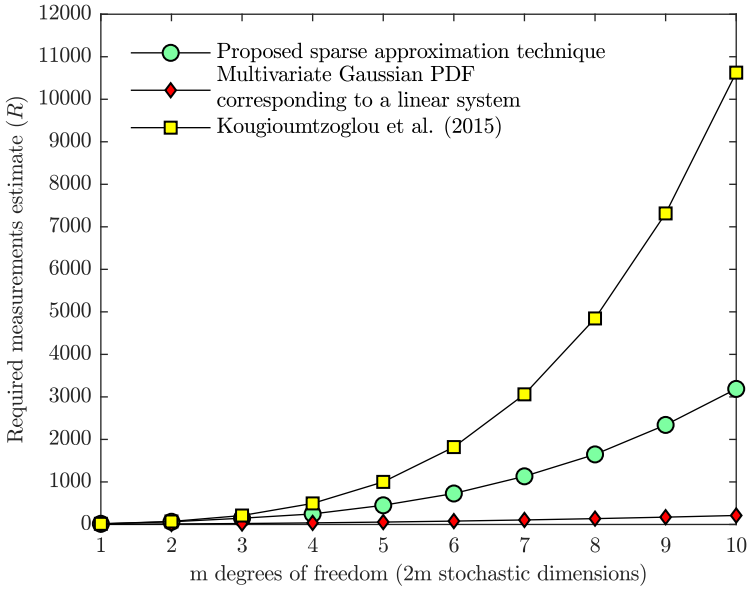

Figure 4.3: Required measurements estimate for a general m-DOF system by utilizing the developed sparse approximation technique, and compared with the technique in [104]; the number of measurements required for a multivariate Gaussian PDF is included for completeness.

4.2.9 Mechanization of the sparse polynomial approximation technique

The mechanization of the developed technique involves the following steps:

(a) Select the polynomial degree l_s and $N = \binom{l_s+2m}{2m}$ points of $\mathbb{R}^{2m}$, either randomly (e.g., uniformly distributed), or by employing optimal point selection methodologies (see, e.g., [186]).

(b) Create the basis matrix $\boldsymbol{D}$.

(c) Relying on Fig. 4.3, select only R out of these N points randomly (e.g., uniformly distributed).

(d) Evaluate $\log\left(p(\boldsymbol{x}, \dot{\boldsymbol{x}})\right)$ at these R points using the WPI technique (Eq. (2.63)).

(e) Estimate the coefficient vector $\boldsymbol{c}$ using StructOMP (or an alternative appropriate optimization algorithm).

(f) The joint response PDF is given by Eq. (4.1).

4.3 Numerical examples

To assess the performance and demonstrate the efficacy of the developed approximation schemes, four examples with distinct features are considered. In Section 4.3.1, two SDOF Duffing nonlinear oscillators subject to Gaussian white noise are considered: one with a standard hardening restoring force (Section 4.3.1.1), and another exhibiting a bimodal response PDF (Section 4.3.1.2). In Section 4.3.1.1 the Kronecker product approach with a 4^{th}-degree polynomial for the spatial dimensions and an one-dimensional wavelet basis for the temporal dimension is used, whereas in Section 4.3.1.2 a basis constructed via a Kronecker product of three one-dimensional wavelet bases is employed. Further, in the example of Section 4.3.1.2 the sparse approximation scheme developed in Section 4.2.4 is utilized

and the obtained results are compared with the analytical exact solution for the stationary response PDF. Next, in Section 4.3.2 a 2-DOF nonlinear oscillator subject to non-stationary time-modulated Gaussian white noise is considered, and the positive definite functions approach of Section 4.2.2 is employed. Moreover, the positive definite functions approach is also employed in Section 4.3.3, where a statically determinate Euler-Bernoulli beam is considered with Young's modulus modeled as a non-Gaussian, non-white and non-homogeneous stochastic field. Finally, in Section 4.3.4 the 20-variate joint response transition PDF of a 10-DOF nonlinear structural system under stochastic excitation is determined by utilizing the sparse approximation scheme of Section 4.2.4.

4.3.1 SDOF Duffing nonlinear oscillator

4.3.1.1 SDOF Duffing oscillator with a hardening restoring force

Consider an SDOF Duffing oscillator, whose equation of motion is given by Eq. (2.34) with parameter values ($\boldsymbol{M} = 1$; $\boldsymbol{C} = 0.1$; $\boldsymbol{K} = 1$; $\boldsymbol{g} = x^3$; and $S_0 = 0.0637$). Assuming quiescent initial conditions, its transition PDF, written as $p(x, \dot{x}, t)$, is a function of the two spatial dimensions, i.e., x and $\dot{x}$, and of the temporal dimension t. In implementing the approximate WPI technique developed herein, the monomial basis is used for the two spatial dimensions, while the wavelet basis is used for the temporal dimension as discussed in Section 4.2.1.2. In particular, utilizing a 4^{th}-degree polynomial, the joint response PDF is sampled at $N = n_s n_t = 15 \times 32 = 480$ locations in the spatio-temporal domain and the expansion coefficient vector $\boldsymbol{c}$ is determined by solving Eq. (4.9). Finally, $p(x, \dot{x}, t)$ is approximated by utilizing the constructed basis and the coefficient vector via Eq. (4.6). The non-stationary marginal PDFs of $x(t)$ and $\dot{x}(t)$ are shown in Fig. 4.4, where it is seen that the oscillator response PDF does not experience any significant changes after about $t = 6$s; that is, the system has reached stationarity effectively. Moreover, the marginal PDFs of $x(t)$ and $\dot{x}(t)$ for two arbitrary time instants are shown in Fig. 4.5. Although the accuracy of the

technique depends, in general, on the choice of the polynomial degree and the number of points in the temporal dimension, it is shown in this example that a 4^{th}-degree polynomial and $n_t = 32$ points are adequate in determining the non-stationary PDF of this Duffing oscillator with high accuracy as compared to pertinent MCS data (50,000 realizations).

To provide a rough comparison and highlight the gain of the proposed technique in terms of computational efficiency, it is worth noting that a brute-force numerical implementation of the WPI technique as described in Section 2.4.3 would require a number of PDF measurements of the order of $\sim 10^6$ (assuming that the temporal dimension is, indicatively, discretized into 1,000 points). Further, the approximation based on polynomials and wavelets employed in this example also requires a smaller number of measurements as compared to the efficient implementation of [104]. Specifically, by utilizing the approximate technique developed in [104] the response PDF needs to be separately determined at every time instant, which (for an indicative discretization of the time domain into 1,000 points) yields approximately 35,000 required PDF measurements via the WPI technique.

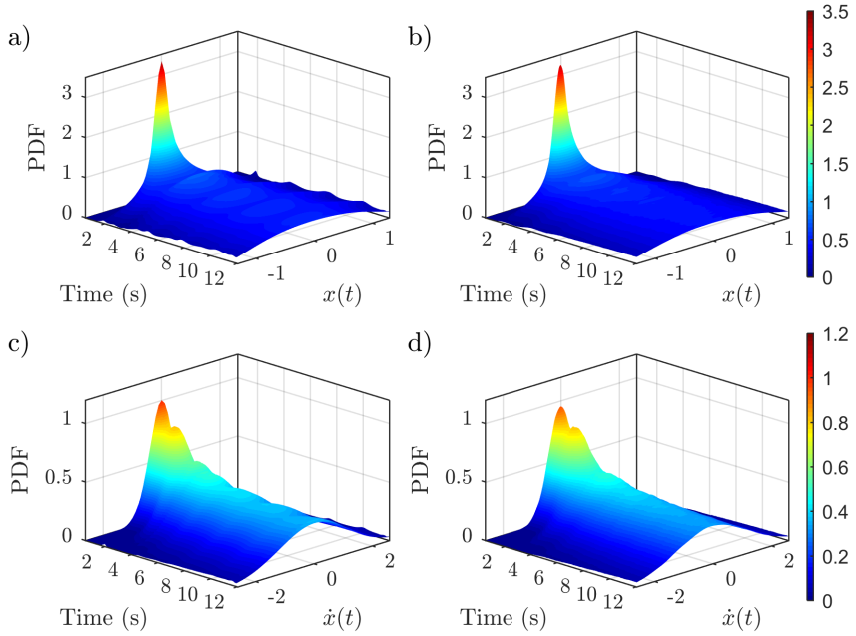

Figure 4.4: Non-stationary marginal PDF of $x(t)$ and $\dot{x}(t)$ for an SDOF hardening Duffing oscillator under Gaussian white noise excitation, as obtained via the WPI technique (a and c); comparisons with MCS data - 50,000 realizations (b and d).

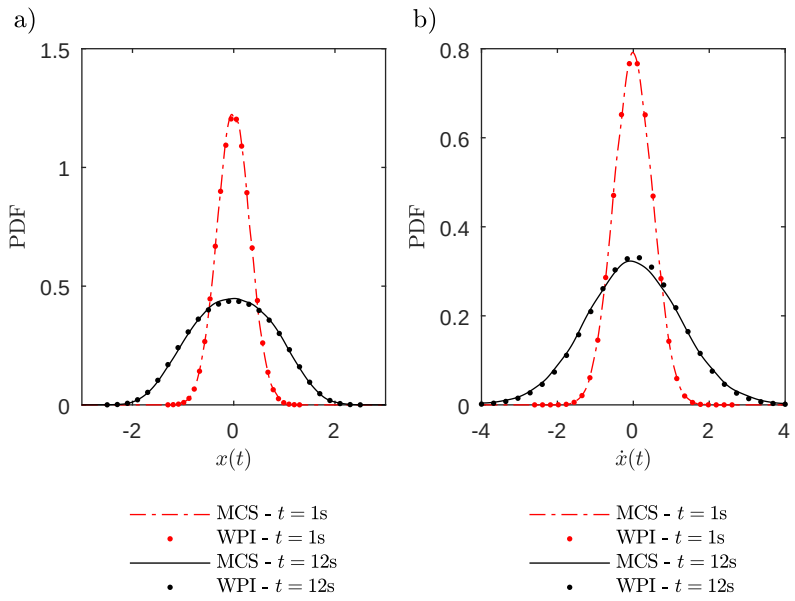

Figure 4.5: Marginal PDFs of $x(t)$ (a) and $\dot{x}(t)$ (b) at time instants $t = 1$s and $t = 12$s for an SDOF hardening Duffing oscillator under Gaussian white noise excitation, as obtained via the WPI technique; comparisons with MCS data (50,000 realizations).

4.3.1.2 SDOF Duffing oscillator with a bimodal response PDF

Although example 4.3.1.1 has shown that utilizing a Kronecker product of a polynomial and a wavelet bases can be adequate for a certain class of problems, the resulting interpolation matrix may often be ill-conditioned. Such is the case of the SDOF oscillator, whose equation of motion is given by Eq. (2.34) with parameter values ($\boldsymbol{M} = 1$; $\boldsymbol{C} = 1$; $\boldsymbol{K} = -0.3$; $\boldsymbol{g} = x^3$) and external excitation as in example 4.3.1.1. In fact, attempting to use the same basis as in 4.3.1.1 has led to ill-conditioning. To bypass this limitation, a multi-dimensional wavelet basis is instead utilized for this case, as discussed in Section 4.2.1.2. In this regard, a mesh is employed for discretizing the three-dimensional spatio-temporal domain characterizing the transition PDF. Specifically, following the procedure delineated in Section 4.2.1.2 the two spatial dimensions are discretized into $n_1 = n_2 = 16$ points and the temporal dimension into $n_t = 32$ points; thus, yielding $N = 8,192$ required measurements via the WPI technique. To put it into perspective, note that a brute-force implementation of the technique would require a number of PDF measurements of the order of $\sim 10^6$, while applying the efficient

implementation of [104] for each and every time instant would yield approximately $35,000$ required measurements (assuming that the temporal dimension is, indicatively, discretized into 1,000 points). Following the determination of the expansion coefficient vector $\boldsymbol{c}$ by solving Eq. (4.6), where all basis matrices correspond to the wavelet basis in each dimension, $p(x,\dot{x},t)$ is approximated based on Eq. (4.1). In this regard, $p(x,\dot{x},t)$ can be approximated at any location by utilizing the constructed basis and the coefficient vector. In Fig. 4.6 the joint response PDF $p(x,\dot{x},t)$ is shown at three arbitrary time instants $t=1,2$ and 6s. Comparisons with corresponding MCS based results demonstrate the relatively high accuracy of the technique for addressing dynamical systems even with relatively complex PDF shapes, such as the bimodal. Finally, in Figs. 4.7 and 4.8 the marginal PDFs of $x(t)$ and $\dot{x}(t)$ are shown for various time instants, as obtained by utilizing the herein developed technique. Pertinent MCS based results (50,000 realizations) are included as well for comparison purposes. Overall, it is seen that for this specific numerical example the gain of the proposed technique in terms of computational efficiency, as compared both to the standard [103] (see also Section 2.4.3) and to the enhanced [104] implementations, is drastic. It is worth noting that the herein developed technique based on global bases can be potentially coupled with sparsity concepts and compressive sampling for further reducing the associated computational cost (see 4.2.4).

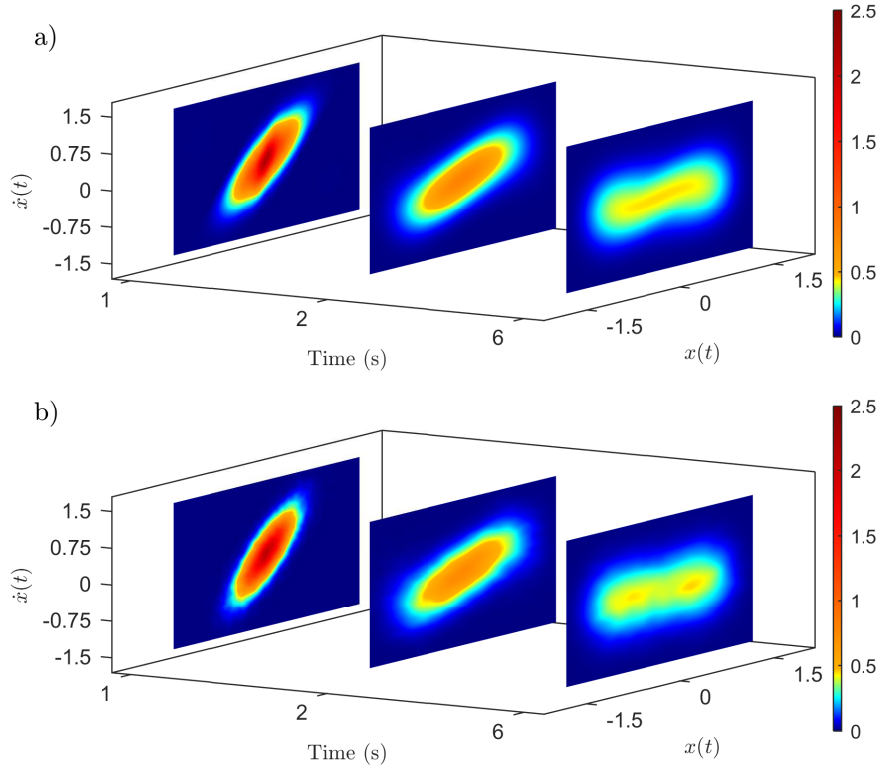

Figure 4.6: Non-stationary joint PDF of $x(t)$ and $\dot{x}(t)$ at time instants $t = 1, 2$ and 6s for an SDOF Duffing oscillator with bimodal response PDF under Gaussian white noise excitation, as obtained via the WPI technique (a); comparisons with MCS data - 50,000 realizations (b).

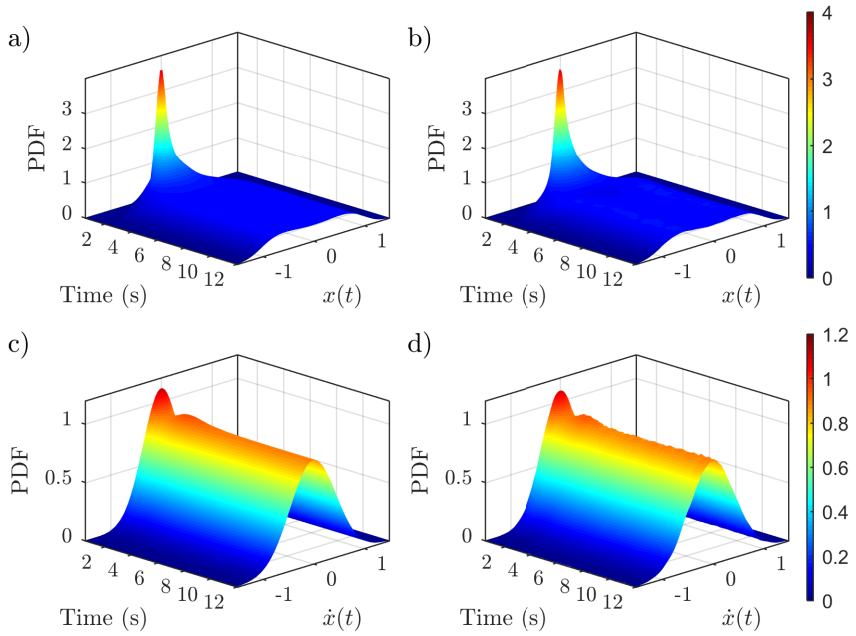

Figure 4.7: Non-stationary marginal PDF of $x(t)$ and $\dot{x}(t)$ for an SDOF Duffing oscillator with bimodal response PDF under Gaussian white noise excitation, as obtained via the WPI technique (a and c); comparisons with MCS data - 50,000 realizations (b and d).

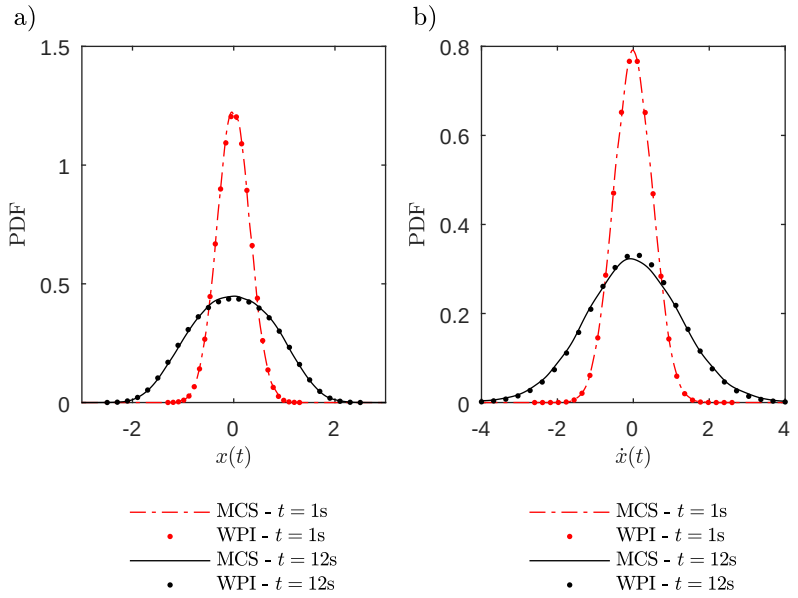

Figure 4.8: Marginal PDFs of $x(t)$ (a) and $\dot{x}(t)$ (b) at time instants $t = 1$s and $t = 12$s for an SDOF Duffing oscillator with bimodal response PDF under Gaussian white noise excitation, as obtained via the WPI technique; comparisons with MCS data (50,000 realizations).

In addition, focusing on the case of determining the response PDF at a given time instant,

as shown in Fig. 4.3 the advantage of the sparse approximation technique of Section 4.2.4 as compared to the implementation of [104] becomes more significant for relatively high-dimensional problems. However, to demonstrate the efficacy of the technique in determining accurately even relatively complex response PDF shapes, the herein considered SDOF Duffing nonlinear oscillator that exhibits a bimodal response PDF is also addressed by utilizing the sparse approximation technique. It is noted that an exact analytical expression exists for the stationary joint response PDF of this oscillator, given by [114]

$$p(x,\dot{x}) = C\exp\left(\frac{-1}{0.0637\pi}\left[\frac{-0.3x^2}{2}+\frac{x^4}{4}+\frac{\dot{x}^2}{2}\right]\right) \tag{4.24}$$

where C is a normalization constant. Thus, in addition to utilizing pertinent MCS data, the accuracy degree of the WPI technique can be assessed by direct comparisons with Eq. (4.24) as well. Next, in implementing the WPI technique summarized in Section 4.2.9, a 4-th degree polynomial is employed for approximating the response transition PDF $p(x_f,\dot{x}_f,t_f|x_i,\dot{x}_i,t_i)$. The number of the expansion coefficients is $N=15$, however, resorting to the sparse approximation technique only $R=9$ PDF measurements obtained by the WPI are used for determining the joint response PDF of the displacement x and the velocity $\dot{x}$ at a given time instant.

In Fig. 4.9 the marginal PDFs of x and $\dot{x}$ referring to time instants $t=1$s and $t=12$s are shown. For the time instant $t=1$s, which corresponds to the transient phase of the oscillator dynamics, the high accuracy degree of the technique is demonstrated by comparisons with MCS data (50,000 realizations). For the time instant $t=12$s, which corresponds to the stationary phase of the oscillator dynamics, the high accuracy degree is demonstrated by comparisons with the exact analytical expression given by Eq. (4.24). Although the accuracy of the technique depends, in general, on the choice of the polynomial degree, it has been shown in this example that a 4-th degree polynomial is adequate in capturing even relatively complex PDF shapes, such as the bimodal.

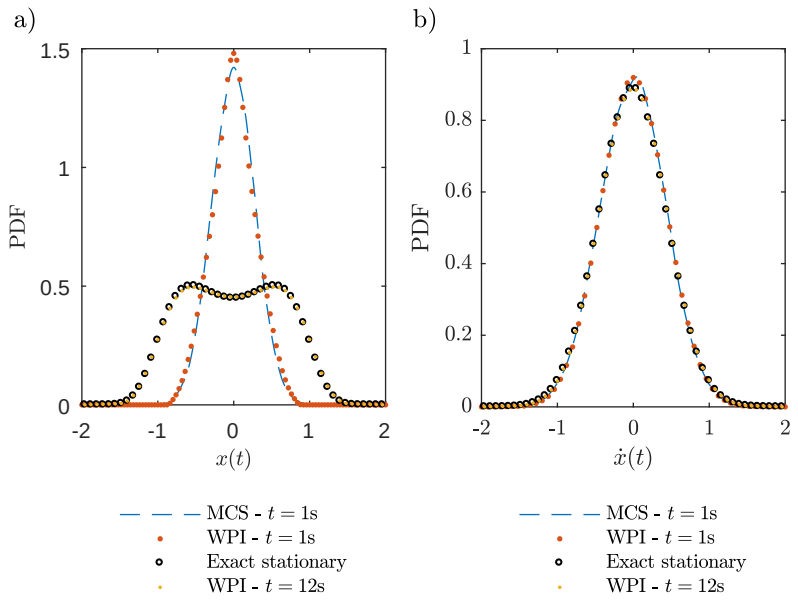

Figure 4.9: Marginal PDFs of $x(t)$ and $\dot{x}(t)$ at time instants $t = 1$s and $t = 12$s for a Duffing oscillator with a bimodal response PDF, as obtained via the WPI technique; comparisons with MCS data (50,000 realizations) and the exact stationary PDF of Eq. (4.24).

4.3.2 MDOF nonlinear oscillator subject to non-stationary time-modulated Gaussian white noise

In this section the efficacy of the mesh-free approximate WPI technique presented in Section 4.2.2 is assessed, in conjunction with a 2-DOF nonlinear dynamical system whose equation of motion is given by Eq. (2.66) with

$$\boldsymbol{M} = \begin{bmatrix} m_0 & 0 \\ 0 & m_0 \end{bmatrix}, \tag{4.25}$$

$$\boldsymbol{C} = \begin{bmatrix} 2c_0 & -c_0 \\ -c_0 & 2c_0 \end{bmatrix}, \tag{4.26}$$

$$\boldsymbol{K} = \begin{bmatrix} 2k_0 & -k_0 \\ -k_0 & 2k_0 \end{bmatrix}, \tag{4.27}$$

and

$$\boldsymbol{g}(\boldsymbol{x}, \dot{\boldsymbol{x}}) = \begin{bmatrix} \epsilon_1 k_0 x_1^3 \\ 0 \end{bmatrix} \tag{4.28}$$

and parameter values ($m_0 = 1$; $c_0 = 0.35$; $k_0 = 0.5$; $\epsilon_1 = 0.2$; and $S_0 = 0.1$). The matrix $\boldsymbol{\Gamma}(t)$ of Eq. (2.67) containing the time-modulating functions $\gamma_1(t)$ and $\gamma_2(t)$ is diagonal with

$$\gamma_1(t) = \gamma_2(t) = \theta_1 + \theta_2(e^{-\theta_3 t} - e^{-\theta_4 t}) \tag{4.29}$$

and parameters values ($\theta_1 = 10^{-3}$; $\theta_2 = 5$; $\theta_3 = 0.4$; and $\theta_4 = 1.6$). The non-stationary excitation power spectrum is, thus, given as

$$\boldsymbol{PS_w} = \begin{bmatrix} PS_w(t) & 0 \\ 0 & PS_w(t) \end{bmatrix}, \tag{4.30}$$

where $PS_w(t) = S_0\gamma_1^2(t) = S_0\gamma_2^2(t)$ is shown in Fig. 4.10.

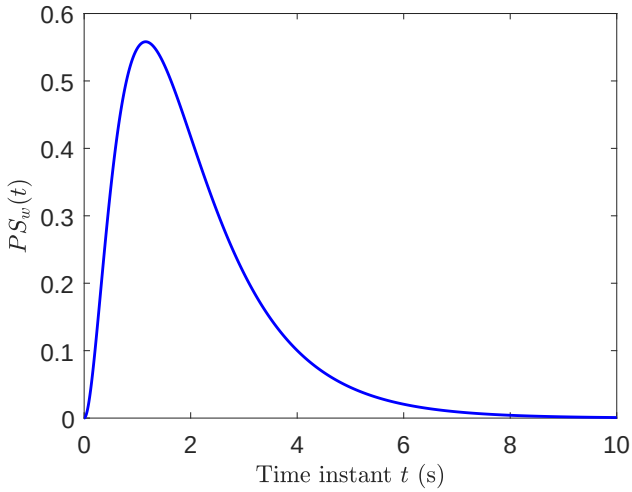

Figure 4.10: Non-stationary Gaussian white noise excitation power spectrum, given by Eq. (4.30), where $PS_w(t) = S_0\gamma_1^2(t) = S_0\gamma_2^2(t)$ and $\gamma_1(t) = \gamma_2(t) = \theta_1 + \theta_2(e^{-\theta_3 t} - e^{-\theta_4 t})$ with parameter values ($S_0 = 0.1$; $\theta_1 = 10^{-3}$; $\theta_2 = 5$; $\theta_3 = 0.4$; and $\theta_4 = 1.6$).

Considering the system initially at rest, the joint response PDF $p\,(\boldsymbol{x}, \dot{\boldsymbol{x}}, t)$ is sampled at $N = 60{,}000$ Halton points (see Section 4.2.2 for more details). Note that this is a rather

challenging example from an approximation theory perspective due to the fact that the response PDF is non-stationary. As a result, the bounds of the effective PDF domain may vary continuously with time in an arbitrary manner. In this regard, if the bounds are pre-specified and fixed, there are measurements of the PDF whose values are effectively zero; thus, causing numerical instabilities in the approximation. This challenge can be addressed by considering "adaptive" bounds, whose time-varying values can be estimated, for instance, via a preliminary MCS analysis with very few realizations (e.g., of the order of 10^2). Next, the leave-one-out cross validation follows and the set of optimal parameters (ϵ_s, ϵ_t) is determined. It is noted that, as discussed in Section 4.2.2.2, a 4^{th}-degree polynomial is also added in the approximation scheme, and thus, the joint response PDF is approximated via Eq. (4.19) with the augmented coefficient vector determined via Eq. (4.18).

In Figs. 4.11 and 4.12 the joint PDFs $p(x_1, \dot{x}_1, t)$ and $p(\dot{x}_1, x_2, t)$ obtained by the approximate WPI technique based on positive definite functions are plotted, respectively. Comparisons with pertinent MCS data (50,000 realizations) demonstrate a relatively high accuracy degree. Further, as shown in Figs. 4.13 and 4.14 for the non-stationary marginal PDFs of $x_1(t)$ and $x_2(t)$, respectively, and based on comparisons with MCS data, the herein developed technique is capable of capturing accurately the evolution in time of the PDF shape and features. Furthermore, in Fig. 4.15 the marginal PDFs of $x_2(t)$ and $\dot{x}_2(t)$ for two arbitrary time instants are shown and compared with respective MCS-based results. In passing, note that an alternative brute-force implementation (see Section 2.4.3) and employing an expansion basis for each and every time instant independently [104] would require approximately 10^9 and 70,000 PDF measurements, respectively (assuming that the temporal dimension is, indicatively, discretized into 1,000 points).

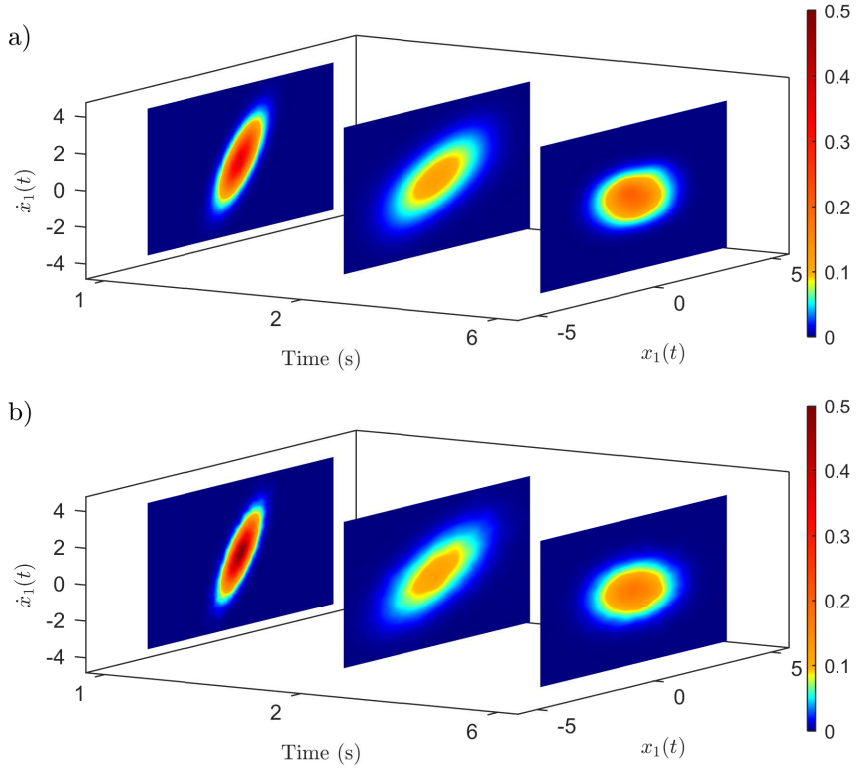

Figure 4.11: Non-stationary joint PDF of $x_1(t)$ and $\dot{x}_1(t)$ at time instants $t = 1, 2$ and 6s for a 2-DOF nonlinear system subject to time-modulated Gaussian white noise, as obtained via the WPI technique (a); comparisons with MCS data - 50,000 realizations (b).

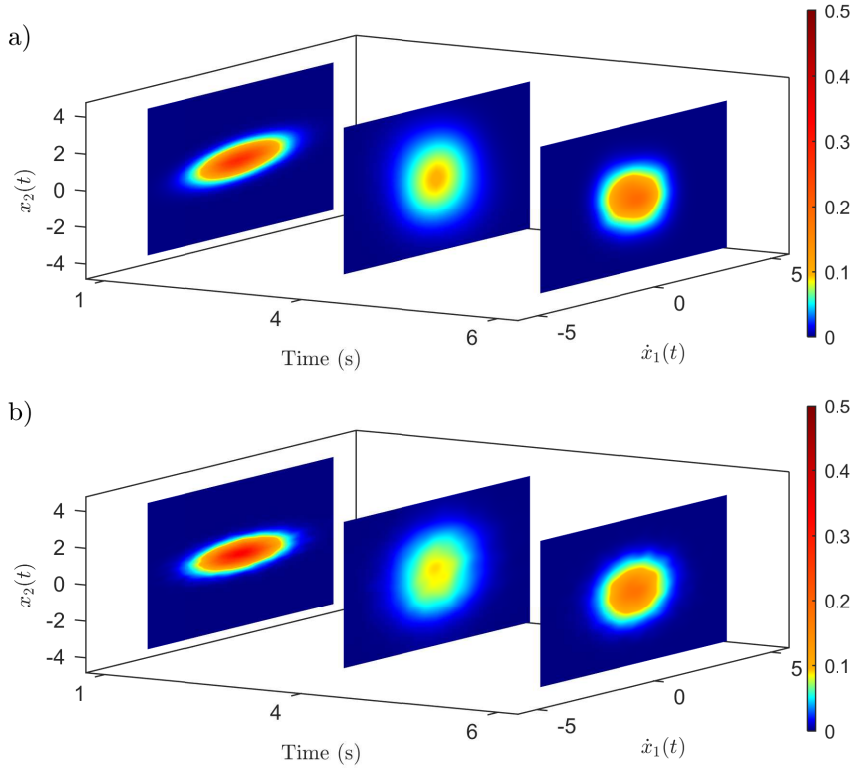

Figure 4.12: Non-stationary joint PDF of $\dot{x}_1(t)$ and $x_2(t)$ at time instants $t = 1, 4$ and 6s for a 2-DOF nonlinear system subject to time-modulated Gaussian white noise, as obtained via the WPI technique (a); comparisons with MCS data - 50,000 realizations (b).

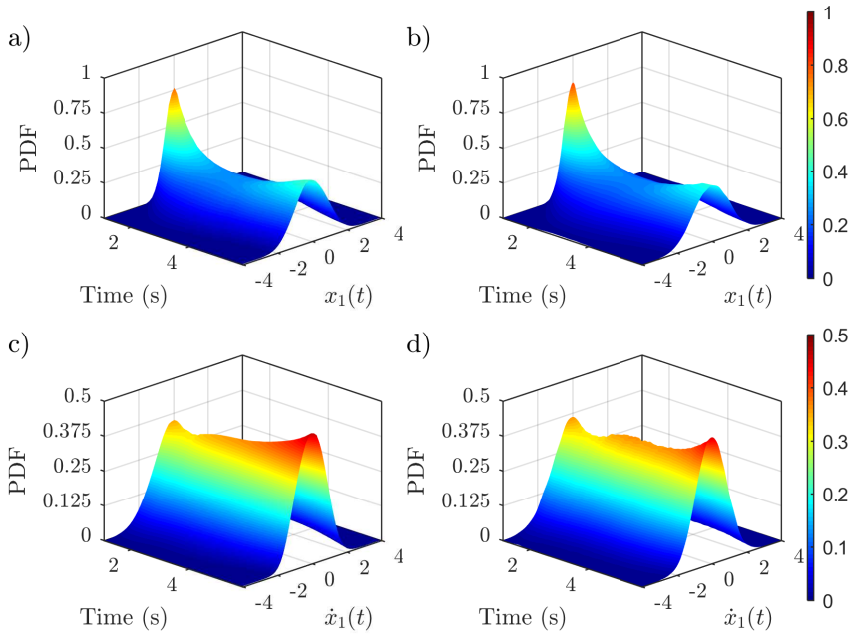

Figure 4.13: Non-stationary marginal PDF of $x_1(t)$ and $\dot{x}_1(t)$ for a 2-DOF nonlinear system subject to time-modulated Gaussian white noise, as obtained via the WPI technique (a and c); comparisons with MCS data - 50,000 realizations (b and d).

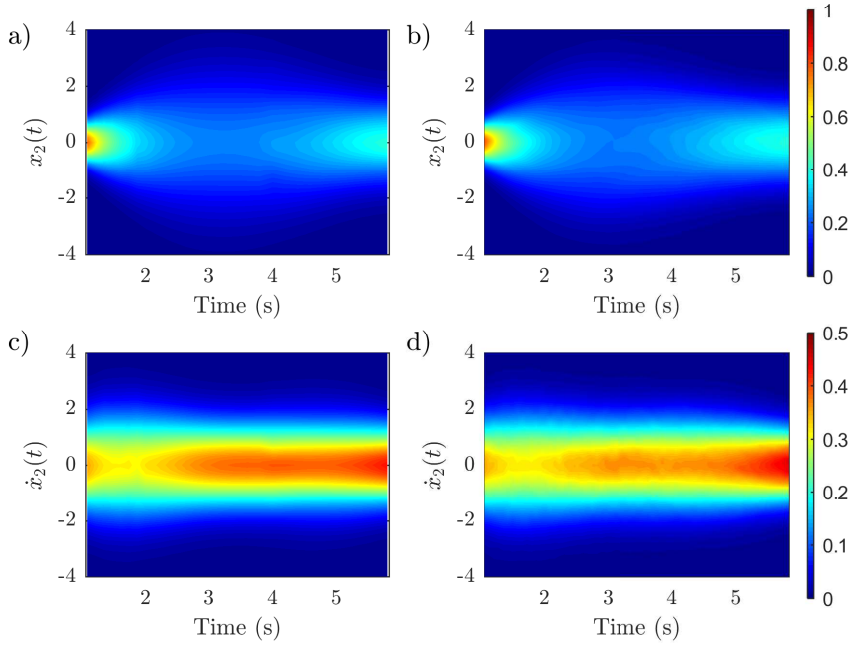

Figure 4.14: Non-stationary marginal PDF of $x_2(t)$ and $\dot{x}_2(t)$ for a 2-DOF nonlinear system subject to time-modulated Gaussian white noise, as obtained via the WPI technique (a and c); comparisons with MCS data - 50,000 realizations (b and d).

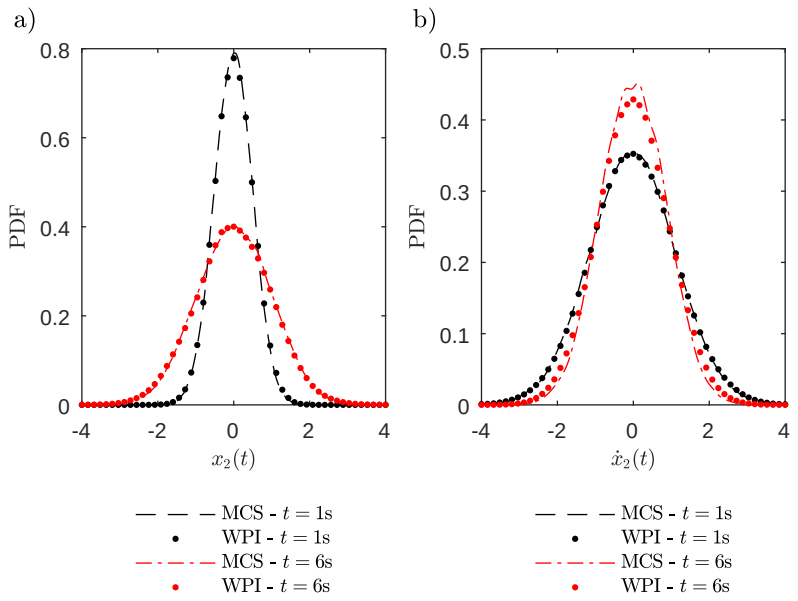

Figure 4.15: Marginal PDFs of $x_2(t)$ (a) and $\dot{x}_2(t)$ (b) at time instants $t = 1$s and $t = 6$s for a 2-DOF nonlinear system subject to time-modulated Gaussian white noise, as obtained via the WPI technique (a); comparisons with MCS data - 50,000 realizations (b).

4.3.3 Beam bending problem with a non-Gaussian and non-homogeneous stochastic Young's modulus

The example considered in this section serves to demonstrate that the WPI formalism delineated in Chapter 2 (see [146] for more details) can account not only for stochastically excited dynamical systems governed by Eq. (2.34) or (2.66), but also for certain engineering mechanics problems with stochastic media properties. In this regard, it has been shown [101, 146] that a class of one-dimensional mechanics problems with stochastic system parameters, such as the herein considered Euler-Bernoulli beam with stochastic Young's modulus, can be cast equivalently in the form of Eq. (2.69). Thus, the left hand-side of Eq. (2.69) can be used for defining an auxiliary Lagrangian function, and the WPI solution technique can be applied in a rather straightforward manner.

In this regard, a statically determinate Euler-Bernoulli beam is considered next whose

response is governed by the differential equation

$$\frac{\mathrm{d}^2}{\mathrm{d}z^2}\left[E(z)I\ddot{q}(z)\right] = l(z) \tag{4.31}$$

where $E(z)$ is the Young's modulus; I is the constant cross-sectional moment of inertia; $q(z)$ is the deflection of the beam; and $l(z)$ denotes a deterministic distributed force. In this static problem the dot above a variable denotes differentiation with respect to the space variable z. Further, as explained in [101] and [146], Eq. (4.31) can be integrated twice and cast in the form

$$-\frac{M(z)}{I\ddot{q}(z)} = E(z) \tag{4.32}$$

where the Young's modulus is modeled as a non-Gaussian, non-white and non-homogeneous stochastic field as

$$\frac{\dot{E}(z)}{E(z)} = w(z) \tag{4.33}$$

with $E(0) = E_M$, and $w(z)$ is the white noise process as defined in Eq. (2.68). It can be readily seen that Eq. (4.33) represents a standard geometric Brownian motion SDE, whose space-dependent response PDF is log-normal (e.g., [138]). Combining Eq. (4.32) and (4.33) yields an equation in the form of Eq. (2.69); that is,

$$\frac{\dot{M}(z)}{M(z)} - \frac{q^{(3)}(z)}{\ddot{q}(z)} = w(z) \tag{4.34}$$

Next, the case of a cantilever beam subject to a single point moment at its free end is considered (Fig. 4.16). Thus, taking into account that $M(z)$ is constant along the length of the beam, i.e., $M(z) = M_0$, Eq. (4.34) becomes

$$-\frac{q^{(3)}(z)}{\ddot{q}(z)} = w(z) \tag{4.35}$$

while based on Eq. (2.80) the expression

$$\mathcal{L}\left[q,\dot{q},\ddot{q},q^{(3)}\right]=\frac{(q^{(3)}(z))^2}{4\pi S_0(\ddot{q}(z))^2} \tag{4.36}$$

can be construed as the corresponding Lagrangian function. In this regard, the EL equation becomes

$$\frac{\partial\mathcal{L}}{\partial q_c}-\frac{\partial}{\partial z}\frac{\partial\mathcal{L}}{\partial\dot{q}_c}+\frac{\partial^2}{\partial z^2}\frac{\partial\mathcal{L}}{\partial\ddot{q}_c}-\frac{\partial^3}{\partial z^3}\frac{\partial\mathcal{L}}{\partial q_c^{(3)}}=0 \tag{4.37}$$

together with the initial conditions for $z_i=0$, $q_c(z_i)=q_i=0$, $\dot{q}_c(z_i)=\dot{q}_i=0$ and $\ddot{q}_c(z_i)=-\frac{M_0}{E_M I}$.

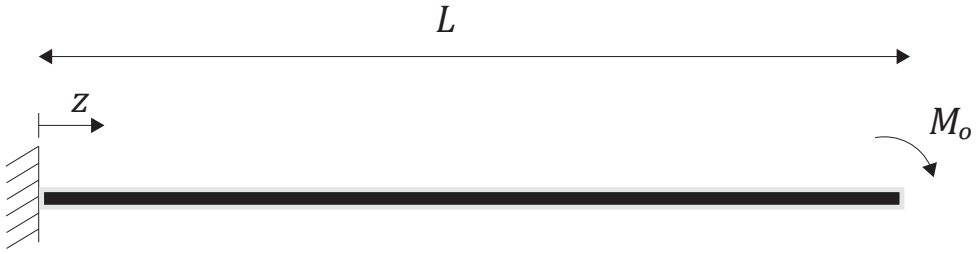

Figure 4.16: Cantilever beam subject to a single-point moment.

Subsequently, the joint response PDF $p\left(q,\dot{q},\ddot{q},z\right)$ is sampled at $N=20{,}000$ Halton points with bounds that vary with z. Specifically, the bounds of the response PDF space-varying effective domain are determined via a preliminary MCS with only a few realizations (see Example 4.3.2 for details). Next, following the evaluation of the augmented coefficient vector via Eq. (4.18), Eq. (4.19) is utilized in conjunction with an 8^{th}-degree polynomial, and $p\left(q,\dot{q},\ddot{q},z\right)$ is determined. In Figs. 4.17 and 4.18 the WPI-based non-stationary (space-dependent) marginal PDFs of $q(z)$ and $\dot{q}(z)$ are shown, respectively, while MCS-based data (50,000 realizations) are also provided for comparison. Moreover, Fig. 4.19 shows the marginal PDFs of $q(z)$ and $\dot{q}(z)$ at $z=0.6$, $z=0.8$ and $z=1$, as obtained via the herein developed technique, and includes comparisons with pertinent MCS data. It is worth mentioning that the considered beam bending problem is significantly challenging from a global approximation point of view, since the response mean varies considerably in the spatial do-

main; thus, rendering necessary the utilization of an adaptive with z effective PDF domain. Nevertheless, it has been shown that the WPI technique in conjunction with positive definite functions for approximating the joint response PDF yields accurate results at a relatively low computational cost. In this regard, note for comparison purposes that alternative implementations, such as the brute-force scheme delineated in Section 2.4.3, would require a several orders of magnitude higher number of PDF measurements. Further, a direct comparison in terms of cost with the enhanced implementation in [104] is not possible as the 4^{th}-order polynomial employed in [104] would be, most likely, an inappropriate choice for approximating the joint response $p\left(q, \dot{q}, \ddot{q}, z\right)$.

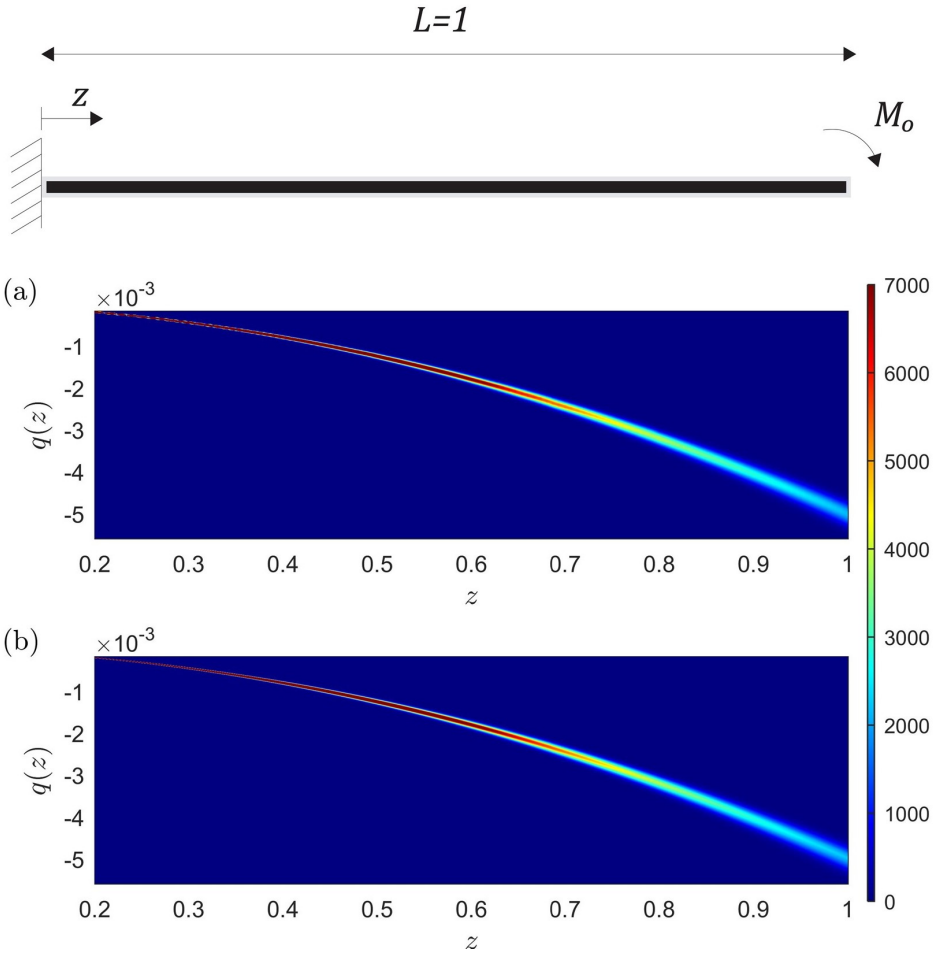

Figure 4.17: Non-stationary (space-dependent) marginal PDF of $q(z)$ for a statically determinate beam with a non-Gaussian and non-homogeneous stochastic Young's modulus, as obtained via the WPI technique (a); comparisons with MCS data - 50,000 realizations (b).

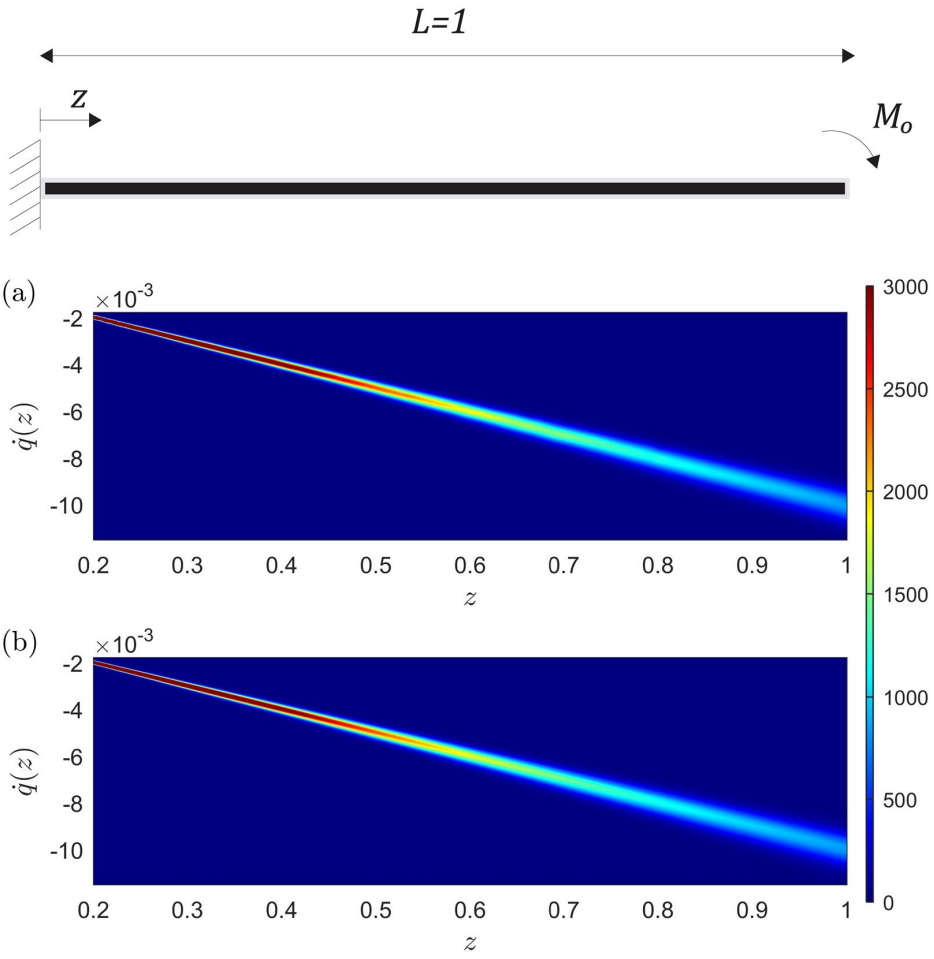

Figure 4.18: Non-stationary (space-dependent) marginal PDF of $\dot{q}(z)$ for a statically determinate beam with a non-Gaussian and non-homogeneous stochastic Young's modulus, as obtained via the WPI technique (a); comparisons with MCS data - 50,000 realizations (b).

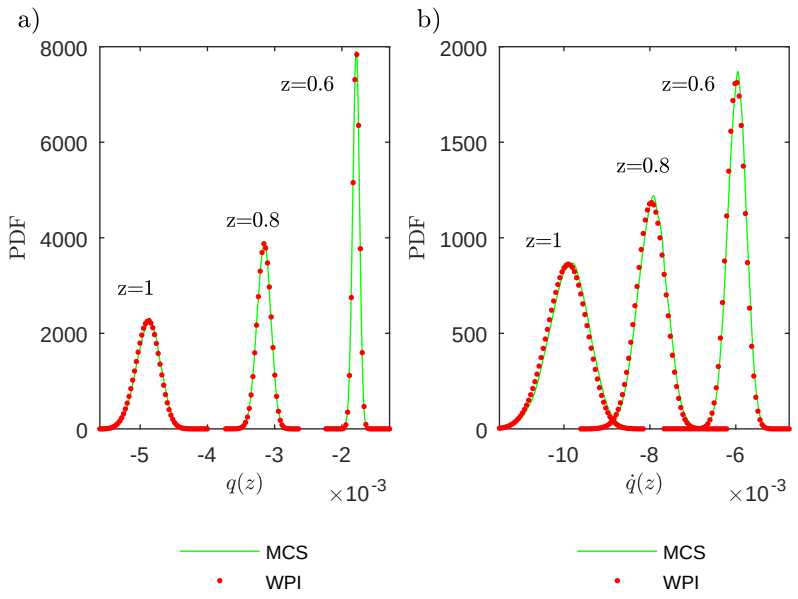

Figure 4.19: Marginal PDFs of $q(z)$ (a) and $\dot{q}(z)$ (b) at $z = 0.6$, $z = 0.8$ and $z = 1$ for a statically determinate beam with a non-Gaussian and non-homogeneous stochastic Young's modulus, as obtained via the WPI technique; comparisons with MCS data (50,000 realizations).

4.3.4 10-DOF oscillator with damping and stiffness nonlinearities

To demonstrate the accuracy and efficiency of the sparse approximation technique developed in Section 4.2.4 in handling relatively high-dimensional problems, a 10-DOF system of the form of Eq. (2.34) with cubic damping and stiffness nonlinearites is considered, where

$$\boldsymbol{M} = \begin{bmatrix} m_0 & \dots & 0 \\ \vdots & \ddots & \vdots \\ 0 & \dots & m_0 \end{bmatrix}, \tag{4.38}$$

$$\boldsymbol{C} = \begin{bmatrix} 2c_0 & -c_0 & \dots & 0 \\ -c_0 & \ddots & \ddots & \vdots \\ \vdots & \ddots & \ddots & -c_0 \\ 0 & \dots & -c_0 & 2c_0 \end{bmatrix}, \tag{4.39}$$

$$\boldsymbol{K} = \begin{bmatrix} 2k_0 & -k_0 & \dots & 0 \\ -k_0 & \ddots & \ddots & \vdots \\ \vdots & \ddots & \ddots & -k_0 \\ 0 & \dots & -k_0 & 2k_0 \end{bmatrix}, \tag{4.40}$$

and

$$\boldsymbol{g}(\boldsymbol{x}, \dot{\boldsymbol{x}}) = \begin{bmatrix} \epsilon_1 k_0 x_1^3 + \epsilon_2 c_0 \dot{x}_1^3 \\ 0 \\ \vdots \\ 0 \end{bmatrix} \tag{4.41}$$

The system is excited by a white noise vector process, whose power spectrum matrix is given by

$$\boldsymbol{P}\boldsymbol{S}_{\boldsymbol{w}} = \begin{bmatrix} S_0 & \dots & 0 \\ \vdots & \ddots & \vdots \\ 0 & \dots & S_0 \end{bmatrix} \tag{4.42}$$

while the parameters values are ($m_0 = 1$; $c_0 = 0.2$; $k_0 = 1$; $\epsilon_1 = 1$; $\epsilon_2 = 1$; and $S_0 = 0.5$). In Figs. 4.20 and 4.21, the joint response PDFs for the displacement $x_1(t)$ and velocity $\dot{x}_1(t)$ corresponding to the first DOF obtained by the herein developed efficient WPI technique are plotted for two time instants $t = 1$s and $t = 2$s, respectively. These arbitrarily chosen time instants refer to the non-stationary (transient) phase of the system dynamics. Comparisons with MCS based PDF estimates are included as well. Fig. 4.22 shows the marginal displacement and velocity PDFs at the above time instants. Figs. 4.23-4.25 show the respective results for $x_{10}(t)$ and $\dot{x}_{10}(t)$. In all cases, comparisons with pertinent MCS data demonstrate a high degree of accuracy for the sparse representation based WPI technique.

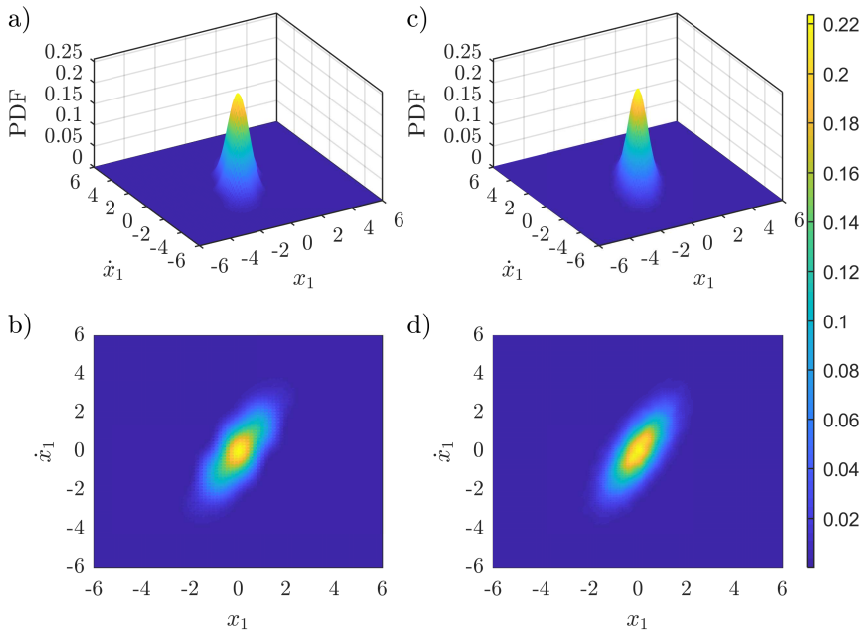

Figure 4.20: Joint PDF of $x_1(t)$ and $\dot{x}_1(t)$ at time $t = 1$s, as obtained via the WPI technique (a - b); comparisons with MCS data - 50,000 realizations (c - d).

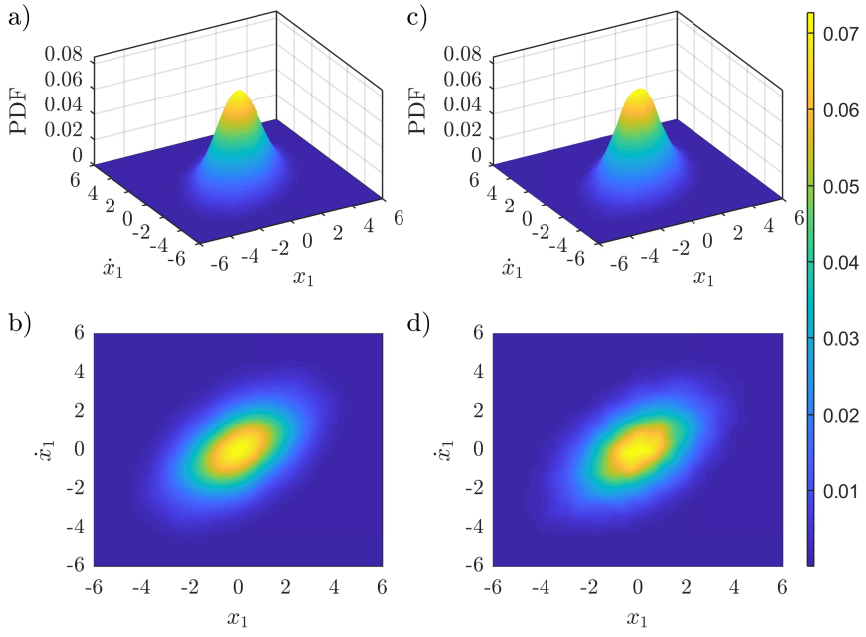

Figure 4.21: Joint PDF of $x_1(t)$ and $\dot{x}_1(t)$ at time $t = 2$s, as obtained via the WPI technique (a - b); comparisons with MCS data - 50,000 realizations (c - d).

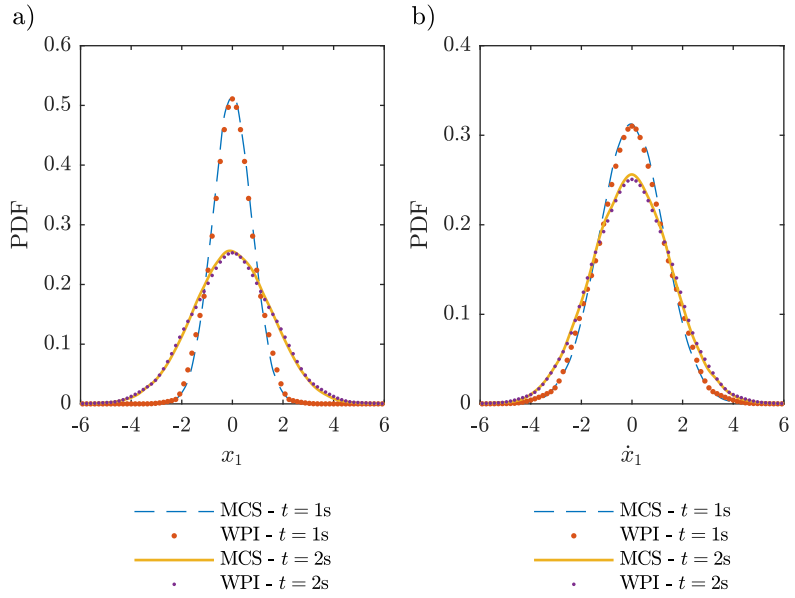

Figure 4.22: Marginal PDF of $x_1(t)$ (a) and $\dot{x}_1(t)$ (b) at time instants $t = 1$s and $t = 2$s, as obtained via the WPI technique; comparisons with MCS data (50,000 realizations).

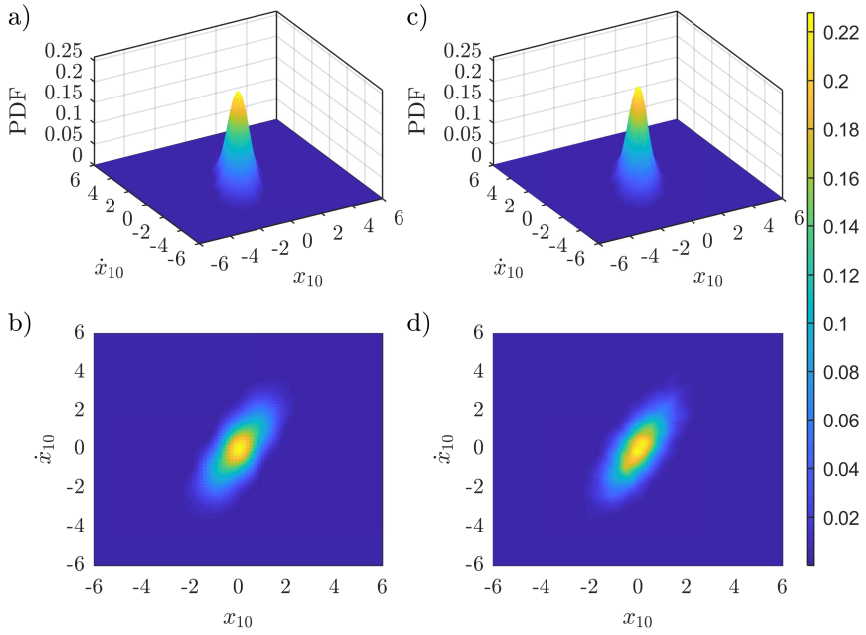

Figure 4.23: Joint PDF of $x_{10}(t)$ and $\dot{x}_{10}(t)$ at time $t = 1$s, as obtained via the WPI technique (a - b); comparisons with MCS data - 50,000 realizations (c - d).

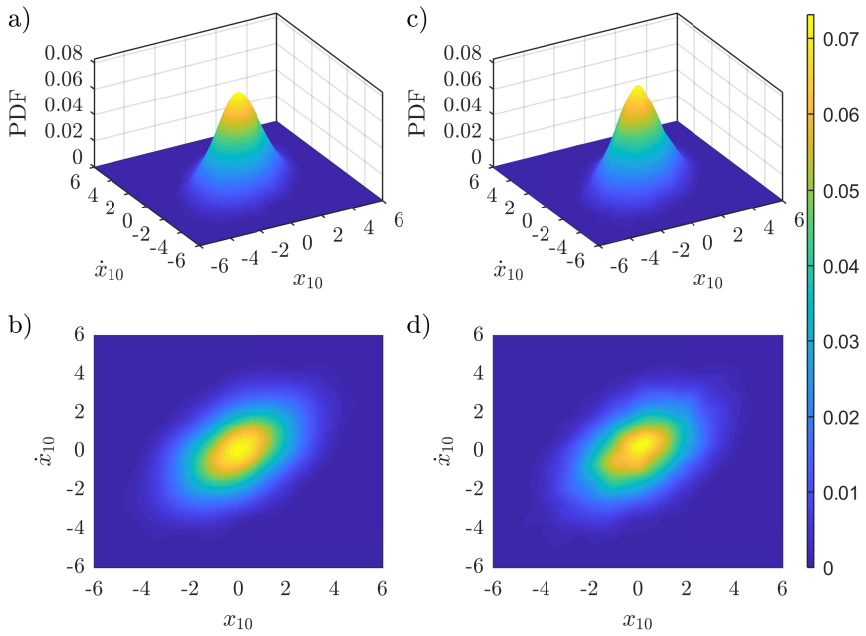

Figure 4.24: Joint PDF of $x_{10}(t)$ and $\dot{x}_{10}(t)$ at time $t = 2$s, as obtained via the WPI technique (a - b); comparisons with MCS data - 50,000 realizations (c - d).

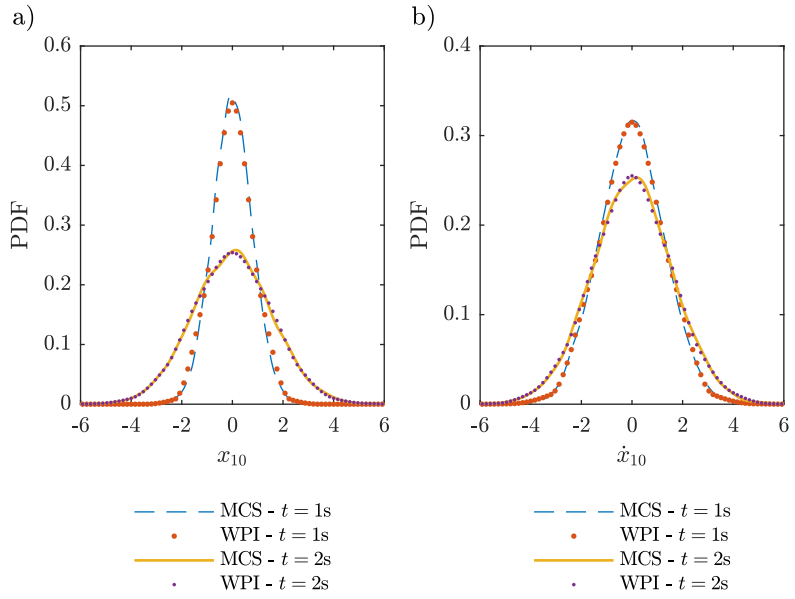

Figure 4.25: Marginal PDF of $x_{10}(t)$ (a) and $\dot{x}_{10}(t)$ (b) at time instants $t = 1$s and $t = 2$s, as obtained via the WPI technique; comparisons with MCS data (50,000 realizations).

Regarding computational efficiency, for such a system with 10 DOFs (or in other words, 20 stochastic dimensions), a brute-force WPI numerical implementation requires $\sim 30^{20}$ func-

tional minimization problems of the form of Eqs. (2.61)-(2.62) to be solved. Fig. 4.3 indicates that the polynomial approximation implementation by Kougioumtzoglou *et al.* [104] requires the solution of only 10,626 functional minimization problems (i.e., measurements of the joint response PDF), whereas resorting to compressive sampling in conjunction with a sparse polynomial approximation technique as developed herein the number of optimization problems to be solved decreases to 3,200. As an indicative order of magnitude, and utilizing a standard PC with up-to-date configurations, the joint response transition PDF of this 10-DOF system is determined in less than an hour by utilizing the herein developed technique. Further, it is noted that according to Fig. 4.3, the technique becomes even more efficient as compared to the one in [104] for increasing number of DOFs m. In other words, the computational efficiency enhancement becomes even more significant for high-dimensional systems. Of course, note that a relatively accurate MCS based response PDF estimate would require the solution of $\sim 10^6$ deterministic problems; thus, rendering the herein developed WPI technique a significantly more efficient alternative.

4.4 Concluding remarks

In this chapter, the WPI technique has been generalized and enhanced for determining directly, and in a computationally efficient manner, the complete time-dependent non-stationary response PDF of stochastically excited nonlinear multi-degree-of-freedom dynamical systems. This has been done, first, by constructing multi-dimensional (time-dependent) global bases for approximating the non-stationary joint response PDF, and second, by exploiting the localization capabilities of the WPI technique for determining PDF points in the joint space-time domain. These points have been used for evaluating the expansion coefficients at a relatively low computational cost. Specifically, two distinct expansions have been constructed: the first is based on Kronecker products of bases (e.g., wavelets), while the second employs positive definite functions. Although the performance of the expansions

in approximating the response PDF is, in general, problem-dependent, it can be argued that positive definite functions appear more versatile and suitable for handling higher-dimensional problems, whereas Kronecker products perform better for lower-dimensional problems, especially when some information regarding the PDF is available a priori.

Further, extending the work by Kougioumtzoglou *et al.* [104] who developed an efficient formulation of the WPI technique for determining the joint response PDF at specific time instants, in this chapter an enhanced formulation based on sparse representations and compressive sampling has been proposed. Specifically, by utilizing an appropriate sparse basis for expanding the system joint response PDF, resorting to the WPI localization features, and employing compressive sampling procedures in conjunction with group sparsity concepts, the computational cost for obtaining the response PDF expansion coefficients can be reduced by potentially several orders of magnitude. It is worth noting that in comparison to the formulation by Kougioumtzoglou *et al.* [104], the enhancement in computational efficiency becomes more prevalent as the number of stochastic dimensions increases; thus, rendering the herein proposed sparse representation approach indispensable, especially for high-dimensional systems.

Several numerical examples pertaining to both single- and multi-degree-of-freedom nonlinear dynamical systems subject to non-stationary excitations have been considered for assessing the reliability of the approximation schemes. Further, to illustrate that the WPI technique can account also for certain engineering mechanics problems with stochastic media properties, a bending beam with a non-Gaussian and non-homogeneous Young's modulus has been included in the numerical examples as well. The latter example has also been found to be significantly challenging from a global approximation perspective, since the response PDF effective domain varies considerably along the spatial dimension. Nevertheless, this challenge can be addressed by utilizing adaptive PDF domain bounds. In the last example, the 20-variate joint response transition PDF of a 10-DOF nonlinear structural system under stochastic excitation has been determined by using the sparse aproximation technique. The

high degree of accuracy exhibited has been corroborated by comparisons with pertinent MCS data for all the considered examples.

Chapter 5

Functional series expansions and quadratic approximations for enhancing the accuracy of the Wiener path integral technique

5.1 Introduction

A WPI-based stochastic response determination technique for diverse dynamical systems /structures is developed in this chapter by resorting to functional series expansions in conjunction with quadratic approximations. The technique can be construed as an extension and enhancement in terms of accuracy of the standard WPI solution approach developed in Chapter 2. Specifically, in comparison to the standard approach, where only the most probable path connecting initial and final states is considered in determining the joint response PDF, the herein developed technique accounts also for fluctuations around it; thus, yielding an increased accuracy degree. An additional significant advantage of the proposed enhancement as compared to earlier developments relates to the fact that low probability

events (e.g., failure probabilities) can be estimated directly in a computationally efficient manner by determining only a few points of the joint response PDF. In other words, the normalization step in the standard approach, which requires the evaluation of the joint response PDF over its entire effective domain, is circumvented. It is worth mentioning that similar approximations have also been employed in other various theoretical physics-related fields (e.g., [21, 66, 97, 107]). The efficiency and accuracy of the technique are assessed in a numerical example, where analytical results are set vis-à-vis pertinent MCS data.

5.2 Functional series expansion and quadratic approximation for non-stationary joint response PDF determination

In this section a novel WPI solution technique is developed based on the functional series expansion discussed in Section 2.3 and on a quadratic approximation. This can construed as an enhancement of the standard most probable path approach (e.g., [37, 103, 146]) to increase the accuracy degree of the determined nonlinear oscillator joint response PDF.

Consider next the one-dimensional integral of the form

$$F(\lambda) = \int_{-\infty}^{\infty} \exp\left[i\lambda f(\tau)\right] \mathrm{d}\tau \tag{5.1}$$

which can provide insight regarding both the multi-dimensional integral of Eq. (2.16) and the functional series expansion of Eq. (2.24). In this context, for $\lambda \gg f(\tau)$ even small changes in $f(\tau)$ cause rapid variations to the phase term $\lambda f(\tau)$, which, in turn, produce oscillations to the integrand $\exp\left[i\lambda f(\tau)\right]$. Consequently, except for regions where the derivative of the function $f(\tau)$ vanishes, constructive and destructive additions of the oscillatory part $\exp\left[i\lambda f(\tau)\right]$ at different τ values lead, eventually, to cancellation of the various added terms within the integral. A rigorous proof of the above heuristic explanation is given by the Riemann-Lebesgue lemma (e.g., [149]) for the case of $\lambda \to \infty$. In this regard, since for large

(but not infinite) λ values the integral is dominated by contributions related to the regions of τ where f' vanishes, the evaluation of $F(\lambda)$ in Eq. (5.1) can be performed by neglecting regions for which f' takes non-zero values. This is typically referred to in the literature as stationary phase approximation and the points for which f' becomes zero are termed stationary or critical points [161]. Next, considering for simplicity that f has only one stationary point at τ_0, and resorting to the stationary phase approximation, only contributions from points in the vicinity of τ_0 are accounted for in the evaluation of Eq. (5.1). In particular, employing a Taylor series expansion of f inserted in F yields

$$F(\lambda) = \int_{-\infty}^{\infty} \exp\left[i\lambda f(\tau_0) + \frac{1}{2} i\lambda(\tau - \tau_0)^2 f''(\tau_0) + \dots\right] \mathrm{d}\tau \tag{5.2}$$

Further, the contributions of terms of order higher than 2 in the expansion of Eq. (5.2) are regarded relatively small compared to the lower-order terms for large λ and small $\tau - \tau_0$ [161], and thus can be neglected. Note that the aforementioned expansion is also known as Laplace approximation for the case of real-valued functions.

Loosely speaking, the same rationale can be adopted when considering multi-dimensional integrals such as in Eq. (2.16) [160, 195]. In this regard, consider a stochastically excited nonlinear SDOF oscillator, whose equation of motion takes the form of Eq. (2.34) with parameters ($\boldsymbol{M} = m_0$, $\boldsymbol{C} = c_0$, $\boldsymbol{K} = k_0$, $\boldsymbol{g} = g$, $\boldsymbol{S_w} = 2\pi S_0$). Its joint transition PDF is expressed as the limit of an L-dimensional integral with $L \to \infty$ in the form of Eq. (2.16), which for the case of an SDOF oscillator becomes

$$\begin{aligned} &p(x_f, \dot{x}_f, t_f | x_i, \dot{x}_i, t_i) \\ &\quad = \lim_{\substack{\epsilon \to 0 \\ L \to \infty}} \int_{-\infty}^{\infty} \dots \int_{-\infty}^{\infty} \left\{ \exp\left(-\sum_{l=0}^{L} \frac{1}{4\pi S_0} \left[m_0 \ddot{x}_l + c_0 \dot{x}_l + k_0 x_l + g(x_l, \dot{x}_l) \right]^2 \right) \right. \\ &\qquad \left. \times \delta(\dot{x}_0 - \dot{x}_i) \left[\prod_{l=0}^{L} \frac{m_0}{\sqrt{4\pi^2 S_0 \epsilon^3}} \right] \right\} \mathrm{d}x_1 \dots \mathrm{d}x_L \end{aligned} \tag{5.3}$$

or, alternatively,

$$p(x_f, \dot{x}_f, t_f | x_i, \dot{x}_i, t_i)$$
$$= \lim_{\substack{\epsilon \to 0 \\ N \to \infty}} \int_{-\infty}^{\infty} \dots \int_{-\infty}^{\infty} \left\{ \exp\left(-\frac{1}{4\pi S_0} f_0(x_0)\right) \exp\left(-\frac{1}{4\pi S_0} f_1(x_1)\right) \right.$$
$$\left. \times \dots \times \exp\left(-\frac{1}{4\pi S_0} f_N(x_N)\right) \delta(\dot{x}_0 - \dot{x}_i) \left[\prod_{j=0}^{L} \frac{m_0}{\sqrt{4\pi^2 S_0 \epsilon^3}}\right] \right\} \mathrm{d}x_1 \dots \mathrm{d}x_L \quad (5.4)$$

where

$$f_l(x_l) = \left[m_0 \ddot{x}_l + c_0 \dot{x}_l + k_0 x_l + g(x_l, \dot{x}_l)\right]^2, \quad \text{for } l = 0, \dots, L \quad (5.5)$$

and x_l is the value of the response process $x(t)$ at time $t_l \in [t_i, t_f]$. Examining next an arbitrarily chosen exponential term in the multi-dimensional integral of Eq. (5.4), and comparing with Eq. (5.1), it is seen that the parameter λ and function f of Eq. (5.1) correspond to the constant $\frac{1}{4\pi S_0}$ and to Eq. (5.5), respectively. Therefore, it can be argued in a qualitative manner that the dominant contribution to the path integral of Eq. (2.56), which is the continuous limit of the multi-dimensional integral approximation of Eq. (5.3), is associated with the path $x_c(t)$ for which the extremality condition of Eq. (2.59) is satisfied. In other words, $x_c(t)$ can be construed as the path for which the stochastic action is stationary with respect to path fluctuations; see also Eq. (2.60). Therefore, according to the representation of Eq. (2.23) a Taylor functional series expansion of the stochastic action takes the form of Eq. (2.24), which for an SDOF oscillator can be written as

$$\mathcal{S}[x] = \mathcal{S}[x_c + X] = \mathcal{S}[x_c] + \delta\mathcal{S}[x_c, X] + \frac{1}{2!}\delta^2\mathcal{S}[x_c, X] + \dots \quad (5.6)$$

where $X(t)$ denotes the fluctuations around the most probable path $x_c(t)$.

It is noted that for quadratic Lagrangian functionals, i.e., functionals with terms whose highest power is less or equal to two, the terms in the expansion of Eq. (5.6) of order higher than two become zero. In the ensuing analysis, although for arbitrary nonlinearity

functions $g(x,\dot{x})$ these higher order terms do not vanish (e.g., [161, 191]), by resorting to the aforementioned stationary phase arguments and assumptions Eq. (5.6) is approximated as

$$\mathcal{S}\left[x\right]=\mathcal{S}[x_c]+\frac{1}{2}\delta^2\mathcal{S}\left[x_c,X\right] \tag{5.7}$$

where

$$\begin{aligned}\delta^2\mathcal{S}\left(x_c,X\right)=\int_{t_i}^{t_f}\Bigg(&\frac{\partial^2\mathcal{L}}{\partial x^2}\bigg|_{x=x_c}X^2(t)+2\frac{\partial^2\mathcal{L}}{\partial x\partial\dot{x}}\bigg|_{x=x_c}X(t)\dot{X}(t)+2\frac{\partial^2\mathcal{L}}{\partial x\partial\ddot{x}}\bigg|_{x=x_c}X(t)\ddot{X}(t)\\&+\frac{\partial^2\mathcal{L}}{\partial\dot{x}^2}\bigg|_{x=x_c}\dot{X}^2(t)+2\frac{\partial^2\mathcal{L}}{\partial\dot{x}\partial\ddot{x}}\bigg|_{x=x_c}\dot{X}(t)\ddot{X}(t)+\frac{\partial^2\mathcal{L}}{\partial\ddot{x}^2}\bigg|_{x=x_c}\ddot{X}^2(t)\Bigg)\,\mathrm{d}t\end{aligned} \tag{5.8}$$

Further, it is worth noting that, according to the rationale of the stationary phase approximation, the truncated expansion of Eq. (5.7) is anticipated to be more accurate for smaller magnitude of the fluctuations $X(t)$ around the most probable path $x_c(t)$.

In Section 5.3, it is shown that the second-order term in Eq. (5.7), which is in general different for each $\{x_f,\dot{x}_f\}$, can be explicitly calculated. Clearly, it is seen that in comparison to the standard most probable path approximation of Eq. (2.31), where the additional terms in the expansion of Eq. (5.8) are treated as a single constant independent of the final states $\{x_f,\dot{x}_f\}$, the herein developed technique is expected to exhibit enhanced accuracy.

Next, considering the nonlinear oscillator Lagrangian functional of Eq. (2.57), substituting into Eq. (5.8) and manipulating, the joint response transition PDF of Eq. (2.56) is approximated as

$$p(x_f,\dot{x}_f,t_f|x_i,\dot{x}_i,t_i)=\theta(0,0,t_f|0,0,t_i)\exp(-\mathcal{S}[x_c,\dot{x}_c,\ddot{x}_c]) \tag{5.9}$$

where the fluctuation factor $\theta(0,0,t_f|0,0,t_i)$ is given as

$$\theta(0,0,t_f|0,0,t_i) = \int_{\mathcal{C}\{0,0,t_i;0,0,t_f\}} \exp\Bigg(- \int_{t_i}^{t_f} p_1^2 \Big\{ \ddot{X}^2(t) + p_2(t)\dot{X}\ddot{X}(t) + p_3(t)\dot{X}^2(t) + p_4(t)X(t)\ddot{X}(t) + p_5(t)X(t)\dot{X}(t) + p_6(t)X^2(t) \Big\} \mathrm{d}t \Bigg) \delta(\dot{X}(t_i)) \prod_{t=t_i}^{t_f} \frac{p_1 \, \mathrm{d}X(t)}{\sqrt{\pi \mathrm{d}t^3}} \tag{5.10}$$

where

$$p_1 = \sqrt{\frac{m_0^2}{4\pi S_0}} \tag{5.11a}$$

$$p_2(t) = \frac{1}{m_0} \left[2 \left(c_0 + g_{\dot{x}} \right) \right] \Big|_{x=x_c} \tag{5.11b}$$

$$p_3(t) = \frac{1}{m_0^2} \left[\left(c_0 + g_{\dot{x}} \right)^2 + g_{\dot{x}\dot{x}} \left(m_0\ddot{x} + c_0\dot{x} + k_0 x + g \right) \right] \Big|_{x=x_c} \tag{5.11c}$$

$$p_4(t) = \frac{1}{m_0} \left[2 \left(k_0 + g_x \right) \right] \Big|_{x=x_c} \tag{5.11d}$$

$$p_5(t) = \frac{1}{m_0^2} \left[2 \left(c_0 + g_{\dot{x}} \right) \left(k_0 + g_x \right) + 2 g_{x\dot{x}} \left(m_0\ddot{x} + c_0\dot{x} + k_0 x + g \right) \right] \Big|_{x=x_c} \tag{5.11e}$$

$$p_6(t) = \frac{1}{m_0^2} \left[\left(k_0 + g_x \right)^2 + g_{xx} \left(m_0\ddot{x} + c_0\dot{x} + k_0 x + g \right) \right] \Big|_{x=x_c} \tag{5.11f}$$

In Eq. (5.11) $g\big|_{x=x_c}$ denotes $g(x_c(t))$; g_x and $g_{\dot{x}}$ represent first order partial derivatives of $g(x,\dot{x})$ with respect to x and $\dot{x}$, respectively; and g_{xx},$g_{x\dot{x}}$, and $g_{\dot{x}\dot{x}}$ denote the respective second order partial derivatives of $g(x,\dot{x})$. It is important to note that the fluctuation factor $\theta(0,0,t_f|0,0,t_i)$ of Eq. (5.10) is treated under the most probable path approximation as a single constant C (see Eq. (2.31)). In other words, it is considered independent of the final states $\{x_f,\dot{x}_f\}$. On the contrary, based on the herein proposed quadratic approximation, $\theta(0,0,t_f|0,0,t_i)$ is expressed as a path integral defined by Eq. (5.10). This path integral depends on the final state $\{x_f,\dot{x}_f\}$ through the most probable path $x_c(t)$. Although the calculation of an arbitrary path integral is typically a highly challenging task [21], it is shown in the following Section 5.3 that this is generally possible for the case of $\theta(0,0,t_f|0,0,t_i)$,

where the fluctuation paths $X(t)$ satisfy the conditions $X(t_i) = X(t_f) = \dot{X}(t_i) = \dot{X}(t_f) = 0$.

5.3 Explicit calculation of the fluctuation factor

Consider a discrete approximation of the fluctuation factor in Eq. (5.10) given by

$$\theta(0,0,t_f|0,0,t_i) = \lim_{\substack{\epsilon\to 0\\ L\to\infty}} \int_{-\infty}^{\infty}\cdots\int_{-\infty}^{\infty}\Bigg\{\exp\Bigg(-p_1^2\sum_{l=0}^{L}\Big[\frac{(X_{l+2}-2X_{l+1}+X_l)^2}{\epsilon^3} + p_2(t_l)\frac{(X_{l+2}-2X_{l+1}+X_l)}{\epsilon^2}(X_{l+1}-X_l) + p_3(t_l)\frac{(X_{l+1}-X_l)^2}{\epsilon} + p_4(t_l)\frac{(X_{l+2}-2X_{l+1}+X_l)}{\epsilon}X_l + p_5(t_l)X_l(X_{l+1}-X_l) + p_6(t_l)X_l^2\epsilon\Big]\Bigg)\delta\left(\frac{X_1-X_0}{\epsilon}\right)\prod_{l=0}^{L}\frac{p_1}{\sqrt{\pi\epsilon^3}}\Bigg\}\mathrm{d}X_1\ldots\mathrm{d}X_L \quad (5.12)$$

Taking into account that $X_0 = X_{L+1} = 0$, and also that $X_1 = 0$ due to the forward difference definition of the first-order derivative at $t = t_i$, utilizing the property $\delta\left(\frac{X_1-X_0}{\epsilon}\right) = \epsilon\delta\left(X_1 - X_0\right)$, and manipulating yields

$$\phi(0,0,t_f|0,0,t_i) = \lim_{\substack{\epsilon\to 0\\ N\to\infty}} \int_{-\infty}^{\infty}\cdots\int_{-\infty}^{\infty}\exp\left(-\frac{p_1^2}{\epsilon^3}\sum_{l_1=2}^{L}\sum_{l_2=2}^{L}X_{l_1}\mathbb{A}_{l_1,l_2}X_{l_2}\right)\epsilon\left(\frac{p_1}{\sqrt{\pi\epsilon^3}}\right)^{L+1}\mathrm{d}X_2\ldots\mathrm{d}X_L \quad (5.13)$$

where

$$\mathbb{A} = \mathbb{B} + \mathbb{C} + \mathbb{D} + \mathbb{E} + \mathbb{F} + \mathbb{G} \quad (5.14)$$

and for each $l \in \{0, \ldots, L\}$

$$\mathbb{B} \quad \text{corresponds to the term} \quad (X_{l+2} - 2X_{l+1} + X_l)^2 \tag{5.15a}$$

$$\mathbb{C} \quad \text{to the term} \quad p_2(t_l)(X_{l+2} - 2X_{l+1} + X_l)(X_{l+1} - X_l)\epsilon \tag{5.15b}$$

$$\mathbb{D} \quad \text{to the term} \quad p_3(t_l)(X_{l+1} - X_l)^2\epsilon^2 \tag{5.15c}$$

$$\mathbb{E} \quad \text{to the term} \quad p_4(t_l)(X_{l+2} - 2X_{l+1} + X_l)X_l\epsilon^2 \tag{5.15d}$$

$$\mathbb{F} \quad \text{to the term} \quad p_5(t_l)X_l(X_{l+1} - X_l)\epsilon^3 \tag{5.15e}$$

$$\mathbb{G} \quad \text{to the term} \quad p_6(t_l)X_l^2\epsilon^4 \tag{5.15f}$$

Specifically, it is straightforward to construct an algorithm that counts for each matrix $\mathbb{B}, \ldots, \mathbb{G}$ how many X_l^2, X_lX_{l+1}, and X_lX_{l+2} exist for each $l \in \{0, \ldots, L\}$ and place the corresponding values in its main, first and second diagonals, respectively. Note that every matrix in Eq. (5.15) is at most pentadiagonal, i.e., a matrix whose only nonzero elements belong to the main diagonal and the first two diagonals above and below it. Further, due to the form of the product $X_{l_1}\mathbb{A}_{l_1,l_2}X_{l_2}$ the integral of Eq. (5.13) is a multi-dimensional Gaussian integral [21]. By resorting to the multi-dimensional Gaussian integral formula [21] the fluctuation factor $\theta(0, 0, t_f|0, 0, t_i)$ can be calculated explicitly as

$$\theta(0, 0, t_f|0, 0, t_i) = \lim_{\substack{\epsilon\to 0 \\ L\to\infty}} \frac{p_1^2}{\pi\epsilon^2} \left[\det(\mathbb{A})\right]^{-1/2} \tag{5.16}$$

5.4 Numerical aspects

This section highlights certain aspects of the numerical implementation of the quadratic approximation of the WPI technique as developed in Sections 5.2 and 5.3. In this regard, note that one point of the transition PDF at a given time instant t_f is obtained by Eq. (5.9), where the fluctuation factor $\theta(0, 0, t_f|0, 0, t_i)$ is determined via Eq. (5.16). Following a brute-force implementation and assuming fixed initial conditions $\{x_i, \dot{x}_i\}$, an effective domain of

final states $\{x_f, \dot{x}_f\}$ is considered for the PDF and is discretized into $N_s \times N_s$ points. These $N_{bf} = N_s^2$ points are the final states $\{x_f, \dot{x}_f\}$ at which the transition PDF is determined via the quadratic approximation of the WPI technique. Next, for each $\{x_f, \dot{x}_f\}$ the most probable path $x_c(t)$ is obtained either by solving a BVP of the form of Eqs. (2.61)-(2.62) or by direct minimization of the stochastic action of Eq. (2.64). Further, following determination of $x_c(t)$, the time domain is discretized into $L+2$ points as in Eq. (2.10) (e.g., $L = 1{,}000$) and the parameter matrices $\mathbb{B}, \ldots, \mathbb{G}$ are evaluated on $x_c(t)$ at these $L+2$ points via Eq. (5.15). Finally, the determinant of the sum $\mathbb{A} = \mathbb{B} + \cdots + \mathbb{G}$ is computed and the L-point approximation of the fluctuation factor $\theta(0, 0, t_f|0, 0, t_i)$ is obtained by utilizing Eq. (5.16). In the numerical example in Section 5.7, the determinant $\det(\mathbb{A})$ is computed by utilizing the *det* built-in function of MATLAB, which calculates the determinant by factorizing the original matrix into lower and upper triangular factors. Note, however, that according to the definition of the matrices $\mathbb{B}, \ldots, \mathbb{G}$ in Eq. (5.15) the sum $\mathbb{A} = \mathbb{B} + \cdots + \mathbb{G}$ is a pentadiagonal matrix (see Section 5.3). Therefore, a more computationally efficient calculation of the determinant is potentially feasible by exploiting this special property of $\mathbb{A}$ (e.g., [24, 168]).

Clearly, compared with the most probable approximation, the enhanced accuracy of the quadratic approximation comes at the expense of some added modest computational cost due to the calculation of the $\det(\mathbb{A})$ in the definition of the fluctuation factor. Note, however, that the herein developed technique can be readily coupled with efficient numerical implementations such as in Chapter 4 (see also [104, 145, 147]). In this regard, sparse representations and efficacious expansion bases for the joint response PDF can be utilized, which require only few points of the PDF to be determined. Thus, the associated computational cost is kept at a minimal level.

5.5 Advantages of the quadratic WPI approximation for reliability assessment applications

According to the most probable path approximation, a given point of the joint response PDF is obtained by Eq. (2.63). Clearly, in Eq. (2.63) the exponential term depends on the specific final state $\{\boldsymbol{x}_f, \dot{\boldsymbol{x}}_f\}$ associated with the specific PDF point, whereas the constant C is the result of normalization (see Eq. (2.65)) following calculation of all the PDF values. In other words, the exponential term in Eq. (2.63) is unique for each final state $\{\boldsymbol{x}_f, \dot{\boldsymbol{x}}_f\}$, whereas the constant C is common among all $\{\boldsymbol{x}_f, \dot{\boldsymbol{x}}_f\}$, and, thus, among all points of the transition PDF effective domain.

On the contrary, in the quadratic approximation the path integral of Eq. (2.56) is approximated by Eq. (5.9). Although, the exponential term in Eq. (5.9) is exactly the same as the respective one in Eq. (2.63), the fluctuation factor $\theta(0,0,t_f|0,0,t_i)$ is different for each final state $\{x_f, \dot{x}_f\}$, and is determined via Eqs. (5.10) and (5.11) in the continuous limit or via Eq. (5.16) as the limit of an L-dimensional integral with $L \to \infty$. In this regard, note that the dependence of $\theta(0,0,t_f|0,0,t_i)$ on the final state $\{x_f, \dot{x}_f\}$ is through the most probable path $x_c(t)$ as shown in Eqs. (5.10) and (5.11). Thus, by exchanging a common across states constant C used in the most probable approximation for a "localized" and state-dependent fluctuation factor $\theta(0,0,t_f|0,0,t_i)$ in the quadratic approximation, it is anticipated that the WPI technique accuracy is enhanced. This is also demonstrated in the numerical example in Section 5.7.

Further, the fact that $\theta(0,0,t_f|0,0,t_i)$ can be separately calculated for each final state $\{x_f, \dot{x}_f\}$ via Eq. (5.16) allows for reliability assessment of the oscillator without possessing the complete transition PDF. Specifically, the probability of specific events can be calculated via Eqs. (5.9) and (5.16) without the need of determining all the points of the transition PDF and then normalizing by utilizing Eq. (2.65). The latter is an additional advantage of the quadratic approximation over the most probable path approach.

5.6 Mechanization of the quadratic WPI approximation technique

The mechanization of a brute-force implementation of the quadratic approximation as developed in Sections 5.2-5.4 involves the following steps:

(a) For a given time instant t_f, consider an effective domain of final states $\{x_f, \dot{x}_f\}$ and discretize it into $N_s \times N_s$ points.

(b) For each final state $\{x_f, \dot{x}_f\}$ determine the most probable path $x_c(t)$ by solving the BVP problem of Eqs. (2.61)-(2.62).

(c) Evaluate the matrices $\mathbb{B}, \ldots, \mathbb{G}$ based on Eq. (5.15).

(d) Compute the determinant of $\mathbb{A} = \mathbb{B} + \cdots + \mathbb{G}$.

(e) Obtain each point of the PDF by utilizing Eqs. (5.9) and (5.16).

5.7 Numerical example

Consider an SDOF oscillator, whose equation of motion is given by Eq. (2.34) with parameter values ($\boldsymbol{M} = 1$, $\boldsymbol{C} = 0.2$, $\boldsymbol{K} = 1$, $\boldsymbol{g} = 0.5x^2$, $\boldsymbol{S_w} = 0.1\pi$). Following a brute-force numerical implementation of the technique developed in Sections 5.2-5.4 for each time instant t_f an effective domain of $\{x_f, \dot{x}_f\}$ final states is considered and discretized into $N_{bf} = 30^2$ points. Next, for each and every final state $\{x_f, \dot{x}_f\}$ the most probable path $x_c(t)$ is determined by solving the BVP problem of Eqs. (2.61)-(2.62) and the fluctuation factor $\theta(0, 0, t_f|0, 0, t_i)$ is calculated by utilizing Eq. (5.16) with $L = 1{,}000$. Finally, for the most probable path approximation the joint response PDF at each time instant t_f is determined via Eq. (2.63), whereas for the quadratic approximation it is determined via Eq. (5.9).

In this regard, Fig. 5.1 demonstrates the accuracy enhancement achieved by using the quadratic approximation for various time instants t_f. Specifically, with blue color the normalized average difference (measured by the ℓ_2-norm) between the most probable path approach

and MCS data (50,000) is shown, while the respective difference for the case of the quadratic approximation is shown with red color. Finally, indicative results for the marginal PDF of $x(t)$ and $\dot{x}(t)$ obtained by the most probable path approach and the quadratic approximation are shown in Fig. 5.2. Comparisons with MCS data in Fig. 5.2 elucidate the accuracy enhancement obtained with the quadratic approximation for the case of the considered nonlinear SDOF oscillator.

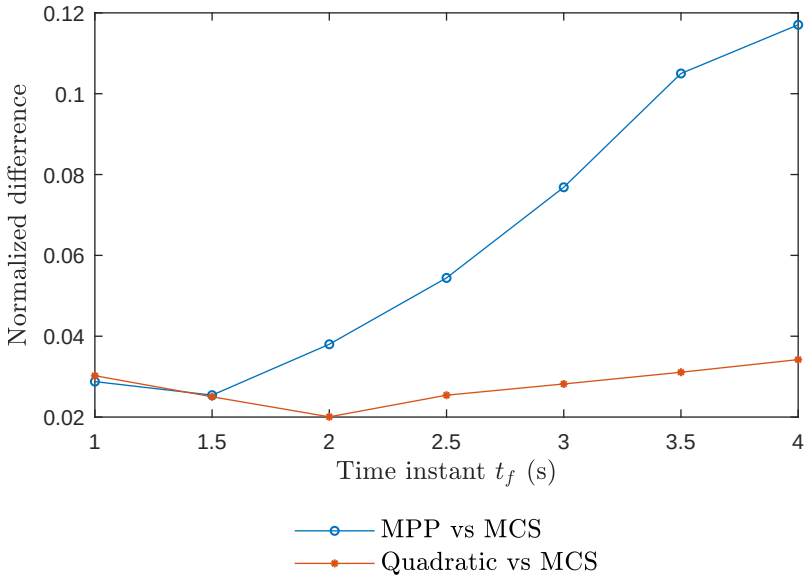

Figure 5.1: Normalized average difference (measured by the ℓ_2-norm) of the marginal PDF of $x(t)$ at various time instants between the most probable path approach of the WPI (MPP) and MCS data (50,000 realizations) - blue line; and between the quadratic approximation of the WPI and MCS data (50,000 realizations) - red line.

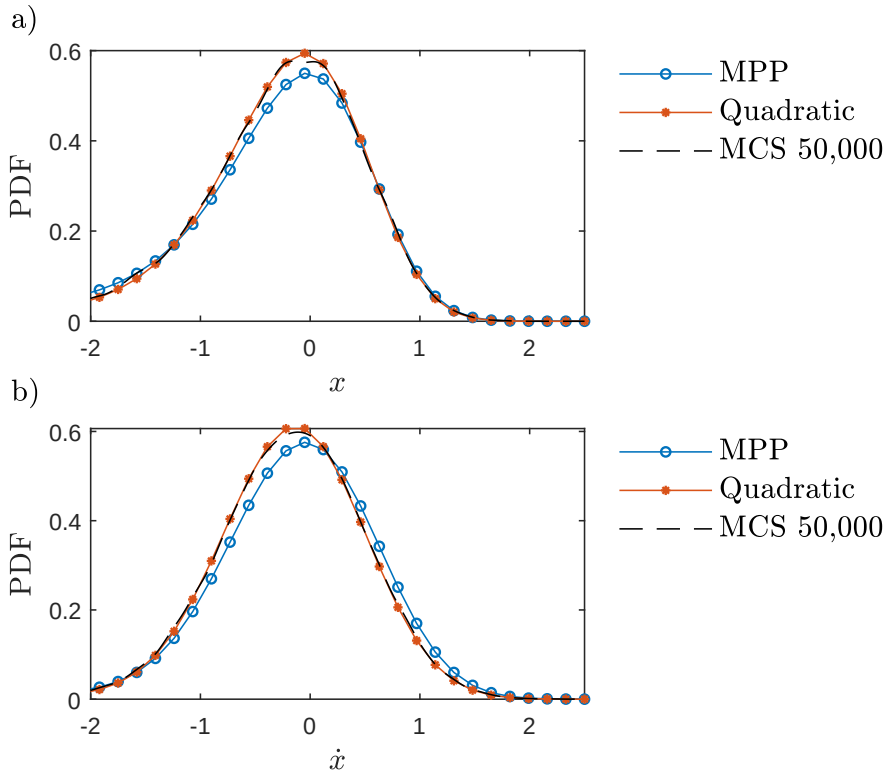

Figure 5.2: Marginal PDF of $x(t)$ (a) and $\dot{x}(t)$ (b) at time instant $t = 4$s, as obtained via the most probable path of the WPI technique (MPP) and the quadratic approximation of the WPI technique; comparisons with MCS data (50,000 realizations).

5.8 Concluding remarks

A novel WPI-based technique has been developed in this chapter for determining the response of a diverse class of stochastically excited nonlinear oscillators by resorting to functional series expansions and a quadratic approximation. Specifically, following a functional series expansion of the stochastic action of Eq. (2.64) a stationary phase argument is developed according to which the contributions of terms of order higher than 2 in the expansion can be regarded as negligible compared to the lower-order terms. As a result, the joint response PDF is approximated by Eq. (5.9) where the exponential term is exactly the same as the respective one in the most probable path approximation of Eq. (2.63), whereas the common across states constant C used in the most probable approximation is exchanged for a "localized" and state-dependent fluctuation factor $\theta(0, 0, t_f|0, 0, t_i)$ in the quadratic approximation. Therefore,

the developed technique can construed as an enhancement of the standard most probable path approach to increase the accuracy degree of the determined nonlinear oscillator joint response PDF. Further, the fact that $\theta(0,0,t_f|0,0,t_i)$ can be separately calculated for each final state $\{x_f,\dot{x}_f\}$ via Eqs. (5.10) and (5.11) allows for reliability assessment of the oscillator without possessing the complete transition PDF. The latter is an additional advantage of the quadratic approximation over the most probable path approach.

Chapter 6

Conclusions and Future Directions

6.1 Summary and major developments

Path integral techniques have proven to be potent tools in theoretical physics. Indicative application areas include the theories of superfluidity, of unified electromagnetic and weak interactions, and of quantum chromodynamics. However, in the field of engineering mechanics and dynamics path integral techniques have been proposed only recently. Specifically, Kougioumtzoglou and co-workers have adapted, extended, and applied the path integral methodology for determining the joint response transition PDF of complex dynamical systems of engineering interest. The developed WPI techniques can address MDOF systems subject to non-white, non-Gaussian and non-stationary excitation processes, whose governing dynamics equations involve complex nonlinearities (e.g., hysteretic) and fractional derivative terms.

As described in Chapter 2, since the analytical evaluation of the path integral is a challenging task for most problems of interest, the standard solution approach (e.g., [100, 103]) resorts to the most probable path approximation. According to this approximation, among all the possible paths that are considered in the path integral expression only the most probable path is taken into account for determining the joint response PDF (see Sections 2.3

and 2.4). Further, the determination of the most probable path requires the solution of a deterministic variational problem, which can either be solved directly or be expressed as a BVP. From a numerical implementation perspective, since the analytical solution of the aforementioned deterministic problem for all final states is also a rather challenging task, the most probable path needs to be separately determined for each and every set of final states (see Section 2.4.3). In this context, for determining all the values of the response PDF, although a brute-force numerical implementation typically yields a prohibitively large number of deterministic problems to be solved (i.e., measurements of the PDF to be collected), Kougioumtzoglou *et al.* [104] showed that by utilizing an expansion basis the response PDF can be approximated with satisfactory accuracy.

In the present thesis, substantial developments have been made concerning the range of problems that the WPI technique can address, its computational efficiency, as well as the related accuracy for determining in a reliable manner the response statistics of complex stochastic dynamical systems.

As explained in Chapters 1 and 3 the need for increasingly sophisticated modeling of excitations has led recently to the use of fractional-order filters for describing stochastic loads acting on structural systems. To enhance the versatility of the technique and address the need for response determination of nonlinear oscillators subject to stochastic excitations modeled via fractional-order filters, an extended WPI technique has been proposed in Chapter 3. In this regard, the original problem of solving a system of coupled multi-term fractional SDEs degenerates either to a set of deterministic fractional BVPs or to a set of deterministic fractional-order optimal control problems.

Further, as explained in Section 2.4.3, even with the enhancement in computational efficiency proposed by Kougioumtzoglou *et al.* [104], the computational cost of the technique is given as a power-law function of the number of stochastic dimensions and thus, restricts the applicability of the methodology to relatively low dimensional systems. To address this issue, several enhancements have been proposed in Chapter 4 that render the

WPI technique a powerful tool for determining efficiently the time-dependent joint response PDF of high-dimensional systems. Concisely, by combining the localization properties of the WPI technique with appropriately chosen global multi-dimensional expansion bases the problem of obtaining the response PDF has been formulated as an approximation problem. Therefore, following the collection of the required number of measurements, the expansion coefficients have been determined by solving a linear system of equations; thus, yielding an analytical expression for the joint response PDF at any point. Moreover, it has been shown that by employing compressive sampling procedures in conjunction with group sparsity concepts, the expansion coefficients can be determined by solving an optimization problem (see Section 4.2.6), and the number of required measurements of the PDF can be reduced by potentially several orders of magnitude. More importantly, it has been shown that this enhancement in computational efficiency becomes more prevalent as the number of stochastic dimensions increases; thus, rendering the herein proposed sparse representation approach indispensable, especially for high-dimensional systems.

Next, a novel WPI-based technique has been developed in Chapter 5 by resorting to functional series expansions and a quadratic approximation. In this regard, following a functional series expansion of the stochastic action (see Sections 2.3 and 5.2) higher-order terms are accounted for, which is equivalent to considering not only the most probable path but also for fluctuations around it. These fluctuations are incorporated into a state-dependent factor by which the exponential part of each PDF value is multiplied; a factor that is considered common across states and is obtained by the normalization condition of the PDF within the most probable path context. As a consequence, the accuracy exhibited by the developed technique is superior to that exhibited by the most probable path approach. Further, the fact that the fluctuation factor can be separately calculated for each state (i.e., for each PDF point) allows for reliability assessment of the oscillator without possessing the complete transition PDF (see Section 5.5).

Overall, the developments in this thesis have increased significantly the versatility, com-

putational efficiency and accuracy of the WPI technique, and have rendered it a potent tool for determining, with a minimal computational cost, the stochastic response of nonlinear oscillators subject to an extended range of excitation processes. Several numerical examples relating to both nonlinear dynamical systems subject to external excitations and a special class of engineering mechanics problems with stochastic media properties have been considered for assessing the reliability of the developed techniques. In all cases, the degree of accuracy and the computational efficiency exhibited has been compared with pertinent MCS data.

6.2 Suggestions for future research

As explained in Chapter 1 a wide range of problems (e.g., in engineering mechanics) are governed by SDEs with stochasticity embedded in the mathematical operator describing the system properties. Further, in other problems, the external excitation is modeled via operators whose input is a combination of stochastic processes and responses of filters subject to stochastic excitations (see also Chapter 3). In this context, a significant extension to the class of problems that the WPI technique can address relates to considering cases for which the stochasticity cannot be uncoupled by the response of the system. Based also on the computational efficiency and accuracy enhancements presented in this thesis, such an extension is anticipated to further increase the range of application areas of the WPI technique.

In terms of rendering the approximation schemes of Chapter 4 even more reliable, indicative future work pertains to exploring alternative sparse expansion bases for representing the time-dependent response PDF of nonlinear systems. Clearly, the performance of expansions in approximating the response PDF is, in general, problem-dependent, and thus, it can be argued that a thorough study regarding the suitability of the various expansion bases for addressing each distinct problem is required. Moreover, by exploring alternative sparse bases

the associated computational cost can be potentially reduced even further as compared to the developments of Chapter 4. In this regard, the recently developed and promising tool of dictionary learning, which given a set of measurements of the function to be approximated determines the optimal basis for representing that function, may be coupled with the WPI technique and the approximation schemes of Chapter 4.

Further, pertaining to the accuracy enhancement proposed in Chapter 5 by utilizing a quadratic approximation, a potential future development relates to exploring higher-order approximations in the functional series expansion. Although, as described in Section 5.2, the contributions of these higher-order terms are significantly smaller than the most probable path and the quadratic terms, such an enhancement is anticipated to improve significantly the accuracy of the technique for addressing stochastic systems with rather complex PDF shapes. Finally, indicative future work with important practical implications relates to developing a WPI-based technique for determining the PDF of the first time that the response of an oscillator reaches, and possibly crosses, a predetermined level; i.e., for determining the first-passage time PDF.

References

1. Agrawal, O. P. Formulation of Euler–Lagrange equations for fractional variational problems. *Journal of Mathematical Analysis and Applications* **272,** 368–379 (2002).

2. Agrawal, O. P. & Baleanu, D. A Hamiltonian formulation and a direct numerical scheme for fractional optimal control problems. *Journal of Vibration and Control* **13,** 1269–1281 (2007).

3. Agrawal, O. P. A general formulation and solution scheme for fractional optimal control problems. *Nonlinear Dynamics* **38,** 323–337 (2004).

4. Agrawal, O. Stochastic analysis of dynamic systems containing fractional derivatives. *Journal of Sound and Vibration* **5,** 927–938 (2001).

5. Alevras, P. & Yurchenko, D. GPU computing for accelerating the numerical Path Integration approach. *Computers and Structures* **171,** 46–53 (2016).

6. Alotta, G., Paola, M. D. & Pirrotta, A. Fractional Tajimi–Kanai model for simulating earthquake ground motion. *Bulletin of Earthquake Engineering* **12,** 2495–2506 (2014).

7. Arnold, L. *Stochastic Differential Equations: Theory and Applications* (Wiley, 1974).

8. Atanacković, T. M., Konjik, S. & Pilipović, S. Variational problems with fractional derivatives: Euler–Lagrange equations. *Journal of Physics A: Mathematical and Theoretical* **41,** 095201 (2008).

9. Au, S.-K. & Wang, Y. *Engineering Risk Assessment with Subset Simulation* (John Wiley & Sons, 2014).

10. Bach, F., Jenatton, R., Mairal, J. & Obozinski, G. Structured sparsity through convex optimization. *Statistical Science* **27,** 450–468 (2012).

11. Baleanu, D. & Trujillo, J. J. On exact solutions of a class of fractional Euler–Lagrange equations. *Nonlinear Dynamics* **52,** 331–335 (2008).

12. Batou, A. & Soize, C. Calculation of Lagrange multipliers in the construction of maximum entropy distributions in high stochastic dimension. *SIAM/ASA Journal on Uncertainty Quantification* **1,** 431–451 (2013).

13. Braess, D. *Nonlinear Approximation Theory* (Springer Science & Business Media, 2012).

14. Bratley, P., Fox, B. L. & Niederreiter, H. Implementation and tests of low-discrepancy sequences. *ACM Transactions on Modeling and Computer Simulation (TOMACS)* **2,** 195–213 (1992).

15. Buhmann, M. D. *Radial Basis Functions: Theory and Implementations* (Cambridge University Press, 2003).

16. Caiafa, C. F. & Cichocki, A. Computing sparse representations of multidimensional signals using kronecker bases. *Neural Computation* **25,** 186–220 (2013).

17. Candès, E. J., Romberg, J. & Tao, T. Robust uncertainty principles: exact signal reconstruction from highly incomplete frequency information. *IEEE Transactions on Information Theory* **52,** 489–509 (2006).

18. Candès, E. J. *Compressive sampling* in *Proceedings of the International Congress of Mathematicians: Madrid, August 22-30,2006 : invited lectures, Vol. 3, 2006, ISBN 978-3-03719-022-7, págs. 1433-1452* (2006), 1433–1452.

19. Cartier, P. & DeWitt-Morette, C. *Functional Integration: Action and Symmetries* (Cambridge University Press, 2006).

20. Chai, W., Naess, A. & Leira, B. J. Filter models for prediction of stochastic ship roll response. *Probabilistic Engineering Mechanics* **41,** 104–114 (2015).

21. Chaichian, M. & Demichev, A. *Path Integrals in Physics, Vol. I: Stochastic Processes and Quantum Mechanics* (Institute of Physics Publishing, 2001).

22. Chen, L. & Zhu, W. Stochastic jump and bifurcation of Duffing oscillator with fractional derivative damping under combined harmonic and white noise excitations. *International Journal of Non-Linear Mechanics* **46,** 1324–1329 (2011).

23. Chen, L., Jakobsen, E. R. & Naess, A. On numerical density approximations of solutions of SDEs with unbounded coefficients. *Advances in Computational Mathematics* **44,** 693–721 (2018).

24. Cinkir, Z. An elementary algorithm for computing the determinant of pentadiagonal Toeplitz matrices. *Journal of Computational and Applied Mathematics* **236,** 2298–2305 (2012).

25. Cohen, A., Devore, R. & Schwab, C. Analytic regularity and polynomial approximation of parametric and stochastic elliptic PDE's. *Analysis and Applications* **09,** 11–47 (2011).

26. Colet, P, Wio, H. S. & San Miguel, M. Colored noise: A perspective from a path-integral formalism. *Physical Review A* **39,** 6094 (1989).

27. Comerford, L., Kougioumtzoglou, I. A. & Beer, M. Compressive sensing based stochastic process power spectrum estimation subject to missing data. *Probabilistic Engineering Mechanics. Special Issue Based on Papers Presented at the 7th International Conference on Computational Stochastic Mechanics (CSM7)* **44,** 66–76 (2016).

28. Cossalter, M., Valenzise, G., Tagliasacchi, M. & Tubaro, S. Joint compressive video coding and analysis. *IEEE Transactions on Multimedia* **12,** 168–183 (2010).

29. Crandall, S. H. Perturbation techniques for random vibration of nonlinear systems. *Journal of the Acoustical Society of America* **35,** 1700–1705 (1963).

30. Crandall, S. H. Non-Gaussian closure for random vibration of non-linear oscillators. *International Journal of Non-Linear Mechanics* **15,** 303–313 (1980).

31. Crandall, S. H. A half-century of stochastic equivalent linearization. *Structural Control and Health Monitoring* **13,** 27–40 (2006).

32. Daniell, P. J. Integrals in an infinite number of dimensions. *Annals of Mathematics* **20,** 281–288 (1919).

33. De Marchi, S. & Schaback, R. Stability of kernel-based interpolation. *Advances in Computational Mathematics* **32,** 155–161 (2010).

34. De Marchi, S., Schaback, R. & Wendland, H. Near-optimal data-independent point locations for radial basis function interpolation. *Advances in Computational Mathematics* **23,** 317–330 (2005).

35. Dehghan, M. & Mohammadi, V. The numerical solution of Fokker–Planck equation with radial basis functions (RBFs) based on the meshless technique of Kansa's approach and Galerkin method. *Engineering Analysis with Boundary Elements* **47,** 38–63 (2014).

36. Di Lorenzo, S., Di Paola, M., Pinnola, F. P. & Pirrotta, A. Stochastic response of fractionally damped beams. *Probabilistic Engineering Mechanics* **35,** 37–43 (2014).

37. Di Matteo, A., Kougioumtzoglou, I. A., Pirrotta, A., Spanos, P. D. & Di Paola, M. Stochastic response determination of nonlinear oscillators with fractional derivatives elements via the Wiener path integral. *Probabilistic Engineering Mechanics* **38,** 127–135 (2014).

38. Di Paola, M & Sofi, A. Approximate solution of the Fokker–Planck–Kolmogorov equation. *Probabilistic Engineering Mechanics* **17,** 369–384 (2002).

39. Di Paola, M., Pirrotta, A. & Valenza, A. Visco-elastic behavior through fractional calculus: An easier method for best fitting experimental results. *Mechanics of Materials* **43,** 799–806 (2011).

40. Di Paola, M., Failla, G., Pirrotta, A., Sofi, A. & Zingales, M. The mechanically based non-local elasticity: an overview of main results and future challenges. *Philosophical Transactions of the Royal Society A: Mathematical, Physical and Engineering Sciences* **371,** 20120433 (2013).

41. Di Paola, M., Failla, G. & Pirrotta, A. Stationary and non-stationary stochastic response of linear fractional viscoelastic systems. *Probabilistic Engineering Mechanics* **28,** 85–90 (2012).

42. Diethelm, K., Baleanu, D. & Scalas, E. *Fractional Calculus: Models and Numerical Methods* (World Scientific, 2012).

43. Donoho, D. L., Tsaig, Y., Drori, I. & Starck, J. Sparse solution of underdetermined systems of linear equations by stagewise orthogonal matching pursuit. *IEEE Transactions on Information Theory* **58,** 1094–1121 (2012).

44. Donoho, D. & Tanner, J. Observed universality of phase transitions in high-dimensional geometry, with implications for modern data analysis and signal processing. *Philosophical Transactions of the Royal Society A: Mathematical, Physical and Engineering Sciences* **367,** 4273–4293 (2009).

45. Donoso, J., Salgado, J. & Soler, M. Short-time propagators for nonlinear Fokker-Planck equations. *Journal of Physics A: Mathematical and General* **32,** 3681 (1999).

46. Doostan, A. & Owhadi, H. A non-adapted sparse approximation of PDEs with stochastic inputs. *Journal of Computational Physics* **230,** 3015–3034 (2011).

47. Doucet, A., de Freitas, N. & Gordon, N. *Sequential Monte Carlo Methods in Practice* (Springer-Verlag, 2001).

48. Drozdov, A. N. & Talkner, P. Path integrals for Fokker–Planck dynamics with singular diffusion: Accurate factorization for the time evolution operator. *The Journal of Chemical Physics* **109,** 2080–2091 (1998).

49. Duarte, M. F. & Baraniuk, R. G. Kronecker compressive sensing. *IEEE Transactions on Image Processing* **21,** 494–504 (2012).

50. Dunne, J. F. & Ghanbari, M. Extreme-value prediction for non-linear stochastic oscillators via numerical solutions of the stationary FPK equation. *Journal of Sound and Vibration* **206,** 697–724 (1997).

51. Einchcomb, S. & McKane, A. Use of Hamiltonian mechanics in systems driven by colored noise. *Physical Review E* **51,** 2974 (1995).

52. Eldar, Y. C. & Kutyniok, G. *Compressed Sensing: Theory and Applications* (Cambridge University Press, 2012).

53. Elishakoff, I. *Probabilistic Theory of Structures* (Courier Corporation, 1999).

54. Elishakoff, I. & Crandall, S. H. Sixty years of stochastic linearization technique. *Meccanica* **52,** 299–305 (2017).

55. Er, G.-K. An improved closure method for analysis of nonlinear stochastic systems. *Nonlinear Dynamics* **17,** 285–297 (1998).

56. Ewing, G. M. *Calculus of Variations with Applications* (Courier Corporation, 1985).

57. Failla, G. & Pirrotta, A. On the stochastic response of a fractionally-damped Duffing oscillator. *Communications in Nonlinear Science and Numerical Simulation* **17,** 5131–5142 (2012).

58. Fasshauer, G. & McCourt, M. *Kernel-Based Approximation Methods Using Matlab* (World Scientific Publishing Company, 2015).

59. Fasshauer, G. E. *Meshfree Approximation Methods with Matlab* (World Scientific, 2007).

60. Fasshauer, G. E. Positive definite kernels: past, present and future. *Dolomite Research Notes on Approximation* **4,** 21–63 (2011).

61. Feynman, R. P. Space-time approach to non-relativistic quantum mechanics. *Reviews of Modern Physics* **20,** 367–387 (1948).

62. Feynman, R. P. & Hibbs, A. R. *Quantum Mechanics and Path Integrals* (McGraw-Hill, 1965).

63. Field, R. V., Grigoriu, M. & Emery, J. M. On the efficacy of stochastic collocation, stochastic Galerkin, and stochastic reduced order models for solving stochastic problems. *Probabilistic Engineering Mechanics* **41,** 60–72 (2015).

64. Fornberg, B. & Flyer, N. *A Primer on Radial Basis Functions with Applications to the Geosciences* (SIAM, 2015).

65. Foucart, S. & Rauhut, H. *A Mathematical Introduction to Compressive Sensing* (Birkhäuser Basel, 2013).

66. Freed, K. F. Wiener integrals and models of stiff polymer chains. *The Journal of Chemical Physics* **54,** 1453–1463 (1971).

67. Gardiner, C. W. *Handbook of Stochastic Methods for Physics, Chemistry, and the Natural Sciences* (Springer-Verlag, 1985).

68. Gasca, M. & Sauer, T. Polynomial interpolation in several variables. *Advances in Computational Mathematics* **12,** 377 (2000).

69. Gavriliadis, P. & Athanassoulis, G. The truncated Stieltjes moment problem solved by using kernel density functions. *Journal of Computational and Applied Mathematics* **236,** 4193–4213 (2012).

70. Gelfand, I. & Fomin, S. *Calculus of Variations* (Prentice Hall, New Jersey, 1963).

71. Gelfand, I. M. & Yaglom, A. M. Integration in functional spaces and its applications in quantum physics. *Journal of Mathematical Physics* **1,** 48–69 (1960).

72. Gemant, A. A method of analyzing experimental results obtained from elasto-viscous bodies. *Physics* **7,** 311–317 (1936).

73. Ghanem, R. G. & Spanos, P. D. *Stochastic Finite Elements: A Spectral Approach* (Courier Corporation, 2003).

74. Gihman, I. I., Skorohod, A. V. & Skorohod, A. V. *Stochastic Differential Equations* (Springer-Verlag, 1972).

75. Goovaerts, M. & Devreese, J. Analytic treatment of the Coulomb potential in the path integral formalism by exact summation of a perturbation expansion. *Journal of Mathematical Physics* **13,** 1070–1082 (1972).

76. Graham-Brady, L. L. *et al.* Probability and materials: from nano- to macro-scale: a summary. *Probabilistic Engineering Mechanics* **21,** 193–199 (2006).

77. Grigoriu, M. *Applied Non-Gaussian Processes: Examples, Theory, Simulation, Linear Random Vibration, and Matlab Solutions* (PTR Prentice Hall, 1995).

78. Grigoriu, M. *Stochastic Calculus: Applications in Science and Engineering* (Springer Science & Business Media, 2002).

79. Grigoriu, M. *Stochastic Systems: Uncertainty Quantification and Propagation* (Springer Science & Business Media, 2012).

80. Grigoriu, M. An efficient Monte Carlo solution for problems with random matrices. *Monte Carlo Methods and Applications* **20,** 121–136 (2014).

81. Guo, S.-S. Nonstationary solutions of nonlinear dynamical systems excited by Gaussian white noise. *Nonlinear Dynamics* **92,** 613–626 (2018).

82. Halton, J. H. On the efficiency of certain quasi-random sequences of points in evaluating multi-dimensional integrals. *Numerische Mathematik* **2,** 84–90 (1960).

83. Hänggi, P. Path integral solutions for non-Markovian processes. *Zeitschrift für Physik B Condensed Matter* **75,** 275–281 (1989).

84. Hasegawa, Y. Variational superposed Gaussian approximation for time-dependent solutions of Langevin equations. *Physical Review E* **91,** 042912 (2015).

85. Hawes, D. H. & Langley, R. S. Numerical methods for calculating the response of a deterministic and stochastically excited Duffing oscillator. *Proceedings of the Institution of Mechanical Engineers, Part C: Journal of Mechanical Engineering Science* **230,** 888–899 (2016).

86. Huang, J., Zhang, T. & Metaxas, D. Learning with structured sparsity. *Journal of Machine Learning Research* **12,** 3371–3412 (2011).

87. Huang, Z. & Jin, X. Response and stability of a SDOF strongly nonlinear stochastic system with light damping modeled by a fractional derivative. *Journal of Sound and Vibration* **319,** 1121–1135 (2009).

88. Ibrahim, R. A. *Parametric Random Vibration* (Dover Publications, 1985).

89. Jain, P., Tewari, A. & Dhillon, I. S. *Orthogonal matching pursuit with replacement* in *Advances in neural information processing systems* (2011), 1215–1223.

90. Jenatton, R., Audibert, J.-Y. & Bach, F. Structured variable selection with sparsity-inducing norms. *Journal of Machine Learning Research* **12,** 2777–2824 (2011).

91. John, V, Angelov, I, Öncül, A. & Thévenin, D. Techniques for the reconstruction of a distribution from a finite number of its moments. *Chemical Engineering Science* **62,** 2890–2904 (2007).

92. Joo, H. K. & Sapsis, T. P. A moment-equation-copula-closure method for nonlinear vibrational systems subjected to correlated noise. *Probabilistic Engineering Mechanics* **46,** 120–132 (2016).

93. Kanai, K. Semi-empirical formula for the seismic characteristics of the ground. *Bulletin of the Earthquake Research Institute* **35,** 309–325 (1957).

94. Kazem, S, Rad, J. & Parand, K. Radial basis functions methods for solving Fokker–Planck equation. *Engineering Analysis with Boundary Elements* **36,** 181–189 (2012).

95. Khader, M. M. & Hendy, A. S. A numerical technique for solving fractional variational problems. *Mathematical Methods in the Applied Sciences* **36,** 1281–1289 (2013).

96. Khandekar, D. C., Lawande, S. & Bhagwat, K. *Path-Integral Methods and Their Applications* (Allied Publishers, 2002).

97. Kitahara, K., Metiu, H. & Ross, J. A stochastic theory of cluster growth in homogeneous nucleation. *The Journal of Chemical Physics* **63,** 3156–3160 (1975).

98. Kleinert, H. *Path Integrals in Quantum Mechanics, Statistics, Polymer Physics, and Financial Markets* (World Scientific, 2009).

99. Koh, C. G. & Kelly, J. M. Application of fractional derivatives to seismic analysis of base-isolated models. *Earthquake Engineering & Structural Dynamics* **19,** 229–241 (1990).

100. Kougioumtzoglou, I. A. & Spanos, P. D. An analytical Wiener path integral technique for non-stationary response determination of nonlinear oscillators. *Probabilistic Engineering Mechanics. Computational Stochastic Mechanics — CSM6* **28,** 125–131 (2012).

101. Kougioumtzoglou, I. A. A Wiener path integral solution treatment and effective material properties of a class of one-dimensional stochastic mechanics problems. *Journal of Engineering Mechanics* **143,** 04017014 (2017).

102. Kougioumtzoglou, I. A. & Spanos, P. D. An identification approach for linear and nonlinear time-variant structural systems via harmonic wavelets. *Mechanical Systems and Signal Processing* **37,** 338–352 (2013).

103. Kougioumtzoglou, I. A. & Spanos, P. D. Nonstationary stochastic response determination of nonlinear systems: A Wiener path integral formalism. *Journal of Engineering Mechanics* **140,** 04014064 (2014).

104. Kougioumtzoglou, I. A., Di Matteo, A., Spanos, P. D., Pirrotta, A. & Di Paola, M. An efficient Wiener path integral technique formulation for stochastic response determination of nonlinear MDOF systems. *Journal of Applied Mechanics* **82,** 101005–101005–7 (2015).

105. Krée, P. & Soize, C. *Mathematics of Random Phenomena: Random Vibrations of Mechanical Structures* (D. Reidel Publishing Company, 1986).

106. Kumar, M., Chakravorty, S. & Junkins, J. L. A semianalytic meshless approach to the transient Fokker–Planck equation. *Probabilistic Engineering Mechanics* **25,** 323–331 (2010).

107. Laing, J. R. & Freed, K. F. A semiclassical magnus approximation to coupled space-time-dependent scattering equations. *Chemical Physics* **19,** 91–117 (1977).

108. Lamping, F., Peña, J.-M. & Sauer, T. Spline approximation, Kronecker products and multilinear forms. *Numerical Linear Algebra with Applications* **23,** 535–557 (2016).

109. Langouche, F, Roekaerts, D & Tirapegui, E. Functional integrals and the Fokker-Planck equation. *Il Nuovo Cimento B (1971-1996)* **53,** 135–159 (1979).

110. Langouche, F., Roekaerts, D. & Tirapegui, E. *Functional Integration and Semiclassical Expansions* (Springer Science & Business Media, 1982).

111. Lee, H. & Tsai, C.-S. Analytical model of viscoelastic dampers for seismic mitigation of structures. *Computers & Structures* **50,** 111–121 (1994).

112. Li, J. & Chen, J. *Stochastic Dynamics of Structures* (John Wiley & Sons, 2009).

113. Liaskos, K. B., Pantelous, A. A., Kougioumtzoglou, I. A. & Meimaris, A. T. Implicit analytic solutions for the linear stochastic partial differential beam equation with fractional derivative terms. *Systems & Control Letters* **121,** 38–49 (2018).

114. Lin, Y.-K. *Probabilistic Theory of Structural Dynamics* (McGraw-Hill, 1967).

115. Liu, Q & Davies, H. The non-stationary response probability density functions of non-linearly damped oscillators subjected to white noise excitations. *Journal of Sound and Vibration* **139,** 425–435 (1990).

116. Lotfi, A. & Yousefi, S. A. A numerical technique for solving a class of fractional variational problems. *Journal of Computational and Applied Mathematics* **237,** 633–643 (2013).

117. Lotfi, A., Yousefi, S. A. & Dehghan, M. Numerical solution of a class of fractional optimal control problems via the Legendre orthonormal basis combined with the operational matrix and the Gauss quadrature rule. *Journal of Computational and Applied Mathematics* **250,** 143–160 (2013).

118. Lutes, L. D. & Sarkani, S. *Random Vibrations: Analysis of Structural and Mechanical Systems* (Butterworth-Heinemann, 2004).

119. Machlup, S & Onsager, L. Fluctuations and irreversible process. II. Systems with kinetic energy. *Physical Review* **91,** 1512 (1953).

120. Mallat, S. *A Wavelet Tour of Signal Processing: The Sparse Way* (Academic Press, 2008).

121. Mann, S. & Haykin, S. The chirplet transform: Physical considerations. *IEEE Transactions on Signal Processing* **43,** 2745–2761 (1995).

122. Mayergoyz, I. D. *Mathematical Models of Hysteresis and Their Applications* (Elsevier Science, 2003).

123. McKane, A., Luckock, H. & Bray, A. Path integrals and non-Markov processes. I. General formalism. *Physical Review A* **41,** 644 (1990).

124. McWilliam, S, Knappett, D. & Fox, C. Numerical solution of the stationary FPK equation using Shannon wavelets. *Journal of Sound and Vibration* **232,** 405–430 (2000).

125. Micchelli, C. A. in *Approximation Theory and Spline Functions* 143–145 (Springer, 1984).

126. Mongillo, M. Choosing basis functions and shape parameters for radial basis function methods. *SIAM Undergraduate Research Online* **4,** 2–6 (2011).

127. Muscolino, G, Ricciardi, G & Vasta, M. Stationary and non-stationary probability density function for non-linear oscillators. *International Journal of Non-Linear Mechanics* **32,** 1051–1064 (1997).

128. Naess, A & Johnsen, J. Response statistics of nonlinear, compliant offshore structures by the path integral solution method. *Probabilistic Engineering Mechanics* **8,** 91–106 (1993).

129. Naess, A & Moe, V. Efficient path integration methods for nonlinear dynamic systems. *Probabilistic Engineering Mechanics* **15,** 221–231 (2000).

130. Náprstek, J. & Král, R. Finite element method analysis of Fokker–Plank equation in stationary and evolutionary versions. *Advances in Engineering Software* **72,** 28–38 (2014).

131. Narayanan, S & Kumar, P. Numerical solutions of Fokker–Planck equation of nonlinear systems subjected to random and harmonic excitations. *Probabilistic Engineering Mechanics* **27,** 35–46 (2012).

132. Natarajan, B. K. Sparse approximate solutions to linear systems. *SIAM Journal on Computing* **24,** 227–234 (1995).

133. Newland, D. E. Harmonic and musical wavelets. *Proceedings of the Royal Society of London. Series A: Mathematical and Physical Sciences* **444,** 605–620 (1994).

134. Newman, T., Bray, A. & McKane, A. Inertial effects on the escape rate of a particle driven by colored noise: An instanton approach. *Journal of Statistical Physics* **59,** 357–369 (1990).

135. Nigam, N. C. *Introduction to Random Vibrations* (The MIT Press, 1983).

136. Niu, B. *Monte Carlo Simulation of Infinite-dimensional Integrals* PhD thesis (Illinois Institute of Technology, 2011).

137. Nutting, P. G. A new general law of deformation. *Journal of the Franklin Institute* **191,** 679–685 (1921).

138. Øksendal, B. *Stochastic Differential Equations: An Introduction with Applications* (Springer, 2003).

139. Oldham, K. B. & Spanier, J. *The Fractional Calculus* (Academic Press, 1974).

140. Olver, P. J. On multivariate interpolation. *Studies in Applied Mathematics* **116,** 201–240 (2006).

141. Opfer, R. Multiscale kernels. *Advances in Computational Mathematics* **25,** 357–380 (2006).

142. Pazouki, M. & Schaback, R. Bases for kernel-based spaces. *Journal of Computational and Applied Mathematics* **236,** 575–588 (2011).

143. Petromichelakis, I., Psaros, A. F. & Kougioumtzoglou, I. A. Stochastic response determination and optimization of a class of nonlinear electromechanical energy harvesters: A Wiener path integral approach. *Probabilistic Engineering Mechanics* **53,** 116–125 (2018).

144. Petromichelakis, I., Psaros, A. F. & Kougioumtzoglou, I. A. *Stochastic response determination of nonlinear structural systems with singular diffusion matrices: A Wiener path integral variational formulation with constraints* in *Computational Stochastic Mechanics CSM8* (2018).

145. Psaros, A. F., Kougioumtzoglou, I. A. & Petromichelakis, I. Sparse representations and compressive sampling for enhancing the computational efficiency of the Wiener path integral technique. *Mechanical Systems and Signal Processing* **111,** 87–101 (2018).

146. Psaros, A. F., Brudastova, O., Malara, G. & Kougioumtzoglou, I. A. Wiener Path Integral based response determination of nonlinear systems subject to non-white, non-Gaussian, and non-stationary stochastic excitation. *Journal of Sound and Vibration* **433,** 314–333 (2018).

147. Psaros, A. F., Petromichelakis, I. & Kougioumtzoglou, I. A. Wiener path integrals and multi-dimensional global bases for non-stationary stochastic response determination of structural systems. *Mechanical Systems and Signal Processing* **128,** 551–571 (2019).

148. Rauhut, H. & Ward, R. Sparse Legendre expansions via ℓ_1-minimization. *Journal of Approximation Theory* **164,** 517–533 (2012).

149. Reed, M. & Simon, B. *II: Fourier Analysis, Self-Adjointness* (Elsevier, 1975).

150. Rippa, S. An algorithm for selecting a good value for the parameter c in radial basis function interpolation. *Advances in Computational Mathematics* **11,** 193–210 (1999).

151. Rish, I. & Grabarnik, G. *Sparse Modeling: Theory, Algorithms, and Applications* (CRC Press, Inc., 2014).

152. Risken, H. *The Fokker-Planck Equation: Methods of Solution and Applications* (Springer-Verlag, 1984).

153. Roberts, J. B. & Spanos, P. D. Stochastic averaging: An approximate method of solving random vibration problems. *International Journal of Non-Linear Mechanics* **21,** 111–134 (1986).

154. Roberts, J. B. & Spanos, P. D. *Random Vibration and Statistical Linearization* (Courier Corporation, 2003).

155. Rossikhin, Y. A. & Shitikova, M. V. Application of fractional calculus for dynamic problems of solid mechanics: novel trends and recent results. *ASME Applied Mechanics Reviews* **63,** 010801 (2010).

156. *Advances in Fractional Calculus: Theoretical Developments and Applications in Physics and Engineering* (eds Sabatier, J., Agrawal, O. P. & Tenreiro Machado, J. A.) (Springer, 2007).

157. Sapsis, T. P. & Athanassoulis, G. A. New partial differential equations governing the joint, response–excitation, probability distributions of nonlinear systems, under general stochastic excitation. *Probabilistic Engineering Mechanics* **23,** 289–306 (2008).

158. Sapsis, T. P. & Lermusiaux, P. F. J. Dynamically orthogonal field equations for continuous stochastic dynamical systems. *Physica D: Nonlinear Phenomena* **238,** 2347–2360 (2009).

159. Schaback, R. & Wendland, H. Kernel techniques: from machine learning to meshless methods. *Acta Numerica* **15,** 543–639 (2006).

160. Schilder, M. Some asymptotic formulas for Wiener integrals. *Transactions of the American Mathematical Society* **125,** 63–85 (1966).

161. Schulman, L. S. *Techniques and Applications of Path Integration* (Wiley, 1981).

162. Shields, M. D. & Kim, H. Simulation of higher-order stochastic processes by spectral representation. *Probabilistic Engineering Mechanics* **47,** 1–15 (2017).

163. Shinozuka, M. & Deodatis, G. Simulation of multi-dimensional Gaussian stochastic fields by spectral representation. *Applied Mechanics Reviews* **49,** 29 (1996).

164. Shokooh, A. & Suárez, L. A comparison of numerical methods applied to a fractional model of damping materials. *Journal of Vibration and Control* **5,** 331–354 (1999).

165. Sobczyk, K & Trcebicki, J. Approximate probability distributions for stochastic systems: maximum entropy method. *Computer Methods in Applied Mechanics and Engineering* **168,** 91–111 (1999).

166. Socha, L. Linearization in analysis of nonlinear stochastic systems: Recent results-Part I: Theory. *Applied Mechanics Reviews* **58,** 178–205 (2005).

167. Socha, L. *Linearization Methods for Stochastic Dynamic Systems* (Springer Science & Business Media, 2007).

168. Sogabe, T. A fast numerical algorithm for the determinant of a pentadiagonal matrix. *Applied Mathematics and Computation* **196,** 835–841 (2008).

169. Soize, C. *The Fokker-Planck Equation For Stochastic Dynamical Systems and its Explicit Steady State Solutions* (World Scientific Publishing, 1994).

170. Sommariva, A. & Vianello, M. Computing approximate Fekete points by QR factorizations of Vandermonde matrices. *Computers & Mathematics with Applications* **57,** 1324–1336 (2009).

171. Soong, T. T. & Grigoriu, M. *Random Vibration of Mechanical and Structural Systems* (PTR Prentice Hall, 1993).

172. Spanos, P. D. Stochastic linearization in structural dynamics. *ASME Applied Mechanics Reviews* **34,** 1–8 (1981).

173. Spanos, P. D. & Zeldin, B. A. Monte Carlo treatment of random fields: A broad perspective. *Applied Mechanics Reviews* **51,** 219–237 (1998).

174. Spanos, P.-T. in *Studies in Applied Mechanics* 459–473 (Elsevier, 1986).

175. Spanos, P. & Zeldin, B. Random vibration of systems with frequency-dependent parameters or fractional derivatives. *Journal of Engineering Mechanics* **123,** 290–292 (1997).

176. Spanos, P. D. & Evangelatos, G. I. Response of a non-linear system with restoring forces governed by fractional derivatives—Time domain simulation and statistical linearization solution. *Soil Dynamics and Earthquake Engineering* **30,** 811–821 (2010).

177. Spanos, P. D. & Failla, G. Wavelets: Theoretical concepts and vibrations related applications. *Shock and Vibration Digest* **37,** 359 (2005).

178. Spanos, P. D. & Malara, G. Nonlinear random vibrations of beams with fractional derivative elements. *Journal of Engineering Mechanics* **140,** 04014069 (2014).

179. Spanos, P. D., Kong, F., Li, J. & Kougioumtzoglou, I. A. Harmonic wavelets based excitation–response relationships for linear systems: A critical perspective. *Probabilistic Engineering Mechanics* **44,** 163–173 (2016).

180. Spanos, P. D., Kougioumtzoglou, I. A., dos Santos, K. R. & Beck, A. T. Stochastic averaging of nonlinear oscillators: Hilbert transform perspective. *Journal of Engineering Mechanics* **144,** 04017173 (2017).

181. Starck, J.-L., Murtagh, F. & Fadili, J. *Sparse Image and Signal Processing: Wavelets and Related Geometric Multiscale Analysis* (Cambridge University Press, 2015).

182. Stefanou, G. The stochastic finite element method: Past, present and future. *Computer Methods in Applied Mechanics and Engineering* **198,** 1031–1051 (2009).

183. Tajimi, H. *A statistical method of determing the maximum response of a building structure during an earthquake* in *Proc. 2nd WCEE, Tokyo* **II** (1960), 781–797.

184. Tarasov, V. E. Fractional mechanics of elastic solids: Continuum aspects. *Journal of Engineering Mechanics* **143,** D4016001 (2017).

185. Tropp, J. A. & Gilbert, A. C. Signal recovery from random measurements via orthogonal matching pursuit. *IEEE Transactions on Information Theory* **53,** 4655–4666 (2007).

186. Van Barel, M., Humet, M. & Sorber, L. Approximating optimal point configurations for multivariate polynomial interpolation. *Electronic Transactions on Numerical Analysis* **42,** 41–63 (2014).

187. Van Loan, C. F. & Pitsianis, N. in *Linear Algebra for Large Scale and Real-Time Applications* 293–314 (Springer, 1993).

188. Vanmarcke, E. *Random Fields: Analysis and Synthesis* (World Scientific, 2010).

189. Wehner, M. F. & Wolfer, W. G. Numerical evaluation of path-integral solutions to Fokker-Planck equations. *Physical Review A* **27,** 2663–2670 (1983).

190. Wendland, H. *Scattered Data Approximation* (Cambridge University Press, 2004).

191. Wiegel, F. W. *Introduction to Path-Integral Methods in Physics and Polymer Science* (World Scientific, 1986).

192. Wiener, N. The average of an analytic functional. *Proceedings of the National Academy of Sciences, USA* **7,** 253–260 (1921).

193. Wio, H. S. *Path Integrals for Stochastic Processes: An Introduction* (World Scientific, 2013).

194. Wio, H. S., Colet, P, San Miguel, M, Pesquera, L & Rodriguez, M. Path-integral formulation for stochastic processes driven by colored noise. *Physical Review A* **40,** 7312 (1989).

195. Wong, R. *Asymptotic Approximations of Integrals* (SIAM, 2001).

196. Xie, W.-X., Xu, W. & Cai, L. Numerical meshfree path integration method for nonlinear dynamic systems. *Applied Mathematics and Computation* **197,** 426–434 (2008).

197. Yang, X. & Karniadakis, G. E. Reweighted ℓ_1 minimization method for stochastic elliptic differential equations. *Journal of Computational Physics* **248,** 87–108 (2013).

198. Yokota, R., Barba, L. A. & Knepley, M. G. PetRBF—A parallel O (N) algorithm for radial basis function interpolation with Gaussians. *Computer Methods in Applied Mechanics and Engineering* **199,** 1793–1804 (2010).

199. Yuan, M. & Lin, Y. Model selection and estimation in regression with grouped variables. *Journal of the Royal Statistical Society: Series B (Statistical Methodology)* **68,** 49–67 (2006).

200. Zhang, X., Zhang, Y., Pandey, M. & Zhao, Y. Probability density function for stochastic response of non-linear oscillation system under random excitation. *International Journal of Non-Linear Mechanics* **45,** 800–808 (2010).

201. Zhang, Y., Comerford, L., Kougioumtzoglou, I. A. & Beer, M. Lp-norm minimization for stochastic process power spectrum estimation subject to incomplete data. *Mechanical Systems and Signal Processing* **101,** 361–376 (2018).

202. Zhu, W. Q. Recent developments and applications of the stochastic averaging method in random vibration. *Applied Mechanics Reviews* **49,** S72–S80 (1996).

203. Zienkiewicz, O. C. & Taylor, R. L. *The Finite Element Method for Solid and Structural Mechanics* (Elsevier, 2005).